

Dissertation

Design and Simulation of the CMS First Level Muon Trigger Track Finder

ausgeführt zum Zwecke der Erlangung des akademischen Grades eines
Doktors der technischen Wissenschaften

eingereicht an der Technischen Universität Wien
Technisch-Naturwissenschaftliche Fakultät

von

Dipl.-Ing. Torsten Wildschek
EP Division
CERN
CH-1211 Genève 23
Schweiz
Matrikelnummer 86 25 501
geboren am 18 01 1968 in Mödling

Genf, im April 1998

Contents

Kurzfassung	1
Abstract	3
1 The Large Hadron Collider (LHC)	5
1.1 The Accelerator	5
1.2 Physics at the LHC	6
2 The CMS Experiment	9
2.1 Overview of the Detector	9
2.2 The CMS Muon System	11
2.2.1 The Task of the Muon System	12
2.2.2 The Setup of the Muon System	14
2.2.3 The Barrel Muon System	15
2.2.4 The Endcap Muon System	20
2.3 Trigger	22
2.3.1 Triggering Concepts	22
2.3.2 CMS Trigger - General	24
2.3.3 The Muon Trigger	26
3 Specification	30
3.1 Input	30
3.1.1 Barrel	31
3.1.2 Endcap	46
3.2 Task of the Processor	50
3.3 Output Quantities	51
3.4 Design Issues and Considerations	53
3.4.1 Requirements	53
3.4.2 Particular Challenges	53

4	Muon Signal and Background Rates	55
4.1	Muon Rates	55
4.2	Background	55
5	Muon Trajectory	59
5.1	Interaction with the Magnetic Field	59
5.1.1	Trajectory in the Bending Plane	62
5.1.2	Trajectory in the (z, R) -Plane	67
5.2	Interaction with Matter	67
5.2.1	Multiple Coulomb Scattering	68
5.2.2	Energy Loss	68
6	Implementation Options	73
6.1	Track Finding	73
6.2	Template Matching/Pattern Comparison	76
6.3	Neural Networks	77
6.4	Histogramming Method	79
6.5	Content-Addressable Memories	80
7	Algorithm	84
7.1	Track Finding	84
7.1.1	Introduction	84
7.1.2	The Pairwise Matching Method	88
7.1.3	Pairwise Matching by Extrapolation	90
7.2	p_T Assignment	97
7.2.1	Bend Angle Method	97
7.2.2	Sagitta Method	101
7.2.3	Implementation in Hardware	105
7.2.4	Resolution	105
7.2.5	Charge Sign	106
7.3	Direction Assignment	107
7.3.1	Pseudo-rapidity η	107
7.3.2	Azimuth ϕ	107
7.4	Quality Assignment	109
7.5	Selection Steps	109
7.6	Feasibility	111
7.6.1	Decoupling	111
7.6.2	η -Dependence	112
7.6.3	ϕ -Dependence	113
7.7	Assessment	115
7.8	Endcap and Overlap Regions	116

8 Hardware	123
9 Simulation Software	125
10 Simulated Performance	127
10.1 Barrel zone	128
10.2 Endcap zone	128
10.3 Overlap zone	133
11 Operation	136
11.1 Operating Instructions	136
11.2 Monitoring and Diagnostics	137
12 Conclusion and Outlook	139
A The Pseudo-Rapidity η	141
Bibliography	143
Acknowledgements	148
Lebenslauf/CV	149

Kurzfassung

Der Large Hadron Collider (LHC) soll im Jahr 2005 am Europäischen Laboratorium für Teilchenphysik (CERN) in Genf den Betrieb aufnehmen. Experimente an diesem Beschleuniger werden in Proton-Proton-Stößen nach Ereignissen suchen, deren Raten weit unter den Untergrundraten liegen. Aufgabe eines Triggers ist es, diesen Untergrund so weit als möglich zu unterdrücken und die Gesamtrate so weit zu reduzieren, daß die Detektordaten auf Magnetband aufgezeichnet werden können.

Thema der vorliegenden Arbeit ist der regionale Myontrigger eines der in Planung befindlichen Experimente, des CMS-Experiments. Einleitend beschreibe ich den Beschleuniger LHC und stelle seine Physikmotivation vor. Anschließend richte ich mein Augenmerk auf den CMS-Detektor, wobei der Schwerpunkt naturgemäß auf dem Myonsystem des Detektors liegt. Der folgende Abschnitt erörtert die wesentlichsten Aspekte der Trigger (Auslösvorrichtungen) unter besonderer Berücksichtigung des CMS-Triggers.

Nach diesen einleitenden Kapiteln arbeite ich die Spezifikation jenes Teils des Triggers, an dem ich mitgearbeitet habe, in allen Einzelheiten aus. Ausgehend vom Entwurf des CMS-Triggers beschreibe ich, wie der regionale Myontrigger in den Gesamttrigger eingebettet ist, und definiere die Ein- und Ausgangsgrößen des Myontriggers. Anschließend leite ich aus den allgemeinen Anforderungen an den CMS-Trigger die besonderen Anforderungen an den regionalen Myontrigger ab.

Danach wird die Umgebung, in der dieser Trigger arbeiten soll, beschrieben. Berücksichtigt werden die Teilchenraten, denen das Myonsystem ausgesetzt ist, ebenso wie die Wirkung des magnetischen Feldes und Materials des Detektors auf die Teilchenbahnen.

Nachdem somit die Aufgabenstellung festgelegt ist, untersuche ich verschiedene Methoden, die in bestehenden Myon- und Spurtriggern eingesetzt werden, im Hinblick auf ihre Eignung im vorliegenden Fall. Meine Schlußfolgerung ist, daß keine dieser Methoden allen gestellten Anforderungen genügt.

Aus diesem Grund war es erforderlich, einen neuen Algorithmus zu ent-

wickeln. Dieser Algorithmus wird in allen Einzelheiten beschrieben, wobei auch die Umsetzbarkeit in Elektronik berücksichtigt wird. Gefolgt wird diese Präsentation von einer Machbarkeitsstudie, die zeigt, daß der vorgestellte Algorithmus machbar ist und die Anforderungen erfüllt.

Um die Leistungsfähigkeit dieser Methode zu untersuchen, entwickelte ich ein Software-Simulationspaket, das kurz vorgestellt wird. Besondere Aufmerksamkeit wird sodann den Simulationsergebnissen gewidmet.

Abschließend beschreibe ich, wie ich mir die Inbetriebnahme des Myontriggers im Jahr 2005 vorstelle.

Abstract

The Large Hadron Collider LHC is scheduled to start operation in the year 2005 at the CERN research center. Experiments at this collider will look for extremely rare physics events hidden in an overwhelming rate of background events. It is the task of the experiment's trigger system to reduce the total event rate to a level that can be recorded permanently for later analysis. The high reduction factor from total rate to recording rate places demands on the experiment's trigger system that go beyond any experienced at previous high-energy physics experiments.

The objective of my thesis has been to design a part of that trigger system, the regional first level muon trigger, of one of the LHC experiments, the Compact Muon Solenoid (CMS) detector. At the beginning, I give a brief introduction to the LHC and its physics motivation, followed by an overview of the CMS detector. The emphasis is on the detector's muon system. Next comes a general introduction to triggering, followed by an overview of the CMS trigger system.

The next part addresses the specifications of the part of the trigger I have been working on. I describe how that device is embedded into the CMS first level trigger and specify its input and output quantities. That is followed by a discussion of the requirements placed on the regional muon trigger with respect to the general trigger requirements.

The environment in which the trigger has to operate is described, giving the particle rates to which the muon system is exposed and detailing the impact of the detector's magnetic field and material on the particles' trajectories.

I then review several methods and techniques employed in previous and existing muon triggers. The conclusion is that none of them meets the requirements stated before.

For that reason a novel algorithm had to be developed. I describe that algorithm in detail and present suggestions for implementing the algorithm in hardware. That is followed by a study of the algorithm's feasibility, and I show that the algorithm is feasible and fulfills the requirements.

To assess the performance of this algorithm, I created a detailed software simulation, of which a brief overview is given. Finally, I present the performance as obtained by simulation.

Chapter 1

The Large Hadron Collider (LHC)

1.1 The Accelerator

The Large Hadron Collider (LHC) [3] will provide proton-proton collisions at energies higher than any achieved to date. The proton beams are bunched such that counter-rotating bunches of protons cross one another every 25 ns in the interaction regions of the experiments built at the Large Hadron Collider. The protons in these bunches each carry an energy of 7 TeV, yielding an energy of 14 TeV in the centre-of-mass frame. When the two counter-moving proton bunches cross, protons from the bunches can collide, producing new particles in inelastic interactions. Such inelastic interactions are also referred to as events.

The probability for such inelastic collisions to take place is determined on the one hand by the cross section for proton-proton interactions, on the other hand by the density and frequency of the proton bunches. The latter quantity, which is characteristic for the collider, is called the luminosity \mathcal{L} . The design luminosity of the LHC is $\mathcal{L} = 10^{34} \text{ cm}^{-2}\text{s}^{-1}$. The proton-proton inelastic cross section σ_{inel} is not known exactly, because it depends on energy and energies as high as those at the LHC have never been reached before. It can, however, be predicted by extrapolation from measured values at lower energies and theoretical models. The event generation software PYTHIA [53] predicts the inelastic cross section to be $\sigma_{inel} = 55 \text{ mbarn}$ at the LHC center-of-mass energy of $\sqrt{s} = 14 \text{ TeV}$. The number of inelastic interactions per second, the event rate, is then given by the product of cross section and luminosity:

$$\mathcal{L} \times \sigma = 10^{34} \text{ cm}^{-2}\text{s}^{-1} \times 55 \cdot 10^{-3} \cdot 10^{-24} \text{ cm}^2 = 5.5 \cdot 10^8 \text{ s}^{-1}$$

This event rate corresponds to 14 events per bunch crossing.

Each of these inelastic collisions creates on average about 25 secondary particles, yielding about 400 particles produced per bunch crossing. This high number of particles generated poses a serious challenge to the detector and its data analysis. The detector is exposed to high radiation doses, its components have to be designed in radiation-hard technology. This provokes the question of why does one create so many events, given the difficulty of coping with the high rates.

Most of the interactions taking place do not contain interesting new physics. The cross sections for interesting events are very small compared to the total inelastic cross section σ_{inel} : For example, the cross section for production of the hypothetical Higgs particle is estimated to be $\sigma_{Higgs} = 10^{-11} \sigma_{inel}$. Looking for the Higgs is like looking for needles in a haystack — and who wants to find many needles, has to search a very big haystack. In other words, to find a sample of very rare events one has to create a huge sample of all kinds of events.

The following table gives an overview of the parameters of the collider that are most important from the point of view of the experiments.

Energy	\sqrt{s}	14 TeV
Luminosity	\mathcal{L}	$10^{34} \text{ cm}^{-2}\text{s}^{-1}$
Bunch crossing interval	BX	25 ns
Total inelastic cross section	σ_{inel}	$\approx 55 \text{ mbarn}$
Events/bunch crossing		≈ 14
Event rate		$\approx 10^9 \text{ Hz}$
Vertex spread along beam	σ_z	5.3 cm
Vertex spread transverse	$\sigma_{x,y}$	15 μm

All of these quantities except the vertex spread have already been introduced in the previous paragraphs. The proton bunches have a finite size, so when they cross one another and produce the events, the vertices of these events are spread over a finite volume, whose dimensions are given by the vertex spread.

In addition to proton-proton operation, the LHC will be able to collide heavy nuclei (Pb-Pb) produced in the existing CERN accelerator complex, giving an energy of 1150 TeV in the centre of mass (2.76 TeV per atomic mass unit and 7.0 TeV per charge).

1.2 Physics at the LHC

The previous section has discussed the machine we plan to use, but to which end do we want to use it? This introduction will not give a detailed descrip-

tion of the physics motivation and potential of the Large Hadron Collider LHC, a complete reference can be found in the Proceedings of the LHC Workshop[2]. The physics potential of the CMS detector is described in chapter 12 of the CMS Technical Proposal[13].

This section will discuss the physics issues of the LHC only with respect to muon detection. As mentioned in the previous section, we are interested in rare events embedded in an overwhelming background of uninteresting events. How can one separate the interesting from the uninteresting events? This is where triggering, explained in section 2.3, comes into play. A trigger is a fast filter that looks at a few characteristics of an event and makes a quick decision on whether to discard the event right away as uninteresting or to keep it for further investigation. One characteristic of events that is convenient for this classification, is the presence of muons in the final state. Muons are more penetrating than most other particles, so these other particles can be blocked by a massive absorber, getting rid of the problem of high particle rates mentioned in the previous section. The muon system is placed behind the absorber, well shielded from the flood of other particles, which makes reconstruction in front of the absorber so difficult. Many of the interesting physics reactions produce muons and can thus be filtered out by looking for muons. Muons are not the only criterion used for fast triggering, but also signals from the calorimeters, which measure the energy released in the primary proton-proton interaction and carried away by the produced particles.

The hypothetical Higgs particle H is believed to be at the origin of mass. Provided it exists and its mass is in the expected range, it can be produced in LHC collisions. These Higgses decay very quickly, the decay products can decay in turn. The final state particles of that decay chain can be detected and be used to reconstruct the original H , thereby confirming its existence and allowing the measurement of its properties such as its mass.

The preferred decay mode of the H depends on its mass, but over a wide range there are muons in the final state:

mass range	decay	muons?
$90 \text{ GeV} < m_H < 130 \text{ GeV}$	$H \rightarrow \gamma \gamma$	no
$130 \text{ GeV} < m_H < 2m_Z$	$H \rightarrow Z Z^* \rightarrow 4l$	yes
$m_H > 2m_Z$	$H \rightarrow Z Z \rightarrow 4l$	yes
$m_H > 700 \text{ GeV}$	$H \rightarrow Z Z \rightarrow 2\nu + 2l$	yes
	$H \rightarrow Z Z \rightarrow 2 \text{ jets} + 2l$	yes

In this table, l stands for lepton, which can be a muon or electron. The two-photon and the four-lepton channels are also crucial for detecting Higgs particles in the minimal supersymmetric standard model (MSSM), a popular extension of the standard model of particle physics.

The search for new heavy vector bosons, which are predicted by other extensions to the standard model, is another application for muon triggers. All of these hypothetical vector bosons have muonic decay modes.

Initially, the LHC will run with a luminosity of $10^{33}\text{cm}^{-2}\text{s}^{-1}$, an order of magnitude lower than the final design luminosity. During this phase, interesting measurements include the precise investigation of the properties of the top-quark t , which has been discovered at the Tevatron collider at FNAL. The dominant decay mode of t is $t \rightarrow W^+ b$ and both decay products can in turn decay to muonic final states.

Another interesting study during low-luminosity operation is the search for CP-violation in the system of the neutral B -meson and its antiparticle \bar{B} . B -mesons can decay to charmonium J/ψ with a branching ratio of about 1 %, J/ψ in turn decays to $\mu^+\mu^-$ with a branching ratio of 6 %. The branching ratios are small, but the expected large $b\bar{b}$ production cross-section of about 500 μbarn compensates for that.

In section 1.1 it was mentioned that the LHC can be operated as a collider of heavy ions. Heavy Ion Physics hunts for the quark-gluon plasma, a deconfined state of hadronic matter. The onset of deconfinement is signaled by the suppression of Υ' and Υ'' production relative to Υ production when compared to pp collisions. Υ decays to $\mu^+\mu^-$ with a branching ratio of 2.5 %, so here again, interesting physics can be triggered on using a muon trigger.

After this survey of the physics potential of muon triggering, the next chapter will present the CMS experiment.

Chapter 2

The CMS Experiment

2.1 Overview of the Detector

The CMS (Compact Muon Solenoid) experiment will be one of two general-purpose experiments at the future Large Hadron Collider (LHC) at CERN. The LHC and its physics motivation have been described in chapter 1.

This chapter will give a brief general introduction to the CMS detector and describe its overall design only insofar as required for understanding the following discussion of the detector's muon system. The muon system will be covered in depth. A complete description of the CMS detector can be found in the Technical Proposal [13]. Figure 2.1 shows a cut view of the detector.

The CMS detector is designed to run at the highest luminosity of the LHC. The Design goal of the detector has been to achieve maximum discovery potential. Meeting this goal requires identification and precise measurement of muons, electrons, photons and measurement of jets and missing energy.

As its name indicates, CMS is a compact solenoidal detector. Its centerpiece is a superconducting solenoid coil producing a magnetic field of 4 Tesla inside the coil. The high field has two advantages, it facilitates a compact detector design and prevents soft charged tracks from reaching the outer layers of the detector. Outside the coil, the iron yoke returns the magnetic flux. The iron is saturated at a magnetic field of 1.8 Tesla.

A design alternative would have been to use a solenoid magnet combined with toroid magnets for the muon spectrometer. The advantages of the CMS solution are the following:

- It uses a single magnet, leading to a compact design. Momentum measurement starts inside the coil and continues outside the coil.
- Track bending due to the magnetic field is in the transverse plane. In the transverse plane the spread of the vertex is small, about 15 μm .

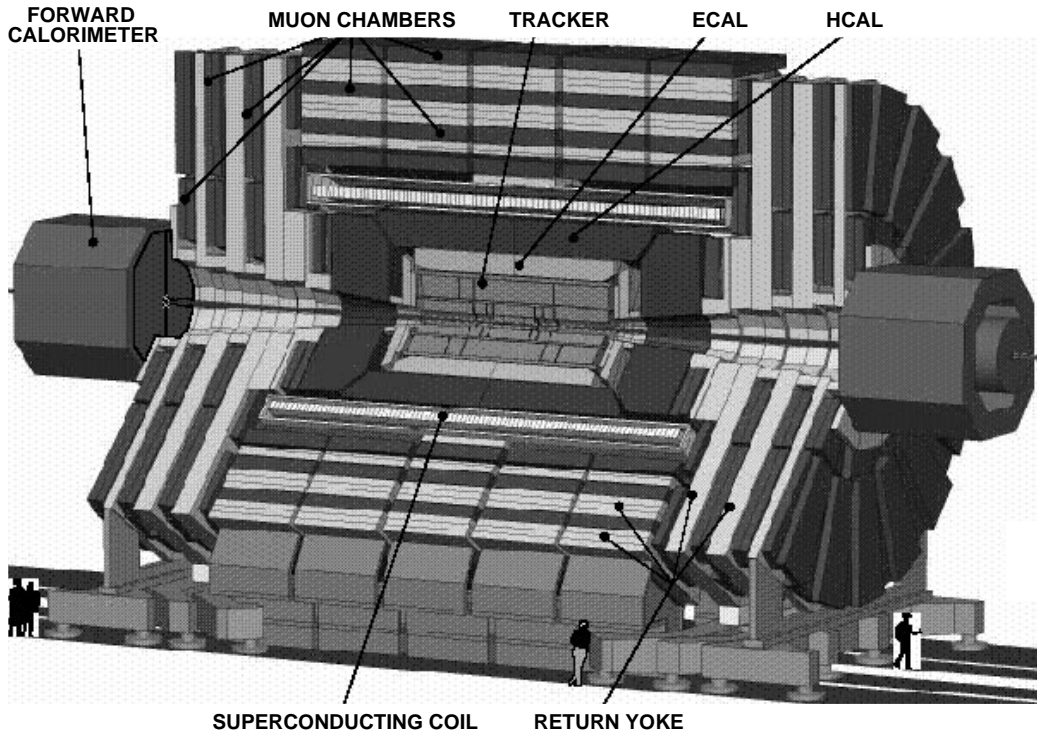


Figure 2.1: Three-dimensional cut view of the CMS detector

This allows basing a trigger on pointing to the vertex and using the vertex constraint for p_t -measurement. In the case of a toroidal muon spectrometer, bending is in the longitudinal plane, where the vertex spread is considerably larger, about 5 cm.

Let us now have a look at the detector components, following a penetrating particle from the interaction point through the detector. Proton bunches traveling in both directions along the beam axis (z -axis in the CMS coordinate system) collide in the interaction region, which has a finite size due to the finite size of the bunches themselves. The interaction region spreads approximately $15 \mu\text{m}$ in the plane perpendicular to the beam (transverse plane) and 5.3 cm along the beam axis. The inner tracker surrounds the interaction region and serves to reconstruct charged tracks, measure their momenta and reconstruct the vertices from which the particles originate. The tracker is followed by the calorimeters, which measure particles' energies by total absorption. The calorimeters are located inside the coil, because the particles would lose fluctuating amounts of energy in the material of the coil, resulting in a degradation of the energy resolution. The electromagnetic calorimeter is made of lead tungstenate PbWO_4 scintillator crystals and measures the energy of photons and electrons. The benchmark physics

process that imposes the most stringent requirements on the electromagnetic calorimeter's performance is the Higgs decay mode $H \rightarrow \gamma\gamma$. Precise determination of the mass of the Higgs boson requires good resolution of the photon energies and their angular separation. The electromagnetic calorimeter is followed by the hadron calorimeter, which measures energies and directions of particle jets. It should provide hermetic coverage to measure 'missing' transverse energy - energy carried off by particles not detectable in the calorimeter, such as neutrinos or the hypothetical lightest supersymmetric particle. Main performance indicators are jet energy resolution and missing energy resolution.

The calorimeters are surrounded by the superconducting coil, which in turn is followed by the flux return yoke. Interleaved with the iron plates of the yoke are the muon chambers, which will be covered in detail in the following sections.

Of importance for the first level muon trigger are only the coil and the muon chambers, the rest of the detector is just absorber from the point of view of first level muon triggering.

Overall dimensions of the detector are given in the following table.

length	20 m
diameter	14 m
mass	12 000 tons

2.2 The CMS Muon System

This section discusses the basis of our special interest in muons based on their interaction properties. It then describes the task of the muon detector itself and other detector components in the identification and measurement of muons. This is followed by a detailed description of the setup of the CMS muon detector.

The acronym CMS stands for Compact Muon Solenoid. This stresses the importance of muon detection to the design of the CMS detector. The identification of muons is based on their penetration depth - muons have a much larger range in matter than other charged particles. Muons, like electrons, interact with the matter they pass mainly due to the electromagnetic interaction. Hadronic particles such as the abundantly produced pions, by contrast, are absorbed due to hadronic interactions with the nuclei of matter. Electrons have a much lower mass than muons and at high energies lose energy primarily through bremsstrahlung. The energy loss through bremsstrahlung is inversely proportional to the particle's mass squared, thus this effect is much smaller for muons than for electrons, resulting in a larger

range for muons.

The muon detector is thus placed behind a massive absorber, which is supposed to absorb all charged particles except muons. Of course, there will always be a certain amount of leakage of particles from the absorber, called punchthrough. This background in the muon system will be discussed in more detail in section 4.2.

Figure 2.2 shows the thickness of absorber in front of each of the four CMS barrel muon chambers as a function of pseudo-rapidity η . Pseudo-rapidity is explained in appendix A. The unit used for giving absorber thickness is the nuclear interaction length, a material constant that indicates the range of a hadron in matter before it interacts inelastically with a nucleus of the target material. This nuclear interaction between the incident hadron and the nucleus creates new hadronic particles, which in turn interact with the material and create yet another generation of hadrons, giving rise to a hadronic shower. The shower terminates when the created particles' energies become so low that they cannot create new particles in interactions. They finally are absorbed by nuclei or come to rest. The depth of the shower is approximately proportional to the logarithm of the incident hadron's energy. That means that the higher the incident particle's energy, the thicker the absorber must be to contain the shower inside the absorber and keep leakage of shower particles to the rear of the absorber low.

So why are muons important for a first level trigger? Muons offer an easy and clean signature: There is a single particle after a massive absorber. At LHC, there will be approximately 20 inelastic interactions per bunch crossing. Each of those interactions has a high track multiplicity, flooding the detector with particles and making pattern recognition in the inner parts of the detector a daunting task. In the muon system, however, charged particle rates are much lower due to the massive absorber, allowing fast and simple algorithms to be employed for track finding.

Important physics channels at LHC involving muons are: The Higgs decay $H \rightarrow ZZ$ where the Z -bosons in turn decay to muons and decays of the heavy quarks t and b (see section 1.2).

After having discussed the special importance attached to muons in the previous paragraphs, the following subsections will describe the task and the setup of the CMS muon detector.

2.2.1 The Task of the Muon System

The tasks of the muon detector are:

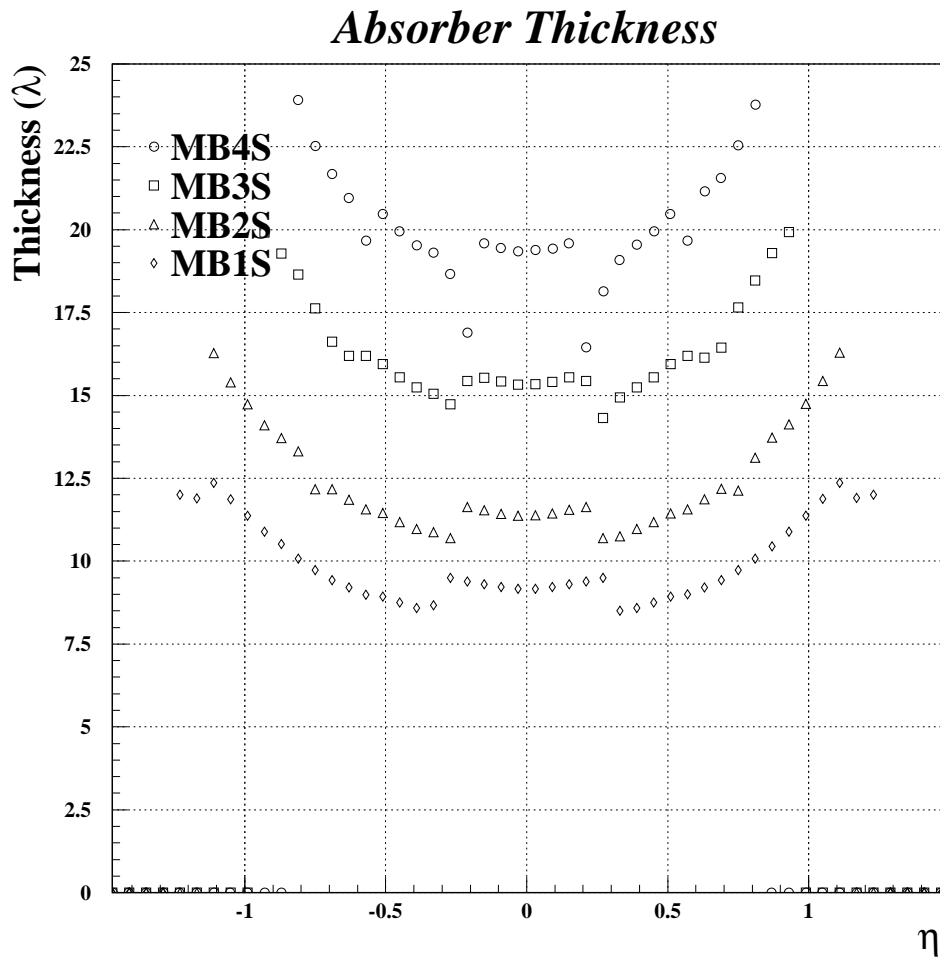


Figure 2.2: Thickness of absorber expressed in units of nuclear interaction length

- Muon identification. As stated above, muon identification is based on the penetration depth of the muons. A massive absorber in front of the muon system serves to filter out other particles. However, in spite of the absorber, the muon detector still is hit by non-muon particles. Therefore its ability to cope with various backgrounds such as punchthrough, neutral backgrounds, muon-induced backgrounds is of utmost importance. Backgrounds will be discussed in more detail in section 4.2.
- Triggering. For the reasons mentioned above, muons provide an important and relatively easy signature for physics processes of interest. They are therefore used for event selection at an early stage.
- Precise momentum measurement. The solenoidal magnetic field bends tracks in the (R, ϕ) -plane. The bending is maximal at the coil. In the flux return yoke the field direction is opposite and tracks are bent back. The bending depends on the particle's momentum and thus can be used for momentum measurement. Interaction of the track with the magnetic field will be discussed in section 5.1 and methods for momentum measurement will be elaborated in section 7.2.

The other detectors have also a rôle to play in the detection and measurement of muons, but not at the first level regional muon trigger, which, due to time constraints, has to make its decision based on information from the muon system alone and treats the other components just as absorber. For higher level triggers and off-line event reconstruction, the inner tracker improves muon momentum resolution. The calorimeter provides isolation criteria at the first level global trigger and higher levels: If a track happens to be found behind a high-energy hadronic shower in the calorimeter, it is likely that the track is not a prompt muon, but debris from the shower.

2.2.2 The Setup of the Muon System

The CMS muon detector consists of two independent systems, the barrel and the endcap muon chambers. This section gives a short introduction to the whole muon system, discusses the features common to the two subsystems and is followed by sections on each of the two subsystems.

Both systems consist of four muon stations interleaved with the iron of the magnetic flux return yoke. The iron decouples adjacent stations in the case of muon-induced background: A muon can emit a bremsstrahlung photon which gives rise to an electromagnetic cascade. The iron between adjacent

stations has to be at least 30 cm thick to absorb all those shower particles and prevent them from reaching the second station.

Figure 2.3 shows a longitudinal cut through the CMS muon system with muon tracks passing at various values of pseudo-rapidity η .

The barrel region covers the η -range $|\eta| < 0.8$. In that η -range, muons pass all four barrel stations. At higher pseudo-rapidities, muons still cross the inner chambers in the barrel region, but for $|\eta| > 0.9$ also hit the endcap chambers. This region, $0.9 < |\eta| < 1.25$, is the overlap zone, where tracks can pass through both barrel and endcap systems. For $|\eta| > 1.25$, tracks pass only the endcap chambers, up to an upper bound of $|\eta| = 2.4$.

The muon stations consist of individual chambers, for mechanical reasons gaps between those chambers are unavoidable. Moreover, the chamber edges are dead areas. The individual chambers of the muon stations are arranged such that overlapping dead areas are minimized. The guiding principle was that every muon of sufficient energy to penetrate all chambers should cross at least three stations in their active area.

The following two subsections will describe the barrel and the endcap muon system in detail. They cover only those detectors on which the trigger presented in this report is based. These detectors are used both for offline event reconstruction and triggering. It should be pointed out that in addition there are muon detectors dedicated solely to triggering. Those devices, resistive plate chambers (RPCs), will not be discussed.

2.2.3 The Barrel Muon System

The barrel muon system consists of four stations. There are two muon stations (MS2 and MS3) inside the iron yoke, the innermost station (MS1) is placed in front of the yoke and the outermost station (MS4) outside the yoke.

The stations consist of individual chambers, these chambers are planar and rectangular. The segmentation of the stations into chambers is dictated by the segmentation of the iron yoke: There are five wheels along the z -axis, each approximately 2.5 m long. Along azimuth ϕ , each wheel is divided into 12 sectors, so one sector covers approximately 30 degrees. Chambers are staggered to avoid that the cracks between the chambers line up and point back to the interaction region.

Figure 2.4 shows a perspective view of the muon chambers in the barrel region.

The innermost muon station (MS1) covers a pseudo-rapidity range up to $|\eta| < 1.2$, the outermost muon station (MS4) up to $|\eta| < 0.8$. In figure 2.5 I show the geometric acceptance at $\eta = 0$ that results from this setup. Muon

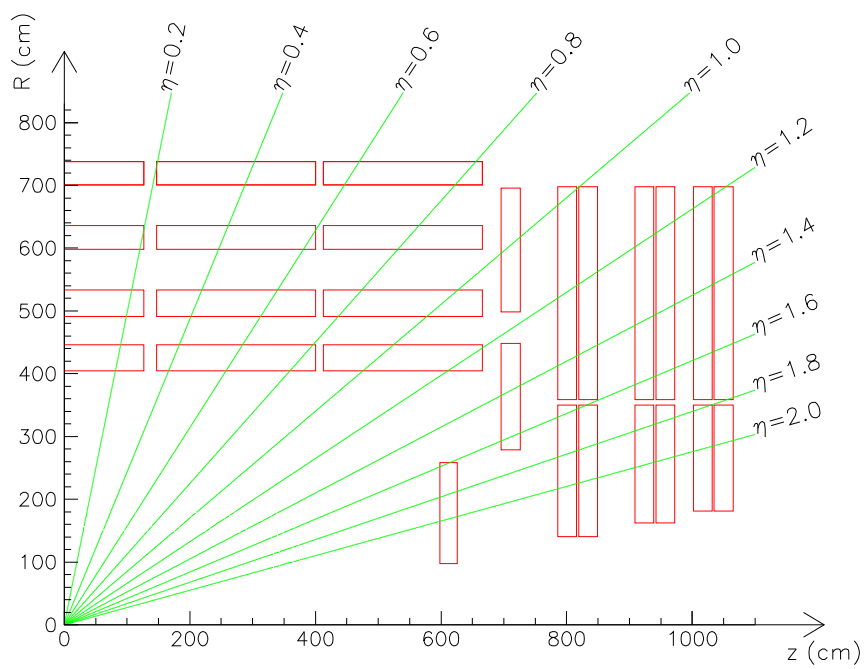


Figure 2.3: Longitudinal view of one octant of the CMS muon system

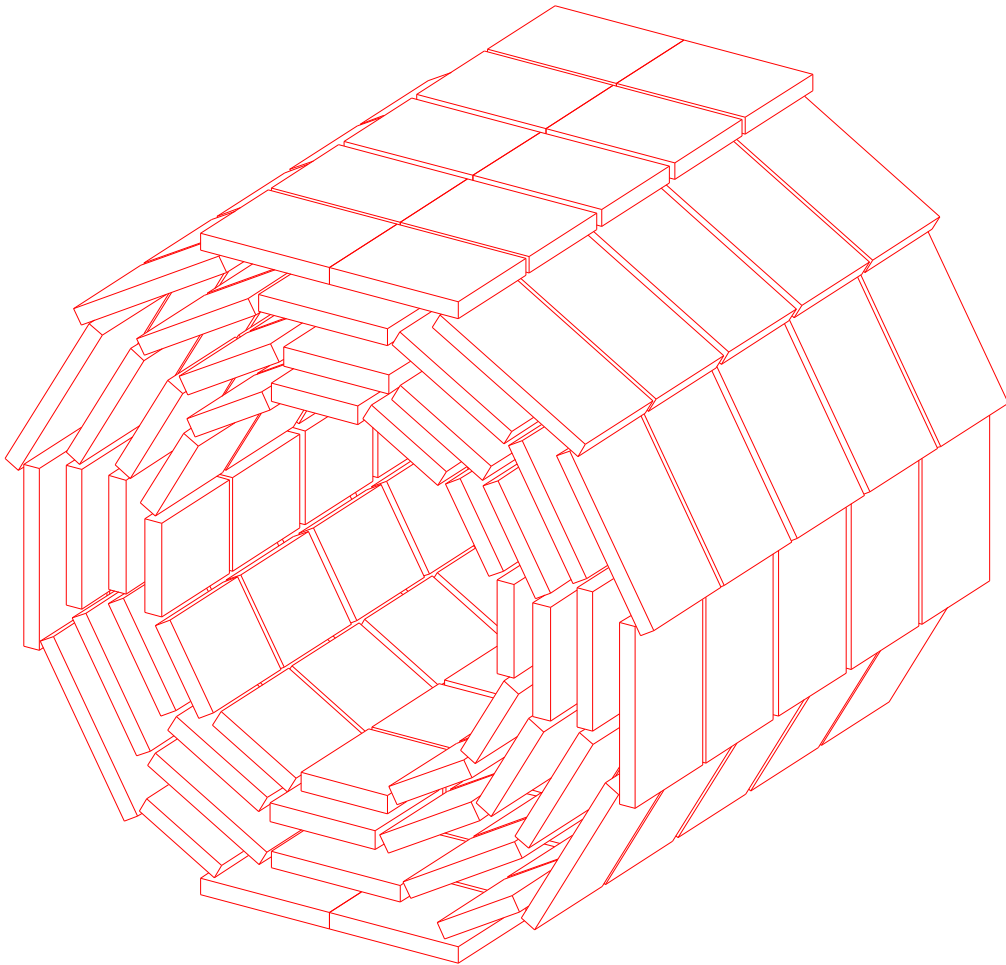


Figure 2.4: Perspective view of the barrel muon detector

chambers in MS4 overlap in ϕ as can be seen from figure 2.4, that is why the acceptance for MS4 reaches practically 100 %. For mechanical reasons, gaps between the chambers can not be avoided in the other stations, and the acceptance curves level off at values below 100 %. The cutoff at low transverse momenta results from the bending of the tracks in the magnetic field and the tracks' energy loss in the material in front of the muon chambers.

After the geometric setup of the barrel muon system, let me now discuss the choice of the detection method and the setup of the individual muon chambers. The magnetic field is mainly contained in the iron yoke and the expected charged particle rates in the barrel region are not very high. This allows the use of drift chambers as detectors.

The basic building block of the drift chambers is the rectangular drift tube, with transverse dimensions $4 \text{ cm} \times 1 \text{ cm}$ and the sense wire running along the axis of the tube. The maximum drift distance is half the cell width of 4 cm, at a drift velocity of roughly $50 \mu\text{m}/\text{ns}$ this results in a maximum drift time of 400 ns (16 bunch crossing intervals). The maximum drift time and hence the cell width is dictated by the need to keep tube occupancies below 1 %. Individual drift tubes are separated by walls. Low-energy muon-induced background (δ -electrons) is thus contained in one cell.

Each chamber comprises 12 layers of drift tubes. These tubes are arranged in three superlayers of four layers each. Drift tubes in adjacent layers are staggered by half a cell width. This staggering enables the use of a mean-timer method to determine the bunch crossing from which the measured particles originate. This mean-timer technique will be discussed in section 3.1.1. Because the drift chambers can determine the bunch crossing, they are called drift tubes with bunch crossing identification or DTBX.

The two outer superlayers are made of tubes with sense wires parallel to the z -axis and hence measure the position in the bending plane ($x - y$ -plane). Not only the track's position, but also the track's crossing angle in the bending plane should be measured with fine resolution. This requires a lever arm between the two superlayers in order to obtain the crossing angle from the position measurements provided by the two superlayers. The distance between the two superlayers is about 23 cm, resulting in an angular resolution of about 1 mrad for a drift cell position resolution of about $200 \mu\text{m}$. The precise measurement in the bending plane is required for measuring the muon's transverse momentum.

The inner superlayer consists of four layers of drift tubes with wires perpendicular to the z -axis and measures the position along the beam direction.

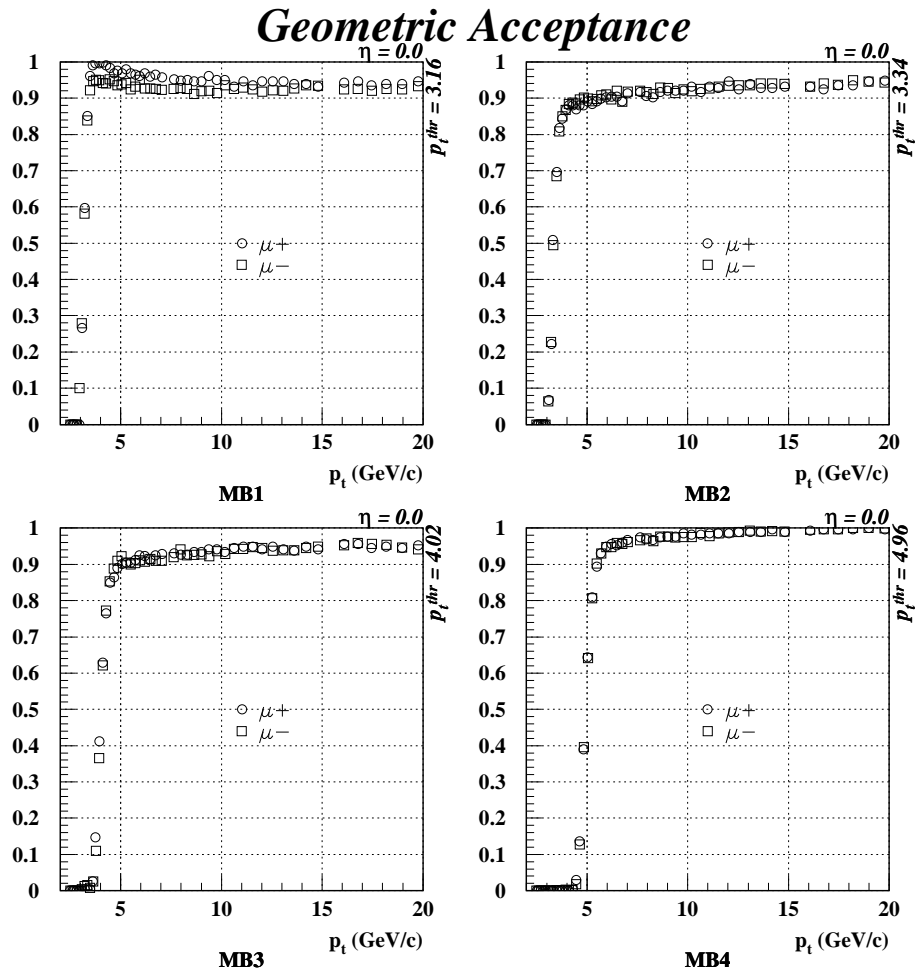


Figure 2.5: Geometric acceptance: probability of a track to give a hit in a station as a function of the track's transverse momentum p_t

2.2.4 The Endcap Muon System

The endcap muon system, like the barrel muon system, consists of four muon stations. The geometric setup of those muon stations, however, is completely different from the one in the barrel. The muon stations are planar and parallel to the $x - y$ -plane. They are arranged as concentric rings between the iron disks, which return the magnetic flux and shield the chambers from background.

The innermost station (ME1) has three rings, the other three stations (ME2–ME4) have two rings each. The rings consist of individual chambers of trapezoidal shape. To avoid cracks, the chambers overlap in azimuth ϕ and the gaps between adjacent rings are not projective, that is they do not point back to the interaction regions. The number of chambers per ring depends on the station and the ring and varies between 36 and 18, that is individual chambers span 10 or 20 degrees in azimuth ϕ .

Figure 2.6 shows a perspective view of the muon chambers in the endcap region. The same design is mirrored for the endcaps at $z > 0$ and $z < 0$.

The η -coverage of the endcap muon system is $0.9 < |\eta| < 2.4$.

The environment in which the endcap muon chambers have to operate is more demanding than the barrel environment. Particle rates, both from muons and from various background, are much higher in the endcap than in the barrel.¹ The stray magnetic field in the gaps between the flux return iron yokes is considerable. Cathode strip chambers (CSCs) have been chosen as detection device for the endcap muon chambers, because they provide the fast response time and fine segmentation required by the high rate environment in the endcap region.

A cathode strip chamber is a multiwire proportional chamber in which one cathode plane is segmented into strips running perpendicular to the wires.

In the CMS endcap muon system each chamber consists of six layers of wires sandwiched between cathode panels. The wires run tangentially and measure radial position. The strips in the cathode planes run radially, measuring the azimuth ϕ . The six layers provide robust local pattern recognition and facilitate the rejection of neutral backgrounds. Moreover, the presence of several layers allows to measure not only position, but also crossing angle.

¹Rates, both from muons and various backgrounds, are discussed in more detail in chapter 4.

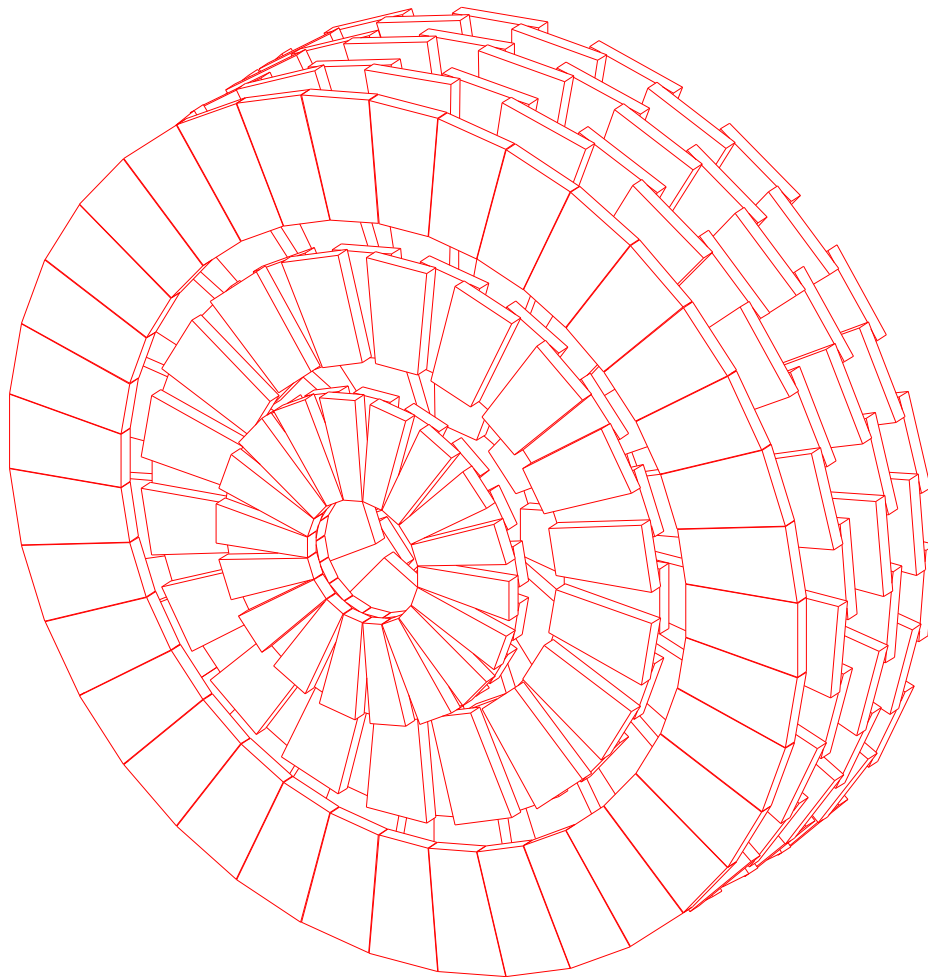


Figure 2.6: Perspective view of the endcap muon detector. The innermost muon station (ME1) with its three rings is in front.

2.3 Trigger

This section presents the CMS trigger, of which the first level muon trigger is a component. It sets out with a general introduction to triggering, and then discusses concepts employed in triggering. It continues with a description of the CMS trigger with emphasis on the first level trigger. A general introduction to the CMS muon trigger concludes this section and sets the stage for the following chapter, which gives a comprehensive specification of the first level muon trigger based on drift tubes and cathode strip chambers.

2.3.1 Triggering Concepts

This subsection states the motivation for building a trigger and introduces general concepts employed in triggering. General introductions to triggering at the Large Hadron Collider LHC can be found in references [46, 12, 22, 47].

High-energy physics at the Large Hadron Collider is essentially devoted to the search for rare phenomena in an overwhelming background of uninteresting interactions. The number of interesting events is small, because they have low cross sections and branching ratios. This means that one needs a selection process to separate the potentially interesting bunch crossings from those that contain no events of interest. In theory, one could write all data to a mass storage device and perform the selection of interesting events off-line. However, the amount of data to be recorded would be enormous. A few numbers from the case of the CMS experiment will serve to illustrate this: Proton bunches from the counter-rotating beams collide in the center of the CMS detector every 25 ns (the bunch crossing interval). On average, about 20 inelastic interactions take place in one bunch crossing. This yields an event rate of up to 10^9 events per second.

In each of those interactions, several particles are created and interact with the detector, resulting in measured data. The amount of raw data for one event, the event size, is about 10^6 Byte. Those figures yield a raw data rate of 10^{15} Byte/s. To visualize this number, let's imagine to store the data on floppy disks. One floppy holds about 1 MegaByte, so one would fill 10^9 floppies in a second. A floppy is about 1 mm thick, so the stack of floppies would grow with a rate of 1000 km per second. We see, that storage of all the raw data produced by the detector is out of question. Moreover, even if somehow one managed to store the data, it still would be a major challenge to process all those data.

The solution is to perform a first preselection of events on-line, before data are written to mass storage. The mechanism to perform this selection is called a trigger, because it triggers the readout of the data from the detector

to mass storage. A reasonable event rate for mass storage (usually magnetic tape) is about 100 events per second. This rate, at which data are written to mass storage, is called the data logging rate. The on-line selection has to reduce the event rate from 10^9 to the data logging rate of 10^2 events per second. The ratio between the interaction rate and the data logging rate is called the reduction factor of the trigger, with the numbers given it evaluates to 10^7 .

To summarize, a trigger is a fast on-line filter that should activate the read-out only for bunch crossings producing interesting events and thus suppresses background events. It processes data generated by the detectors after each bunch crossing and decides whether to accept the bunch crossing and write data to mass storage or to reject that bunch crossing and discard the data. It should be pointed out that bunch crossings discarded by the trigger are lost forever. The trigger should be able to efficiently select potentially interesting events while maintaining sufficient discrimination power against unwanted background events.

The filtering is usually done in several stages, called trigger levels. The idea is to perform stepwise rate reduction until the rate is so low that the data can be written to mass storage. The trigger levels have successively longer processing times. Each level has a lower input rate, uses more data from the detector, employs more sophisticated algorithms and thus takes more time for its decision than the level preceding it. Higher level triggers are finer filters than lower levels.

Some terminology is required for the following discussion. The time a trigger takes for its accept/reject decision is called its latency. Triggers can have a constant latency, meaning that the latency does not depend on the complexity of the event under processing; such a trigger is called synchronous. If the trigger cannot accept data from the bunch crossing following an accepted bunch crossing, it is said to have dead-time. Otherwise it is called dead-time free.

At the Large Hadron Collider the size of a detector is large compared to the distance between the circulating proton bunches. That is to say, that while one bunch crossing takes place, the particles from the previous crossings are still moving in the detector. Particles from different bunch-crossings exist simultaneously in the detector. Detector response times are even much longer than the bunch crossing interval. This fact makes bunch crossing identification, determining which bunch crossing a measured signal belongs to, a very challenging task.

To identify the bunch crossing, the detector either has to have an excellent intrinsic time resolution, this is the case for the dedicated muon trigger detector based on resistive plate chambers, which has a time reso-

lution better than 2 ns. Or the detector has to have a low occupancy such that the correlation of signals from several channels allows assignment of the bunch crossing, e.g. using the mean-timer technique based on drift cells for the barrel muon chambers².

An important technique employed by the first level trigger is pipelining. The motivation is the following: Bunch crossings occur every 25 ns. That means that every 25 ns the trigger accepts input data and every 25 ns it has to issue a decision on whether to pass this crossing on to the next trigger level. Does that mean that there are only 25 ns available for reaching its decision? That would be a very severe restriction on possible algorithms. Fortunately, the answer to that question is no. The trigger's processing time can be longer than the bunch crossing interval.

To this end, the algorithm has to be divided into stages, each stage may take at most 25 ns (1 bunch crossing interval). The data move from stage to stage in lockstep with the 25 ns clock. If one component takes more than 25 ns for its processing, it has to be split up into separate pipeline stages. The stages are connected by intermediate buffer registers. This technique is called pipelining, because the data 'flow' from stage to stage like in a pipe.

Pipelining has been used for the first time by the two HERA experiments ZEUS [54] and H1 [20].

2.3.2 CMS Trigger - General

This section summarizes the parameters relevant for the CMS trigger and data acquisition and discusses the requirements and framework of the first level trigger.

The following table lists the fundamental parameters relevant for the CMS trigger:

bunch crossing (BX) frequency	40 MHz
events/BX	20
event rate	10^9 Hz
data logging rate	100 Hz
reduction factor	10^7
event size	10^6 Byte

The next table presents the basic parameters of the CMS data acquisition system:

²This technique is described in section 3.1.1.

Detector	# Channels	Occupancy (%)	Event size (kByte)
Pixel	80 000 000	0.01	100
Inner Tracker	16 000 000	3.0	700
Preshower	512 000	10.0	50
Calorimeters	125 000	5.0	50
Muons	1 000 000	0.1	10

The first level trigger determines if the event should be discarded right away or be preserved for further processing by the second level trigger.

The CMS first level trigger is synchronous, that means that it reaches its decision after a fixed time (trigger latency). The first-level trigger latency will be much longer than the bunch crossing interval of 25 ns. During processing of the first-level trigger, data from all detector channels have to be buffered in a pipeline (analogue or digital) until the first level trigger's decision is received. If the first level trigger decides to accept the bunch crossing, all the data are read out and used by higher level triggers to refine the decision.

Due to the high number of channels (about 10^8), the first level trigger latency should be kept to a minimum in order to keep the cost for the pipeline low.

CMS has decided to restrict the first level trigger latency to 128 bunch crossings ($3.2 \mu\text{s}$). For reasons of ease of access and maintenance, most of the trigger electronics will not be located on the detector, but in the counting room. The drawback of that arrangement is that most of the trigger latency is actually lost to propagation delays in the optical links between detector and counting room, and only a fraction of the total latency is available for processing the trigger algorithm. The time available is too short to use freely programmable devices such as microprocessors or digital signal processors, the first level trigger has to employ custom processors. It must still be flexible enough, however, to accommodate higher than expected backgrounds or modifications to trigger algorithms, should hints for unexpected physics appear. It must be able to cope with hot (noisy) and dead channels, so it should provide the possibility of selectively turning off individual channels.

The latency of the trigger is longer than the bunch crossing interval, so it has to employ a pipelined design. Particle rates in the inner tracker are very high, so track finding in the tracker is too involved for the first level trigger. It receives input only from the muon system and the calorimeters. CMS requires all components of the first level trigger to be dead-time free.

The CMS second level trigger has been designed for a maximum input rate of 100 kHz, so the first level output rate should be designed to be 30 kHz to provide sufficient contingency.

After describing the general characteristics of the first level trigger, let us

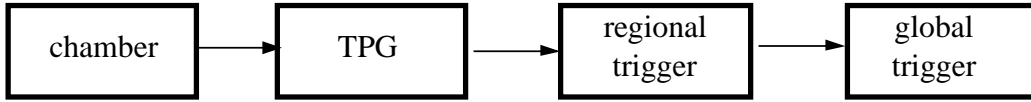


Figure 2.7: The trigger chain: from chamber data to global trigger

now have a look at the trigger chain, the signal path from the chamber level to the decision of the trigger. Figure 2.7 shows that trigger chain.

Only a minimum of trigger electronics should be located on the detector, because the high radiation levels in the experiment's cavern do not permit access to the detector area during machine operation. On the detector only trigger primitive generation (TPG) takes place. In the case of the muon detector the chamber trigger logic generates trigger primitives, e.g. a point or a point plus direction (track segment).

The trigger primitives are transferred via optical links to the regional trigger which is placed in the counting room. There is a regional trigger for each subdetector taking part in the trigger decision, in the case of the first level there is the muon regional trigger and the calorimeter regional trigger.

The global trigger combines information from the regional triggers and makes the final first level accept/reject decision, which initiates the readout of data from the pipelines sitting on the detector.

2.3.3 The Muon Trigger

This section covers the requirements and task of the first level muon trigger of the CMS detector. It serves as introduction to the detailed specification of the trigger component based on drift tubes and cathode strip chambers, which will be given in chapter 3.

The first level muon trigger is based on two independent systems. One consists of dedicated trigger detectors (resistive plate chambers RPCs) and will not be described in this report. The other is based on the muon chambers that are used for offline reconstruction, which are drift tubes (DTBX) in the barrel region (section 2.2.3) and cathode strip chambers (CSC) in the endcap (section 2.2.4). Those detectors are superior to the RPCs in that they have a finer spatial resolution, allowing a better momentum measurement. Moreover they have a multilayer design, reducing their susceptibility to background. Their downsides compared to the RPCs are that their intrinsic time resolution is worse, requiring complicated algorithms to extract the bunch crossing information. Their geometry is not projective, making the track finding more difficult and requiring more data exchange between processors

for subregions of the detector.

Those two independent systems provide

- Redundancy: If one fails, the other one is still available.
- Complementarity: Intelligent combination of the outputs of the sub-systems yields improved performance of the combined system.

The first level muon trigger has the following tasks:

- Muon identification. It should find muons passing through the muon detectors and distinguish them from the various backgrounds.
- Bunch crossing identification. The first level trigger should not only find a muon, but also determine from which bunch crossing it originates.
- Measurement of transverse momentum. Interesting events tend to have a lot of momentum leaving the interaction region in the direction perpendicular to the beam axis. Muons with high transverse momenta p_t are therefore more interesting than those having low momenta. The global first level trigger should be able to apply a p_t -cut, that means to accept events having one or more muons with p_t above a defined threshold. The p_t -measurement should have a fine resolution to be able to tune the rate after the p_t -cut to the level acceptable to the second level trigger.
- Measurement of muon location. This is required by the global trigger to correlate information from the two independent muon triggers with each other and the calorimeter trigger.

The requirements to the first level muon trigger are the following:

- Output rate. As stated above, the total first level output rate should not exceed 30 kHz. This rate includes the calorimeter and the muon system, so about one half of that rate is for muons.
- Flexibility. There is a large uncertainty on the event and particle rate estimates. The detailed physics of the processes that will take place at LHC is not fully known, the magnetic field of the CMS detector might have to be lower than planned due to quenching problems in the superconducting coil, resulting in particles of lower transverse momenta reaching the muon system. The accelerator background rates could be much higher than anticipated, other backgrounds depend strongly on the details of detector geometry that are not yet fully known. So the

trigger must have ‘switches’ that enable it to cope with possibly much higher rates than expected today. Older colleagues have pointed out that all previous hadron collider experiments had to cope with higher rates in their muon systems than they had expected.

The trigger has to be able to accommodate unexpected physics or a shift in physics interests. It must cope with chamber misalignment (the fact that chambers are not in their nominal positions) and noisy or dead detector channels. Moreover, the simulation of the detector that is used today for designing the trigger algorithms will very likely not be an exact description of the detector that is going to be built a couple of years from today. So the trigger will have to be tuned after the first data are available.

- High acceptance. Muons should be found with a high probability.
- High purity of the output sample. While real muons should be found with a high efficiency, backgrounds should be suppressed. A sharp p_t -cut by the global muon trigger requires fine p_t -resolution.
- Bunch crossing assignment. The time resolution of the trigger primitives has to be better than 25 ns. This requires either that the detector itself has a time resolution better than 25 ns or that the occupancy is sufficiently low that the bunch crossing can be extracted from the correlation of several channels.
- Latency. The total first level latency is 3.2 μ s. This includes cable propagation delays and the global first level trigger, so the time actually available for the first level muon trigger is only a fraction of that.
- Deadtime-free. CMS requires the first level trigger to have no dead time.
- Triggering on muons with low transverse momentum p_t . The trigger algorithms should have a high acceptance for low p_t muons. The lower bound on the p_t of detectable muons should be determined only by the range of muons due to bending in the magnetic field and energy loss in the material in front of the muon stations. The trigger algorithm itself must not introduce a p_t -cutoff. This requirement is motivated by low luminosity physics, e.g. CP-violation in the B -system ($B \rightarrow \mu X$).
- Full geometric coverage as defined by the muon system itself.

- Technology. To be on the safe side, it is required that any design can be implemented employing today's technology. One should not throw dice and speculate on technological progress.

The most important figure of merit for a muon trigger is the set of efficiency curves, which show the probability for a muon to be accepted for a given p_t -threshold as a function of the muon's transverse momentum p_t . Another important quantity is the purity of the resulting sample: How many of the found muons are really muons and not background?

Chapter 3

Specification

This chapter gives a full specification of the first level regional muon trigger that is based on drift tubes and cathode strip chambers. The trigger processor receives its input from the chamber trigger logic and provides output to the global muon trigger, which combines the information received from the device described here with the data received from the RPC-based regional muon trigger [6]. This chapter first defines the input quantities received from the chamber trigger logic, then states the task of the trigger processor and concludes by defining the output quantities sent from the regional muon trigger to the global muon trigger.

3.1 Input

The regional muon trigger receives input from two sources: In the barrel there are drift tubes with bunch crossing identification (DTBX), in the endcap there are cathode strip chambers (CSCs). Those chambers are equipped with chamber trigger logic, which performs local pattern recognition and generates trigger primitives. Fig 2.7 shows the trigger chain of the first level trigger all the way from the chamber trigger logic to the global trigger. The chamber trigger logic acts as trigger primitive generator (TPG). This section discusses the interface between TPG and the regional trigger, first for the DTBX in the barrel, then for the CSCs in the endcap region.

Some general remarks about input quantities are appropriate at this place. The first remark concerns their resolution. The resolution of an input quantity is a tradeoff between what can be delivered by the TPG and what is desired by the regional trigger. Having a finer resolution can of course improve the performance, but it comes at the price of higher hardware expense.

The second remark concerns the representation of input quantities. Some input quantities are used only as index into a look-up table, that is they are presented as address to a memory. In this case it does not matter whether the representation of the quantity is a linear function of the quantity, that is the quantity's encoding can be non-linear. In other cases, however, an input quantity may have to be subtracted from another quantity, in this case the encoding should be linear. In the following discussion both types of encoding will be encountered.

It should be pointed out that the definition of the inputs was and is not a 'datum' in the sense that it is fixed and cannot be influenced. There is an interaction between the requirements of the regional trigger and the requirements and capabilities of the trigger primitive generation, and the definition of the inputs is still evolving.

3.1.1 Barrel

The barrel muon system consists of drift chambers described in section 2.2.3. Drift chambers determine the particle position by measuring a drift time: The incident particle creates electrons and positive ions in the detector gas. The created electrons drift from the point of their creation to the chamber's sense wire, the drift time depends on the distance they have to drift. However, the drift cell only sees a pulse at a given point in time, say T , but it by itself does not know when the particle crossed the chamber (this point in time is usually called the T_0), so it cannot determine the drift time $t = T - T_0$. The way of determining T_0 is to either couple the drift chamber with a detector that has a fine time resolution and thus measures T_0 directly, or to build redundancy into the drift chambers so that they can determine t_0 from their own signals. The latter is the approach taken by the CMS barrel drift chambers. The maximum drift time in the drift tubes is about 400 ns, 16 times the bunch crossing interval. For that reason, extracting the bunch crossing information from the pulses measured on the sense wires is not a straightforward task. The chamber trigger logic employs a mean-timing technique to measure T_0 and identify the bunch crossing from which the particle originates. This technique will be explained using the simplified geometry shown in figure 3.1. The figure shows a track passing through two layers of drift cells at perpendicular incidence. The two layers of drift cells are staggered by half a cell width.

Then the following relationship holds:

$$d_1 + d_2 = D$$

where d_1 (d_2) is the distance between the track and the sense wire of the first

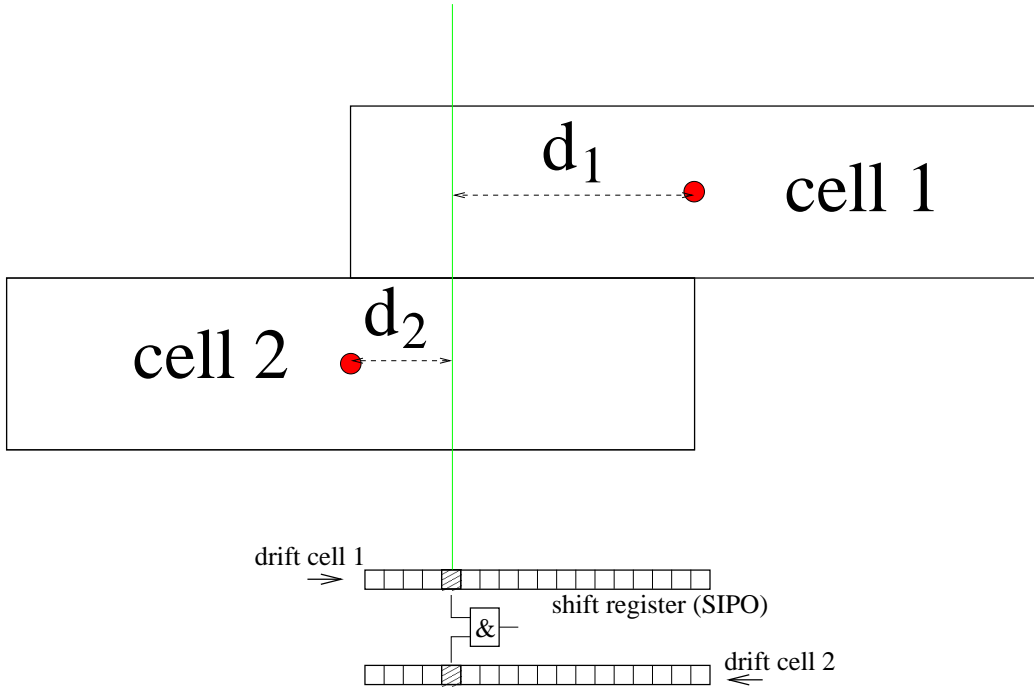


Figure 3.1: Principle of the mean-timer for a track with perpendicular incidence

(second) cell respectively, and D is the spacing between adjacent sense wires, which equals the maximum drift distance of 2 cm.

If the relationship between distance and drift time is linear, it follows that

$$t_1 + t_2 = t_{max}$$

where t_1 (t_2) is the drift time in the first (second) cell respectively, and t_{max} is the maximum drift time of 400 ns. Since $t_i = T_i - T_0$, $i = 1, 2$, where T_i is the point in time where the sense wire of cell i determines its pulse, it is possible to extract T_0 from T_1 and T_2 .

The hardware implementation of this *Bunch- and Track-Identifier* BTI ([14, 28, 27]) employs a shift register (SIPO serial in, parallel out) clocked with the bunch crossing frequency or a multiple. After the maximum drift time of 400 ns there is a coincidence of register cells, which can be detected by the AND-circuit shown in the figure.

For this algorithm to work, a linear distance-drift time relationship is important. This in turn requires a drift velocity that is constant over the cell. The electric field in the cell has to be carefully shaped to ensure that. The distance-drift time relationship is sensitive to magnetic fields. In most of the barrel region, the magnetic field is confined to the iron yoke, but in some

regions at the barrel/endcap interface stray fields reach into the chamber and adversely affect its performance.

The algorithm, as described up to now, works only for perpendicular incidence of the particle. However, if it is modified to include data from at least three drift tube layers, it works for inclined tracks up to a crossing angle of about 45 degrees and measures both position and crossing angle. As mentioned in section 2.2.3, each superlayer consists of four layers of drift cells, so there is redundancy built into the system. A track in a superlayer can be found as an alignment in three or all four of the layers, so the system is able to cope with a single inefficient layer. An alignment of three superlayers is called a low level trigger (L), an alignment of all four superlayers is called a high level trigger (H).

This local pattern recognition operates in all three superlayers of each muon chamber. Two of those superlayers measure the position in the bending plane. The data from these two superlayers are combined by the *Track Correlator*, which checks whether track stubs in the two superlayers line up. Those two superlayers are separated by a distance of about 20 cm, allowing a measurement of the crossing angle that is more precise than the one obtained from a single superlayer. The single superlayer has a lever arm of only 3 cm compared to the 20 cm for the combination of the two superlayers.

To summarize, the local chamber trigger logic generates trigger primitives, which will be called track segments from now on. A track segment comprises the following information: A position at which the track crossed the chamber and the angle under which the track crossed the chamber. In addition, it outputs quality information, which indicates how many of the layers and superlayers contributed to the trigger primitive.

Let us now take a more detailed look at those quantities.

First, I shall discuss the position measurement. The best possible resolution that can be delivered by the BTI is 0.625 mm. The drift velocity is $50 \mu\text{m}/\text{ns}$, and the shift register is clocked with 80 MHz, twice the bunch crossing frequency, yielding a clock cycle of 12.5 ns. The position can thus be resolved with $50 \mu\text{m}/\text{ns} \times 12.5 \text{ ns}$, giving a step size of 0.625 mm.

The resolution to be actually used in the design is a tradeoff between performance, in particular momentum resolution, on the one hand and the hardware expense for transferring and processing the higher number of bits required for fine resolution on the other hand. To determine the required resolution, I made a simulation assuming different position resolutions and determining the p_t -resolution in dependence on position resolution. In those simulations, I employed two algorithms for determining transverse momentum. The first algorithm determines transverse momentum p_t from the bend angle computed from the difference of azimuthal positions in stations 1 and

2. This algorithm is similar to the one employed in the actual design of the regional trigger.

Figure 3.2 shows the p_t -resolution as a function of p_t for various values of position resolution.

The second algorithm for p_t -measurement uses a full track fit as it is employed in off-line event reconstruction. A track fit is an iterative procedure that uses matrix multiplications and is clearly not an option for use in a first level trigger, given the time constraints specified in section 3.4.1. However, it gives the best p_t -resolution that can possibly be achieved with the given data, and thus serves as reference to compare how efficiently the actual design makes use of the information provided to it. The result is shown in figure 3.3.

Those two plots show that for a position resolution of 1.25 mm, the track fit does not perform noticeably better than the simple algorithm using just the positions in stations 1 and 2. Moreover, it is obvious that the resolution worsens dramatically with increasing p_t at a position resolution of 2.5 mm or above. I thus decided that 1.25 mm would be an appropriate position resolution.

It should be noted already here that the quantity I really want as ‘position’ is not the linear position relative to the chamber, but rather the azimuthal angular position with respect to the axis of the sector to which the chamber is assigned. See figure 3.7 for a definition of the latter quantity, denoted $\Phi_{position}$ in that figure. There are several reasons for that preference. First of all, the azimuthal position is the natural quantity for determining transverse momentum p_t , as will be explained in section 7.2.

Secondly, there is a problem of reference planes: If the track is found only in one of the two superlayers, the reference plane for the position measurement is the plane of that superlayer. If the track is found in both superlayers and track segments from the two superlayers align, the reference plane is the plane in the center between the two superlayers. So there is a total of three reference planes, either of the two superlayers or the center of the chamber. For the angular position Φ , that does not really matter: Position resolution is most critical at high momenta, but for a track of infinite momentum Φ is the same in all three reference planes. If the linear position were used, the regional trigger processor would have to take into account not only the measured position, but also its reference plane, making the design more complex and increasing hardware expense. The third argument in favour of transmitting the azimuthal and not the linear position is chamber alignment: The muon chambers will not be in their nominal positions. So the conversion from linear position to azimuthal position has to take that into account. It is more natural to perform that alignment in the chamber trigger logic because the people working on the chambers are also

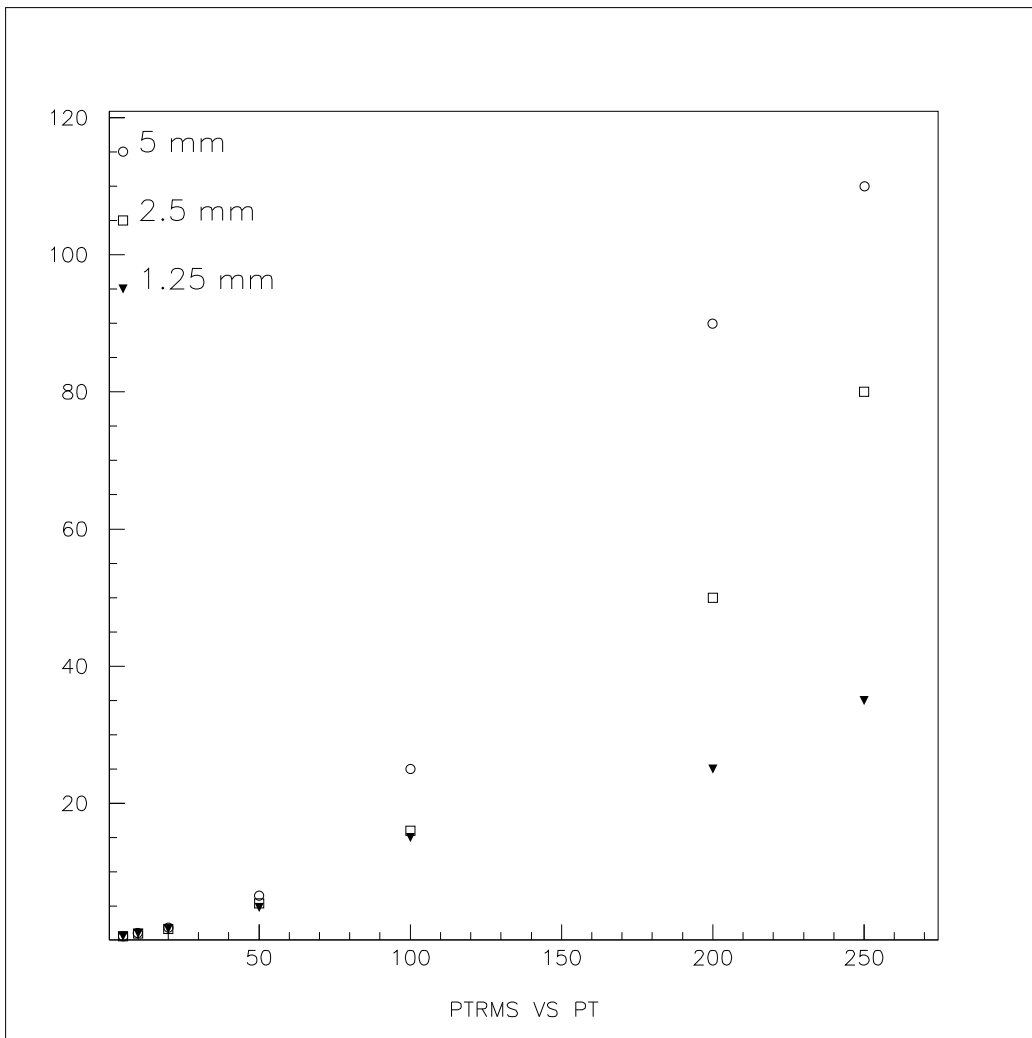


Figure 3.2: p_t -resolution using the difference between the azimuthal hit coordinates in station 1 and station 2 as a function of the track's transverse momentum p_t for several values of the chamber's position resolution; momentum is given in GeV/c.

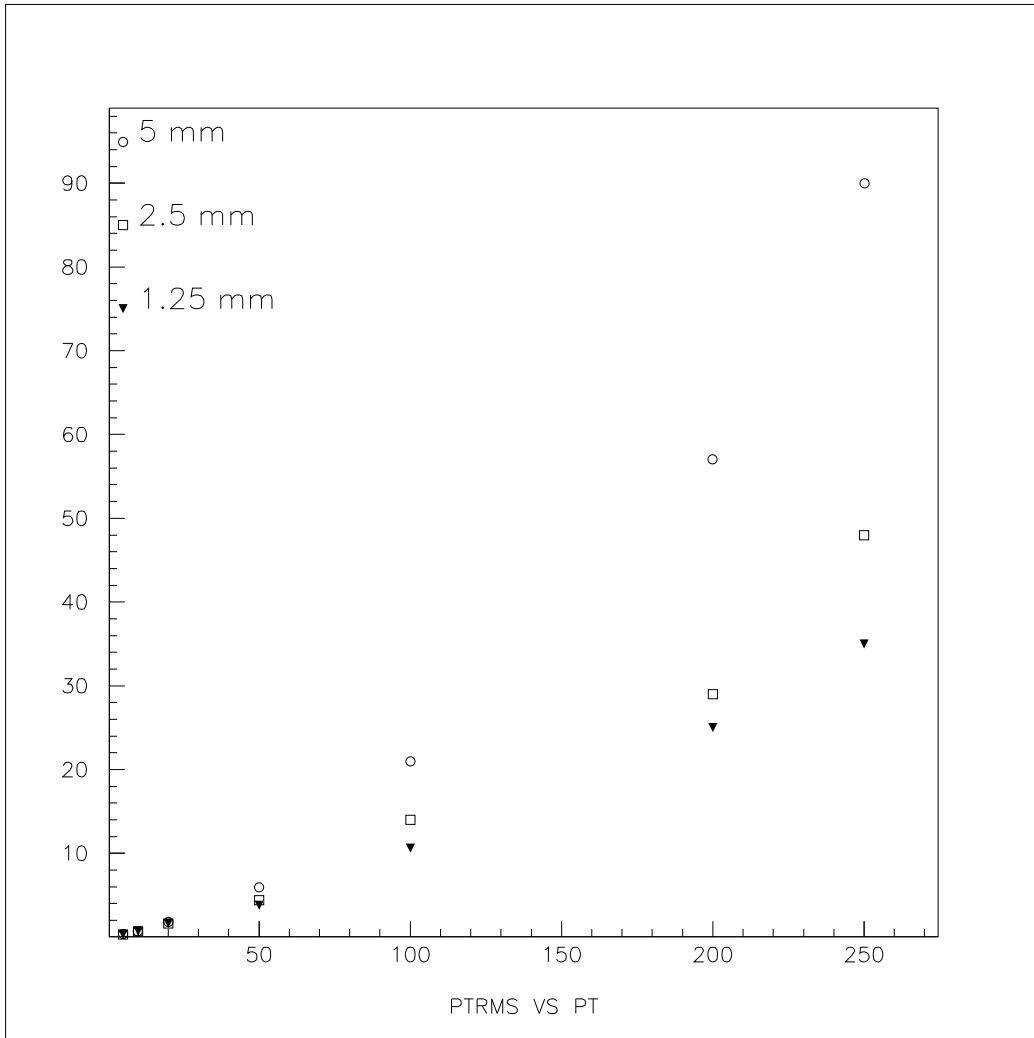


Figure 3.3: p_t -resolution using a track fit as a function of the track's transverse momentum p_t for several values of the chamber's position resolution; momentum is given in GeV/c.

the experts on alignment of their chambers. Finally, the outer chambers are wider than the inner chambers. So, if one used the same resolution in linear position, one would need a wider data word for the position in the outer chambers. Resolution of linear position in the outer chambers, however, is less important than in the inner chambers, so that would be a waste of bandwidth. Transmitting the azimuthal positions in a data word of fixed width for all stations, automatically yields a coarser linear resolution in the outer chambers, while providing an approximately constant resolution in the physically relevant quantity.

How many bits are required to encode the desired position resolution? Answering this question requires a prior discussion of the logical segmentation of the muon detector along azimuth ϕ . Each chamber in the muon system is assigned to a logical sector. Since neighboring chambers overlap and are staggered, those logical sectors overlap, as shown in figure 3.4. The azimuthal angle covered by one logical sector is 0.4 rad (23°). This number includes a safety margin for chamber misalignment. Using the distance between the chamber and the origin and the range mentioned above one can compute the number of bits required. To have a linear position resolution of 1.25 mm in station 2 and 2.5 mm in station 4 requires coding the position in 12 bits.

So far I have discussed the nominal resolution of the position. Due to effects such as the presence of δ -electrons created by the muon in the tube walls, the actual resolution can be worse than that. Figure 3.5 shows the measurement error for the linear position in dependence on the quality of the track segment: H stands for a high level trigger in one of the superlayers, L for a low level trigger, so the combination HL means that there was a high-level trigger in one of the superlayers and a low-level trigger in the other superlayer. For HH track segments the resolution found by simulation corresponds approximately to the nominal resolution of 1.25 mm. The RMS of the distribution shown in the plot is 0.46 mm, from the nominal binning of 1.25 mm one expects an RMS of $1.25 \text{ mm}/\sqrt{12} = 0.36 \text{ mm}$. For track segments of lower quality, the resolution can be considerably worse than expected.

The final question is how the position data should be encoded. The trigger algorithm relies on subtracting positions both for track finding and p_t -assignment (section 7). Therefore the encoding should be linear. Moreover, the azimuthal position is defined with respect to the sector axis, so it is a signed quantity, hence it should be encoded in two's complement.

In addition to a track's position, the mean-timer algorithm implemented in the BTI (Bunch- and Track-Identifier) measures the track's crossing angle. Here again, a question arises on which quantity should actually be output: The crossing angle of the track, that is the angle of the track direction with

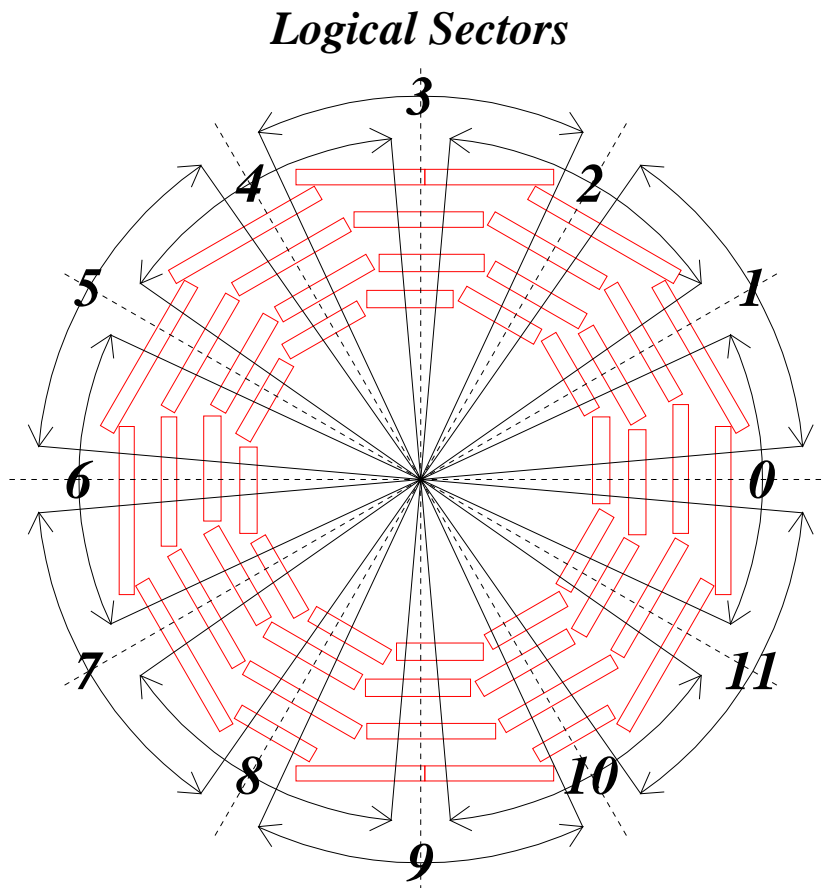


Figure 3.4: Segmentation of the barrel muon detectors into logical sectors

Error on x for better TS

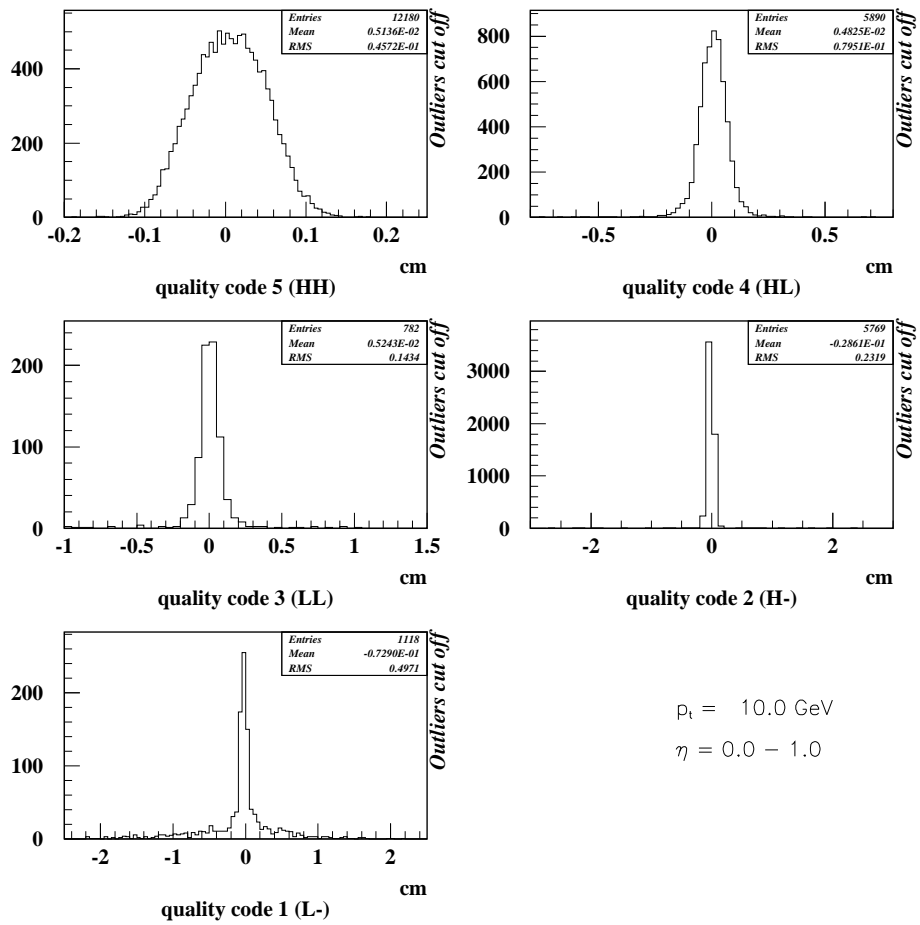


Figure 3.5: Measurement error on linear position for the better track segment (TS) in a chamber

respect to the chamber normal, or the bend angle, that is the angle between the track direction and a radius line passing from the origin through the point where the track passed the chamber. The bend angle is illustrated in figure 3.7, where it is denoted as Φ_{bend} . Again, the crossing angle is the quantity directly determined by the trigger primitive generation, the bend angle is the natural quantity for track finding and p_t -assignment.

The measurement range of the crossing angle is about $\pm 45^\circ$. This limits the acceptance at low transverse momentum p_t and thus introduces a p_t -cutoff. Moreover, due to the asymmetric arrangement of the chambers with respect to their sector axis, muons of different charge sign are affected in a different way, resulting in a muon sign bias. This means that, depending on the geometric configuration finally chosen, μ^+ might have a higher probability to be found by the BTI than μ^- .

The BTI can output 401 possible values in the angular acceptance range, those values are equidistant in the tangent of the crossing angle. This means that there is a very fine nominal resolution (step size 0.1°) at large crossing angles. At these large crossing angles, however, p_t is low and therefore multiple scattering and energy loss fluctuations dominate, the angular resolution hence is not critical. Therefore one can compress the data without losing in performance by encoding the angle data in such a way that the step size at high crossing angles is increased. The angle value is only used as address in look-up tables, therefore a non-linear encoding can be chosen.

Figure 3.6 shows the measurement error for crossing angle in dependence on the quality of the track segment. The actual angle resolution strongly depends on whether the track segment includes both superlayers of the chamber or only one. If it includes both superlayers, the angle can be determined using the 20 cm distance between the two superlayers as lever arm, yielding a resolution as good as $1.25 \text{ mm}/20 \text{ cm} \approx 6 \text{ mrad}$ at normal incidence. If, however, the track segment includes only one superlayer, the angle measurement can be made only using the short lever arm given by the distance between the outermost layers of that superlayer, which is 3 cm. This effect can be clearly seen in the resolution plots.

The third quantity output for each track segment is the segment's quality. It indicates how many layers and superlayers contributed to the measurement. The possible values are, in order of decreasing quality: HH, HL, LL, H-, L-, where the notation xy means that one superlayer gave a level x and the other superlayer gave a level y . Each superlayer can give an H: high-level trigger (all four layers of that superlayer aligned), an L: low-level trigger (three out of the four layers aligned) or -: nothing at all.

What the quality tells us about the track segment is first, how confident we can be that it is a real track and not just a ghost. Secondly, it indicates

Error on angle for better TS

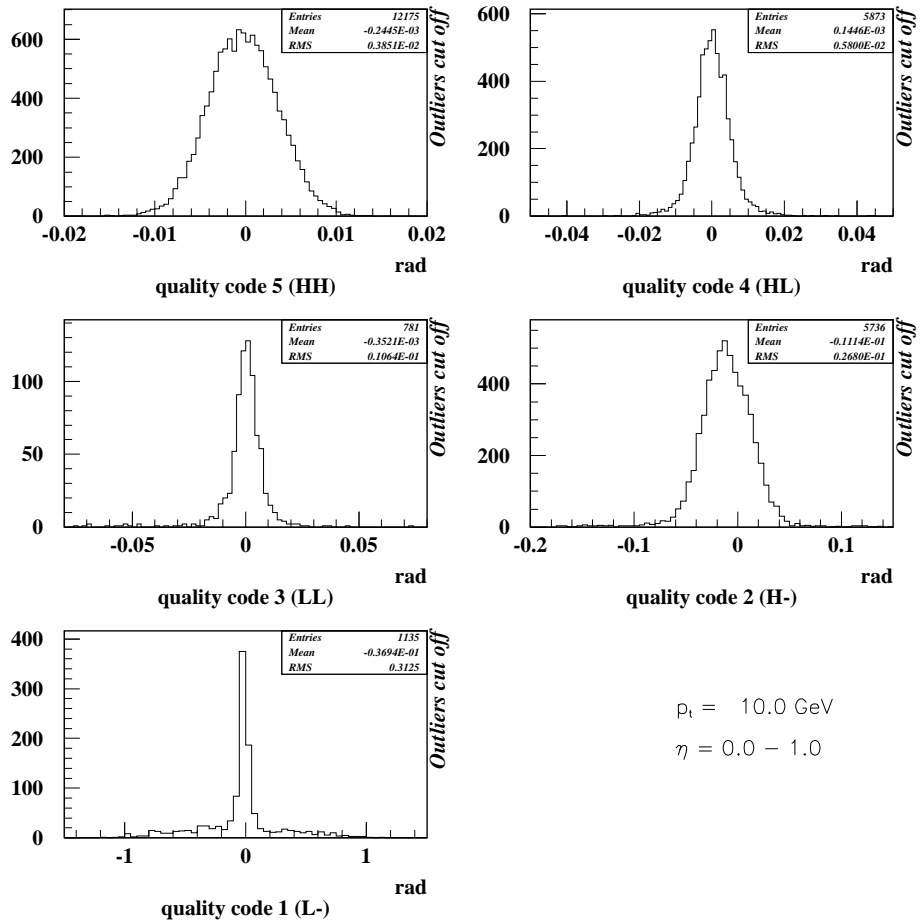


Figure 3.6: Measurement error on crossing angle

which resolution to expect.

The previous paragraphs have defined all the quantities transferred for each track segment found by the chamber trigger logic. The next parameter that had to be determined was the number of track segments that may be output by each chamber.

Here again, a tradeoff has to be made between hardware expense for storing, transferring and processing additional track segments and the possibility that muons are lost due to overcrowding in the chambers. For instance, a muon initiates an electromagnetic shower in the iron in front of a muon chamber and some of the shower particles penetrate the chamber and give track segments. The chamber trigger logic applies some selection criteria and the muon could lose out to the unwanted shower particles in the selection and be pitched overboard.

For the reason mentioned above, it was clear that one track segment per chamber is not sufficient. An estimate of the particle rate per chamber and bunch crossing yields the following result: The muon chambers are about 2.5 m long and between 2 m and 4 m wide, so their area is about 8 m². The particle rate in the barrel is believed to be less than 10 Hz/cm²[13], yielding an average number of 0.02 particles per chamber in each bunch crossing. So it seems reasonable to assume that two track segments per chamber should be sufficient. Detailed simulation of full events has borne out that assumption. However, there is some concern that the innermost muon station MB1 could be exposed to higher than expected punchthrough from the calorimeter. At present, this concern does not appear to justify the additional hardware cost associated with transmitting and processing three or more track segments per chamber in MB1.

The preceding paragraphs can be summarized as follows: The muon chambers in the CMS barrel muon system are equipped with a chamber trigger logic, which generates trigger primitives. Up to now only the trigger primitive generation in the bending plane projection has been discussed. The trigger primitive generated in the bending plane is the track segment, a triple of values:

- Position. Azimuthal angle of the hit relative to the axis of the ϕ -sector to which the chamber is assigned.
- Angle. The angle between the track and the radius vector at the crossing point in the bending plane projection (bend angle).
- Quality. How many of the layers and superlayers in the chamber contributed to the track segment.

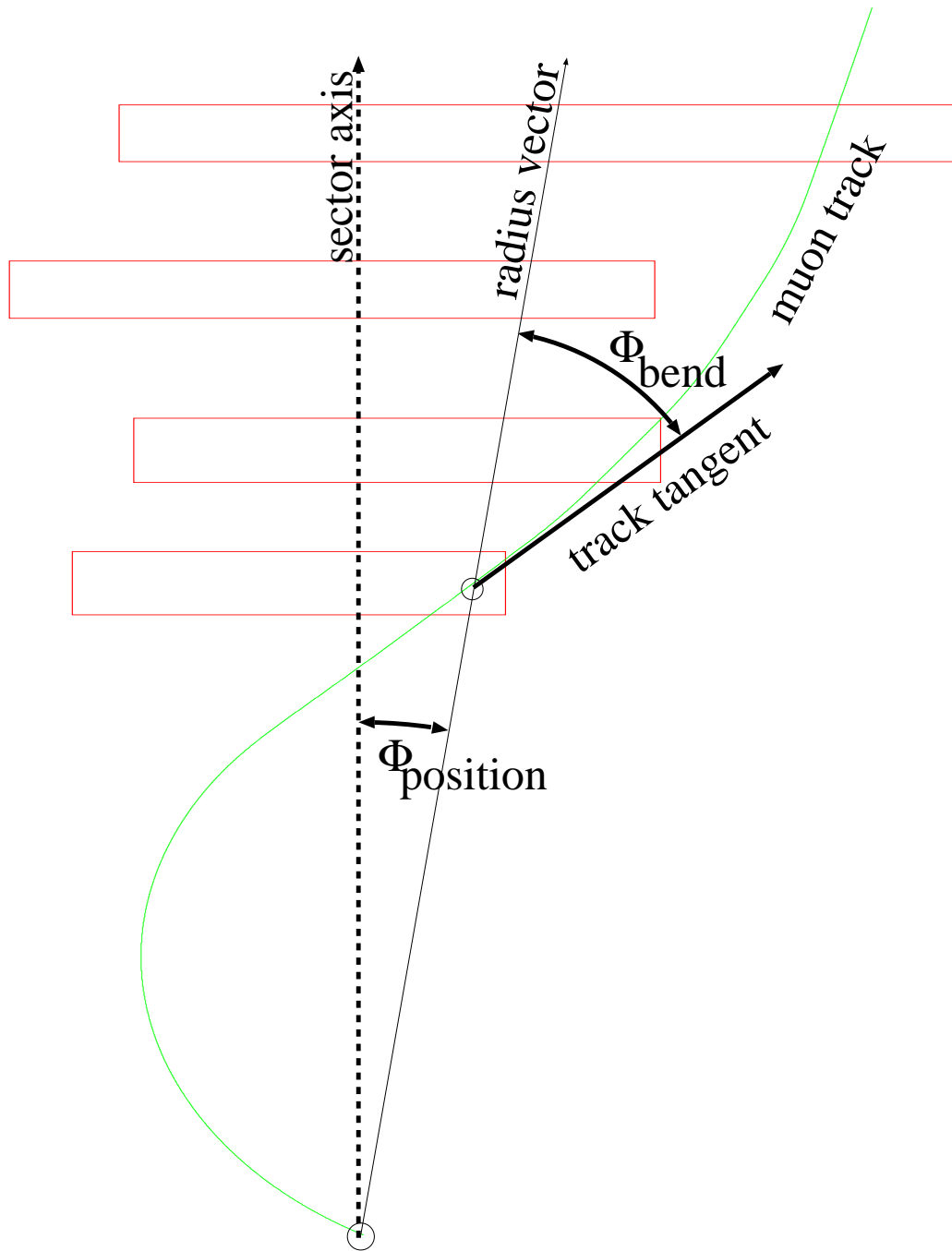


Figure 3.7: Definition of the input quantities position and bend angle

Figure 3.7 shows the definition of the quantities position and angle. The following table gives an overview of the input quantities.

quantity	# of bits	resolution
position	12	1.25 mm – 2.5 mm
bend angle	≤ 9	10 mrad
quality	3	—

The non-bending projection ((z, R) -projection) is based on the middle superlayer with sense wires perpendicular to the z -axis. The *Bunch- and Track-Identifier* works in the same way as in the bending plane projection, but there is no *Track Correlator* because there is only one superlayer for this projection. The crossing angle is not output separately, because it is assumed that all tracks point back to the interaction region, so position and crossing angle are strongly correlated. The position is not needed for p_t -assignment, so fine resolution is not an issue and the length of the chamber along z is divided into 96 bins. Hit data is unencoded, that means the output for a chamber is simply a word of 96 bits, with a bit set meaning that there is a track in the corresponding bin. Moreover there is one quality bit for each bin, indicating whether the *Bunch- and Track-Identifier* found a high-level (H) or a low-level (L) trigger.

Two important figures of merit for the trigger primitive generation are its efficiency and its purity. Efficiency means the probability to find what one wants to find and purity is the probability that what one finds is what one wanted to find.

Figure 3.8 shows the efficiency of trigger primitive generation. The plotted quantity is the probability that a muon track passing the chamber in the active region will generate a trigger primitive at the correct bunch crossing. The efficiency at low transverse momenta is limited by the angular acceptance of the mean-timer algorithm – tracks of low p_t are strongly bent and cross the chamber at a higher crossing angle, hence they are less likely to fall into the angular acceptance range (roughly $\pm 45^\circ$). By contrast, at high momenta the efficiency drops due to secondary particles created by the muon itself.

The purity of trigger primitive generation is not 100 %. Some of the trigger primitives sent to the regional trigger are not associated with a real track passing through the chamber — the trigger primitives found by the chamber trigger logic are contaminated by ‘noise’. Two kinds of noise can be distinguished in this context. Temporal noise means that a track segment is assigned to the wrong bunch crossing. It happens frequently that one track segment is found at the correct bunch crossing, but in addition spurious track segments are found at bunch crossings before or after the correct one.

BTI Efficiency

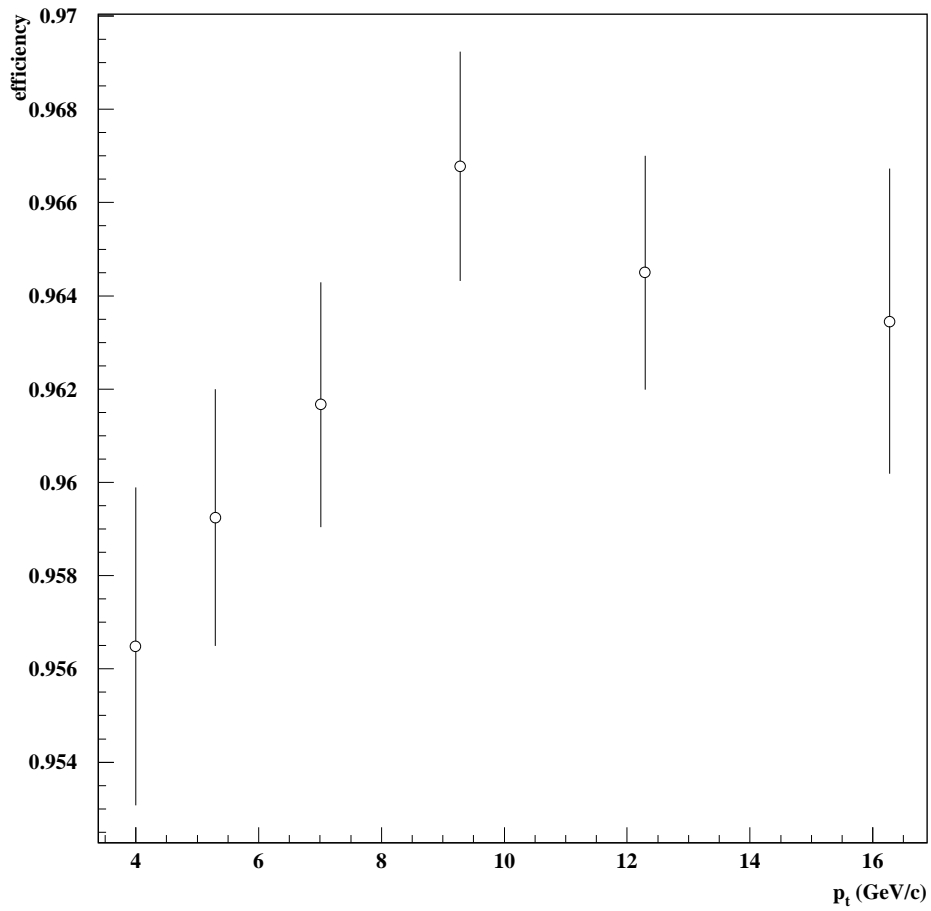


Figure 3.8: Efficiency of trigger primitive generation

The probability that at least one track segment is found at a wrong bunch crossing for a track passing through a single chamber is about 20 %.

The second kind of noise is spatial noise. A track passing through the chamber gives a track segment at the right position and angle, but additional ghost track segments at other positions or angles are produced along with the correct track segment. Figure 3.9 shows the probability that a single muon passing through a chamber will give a second track segment in the same chamber.

One mechanism of ghost generation is due to the left-right ambiguity of drift tubes. Figure 3.10 explains this mechanism. Figure 3.10 shows a real track that passes through the superlayer under orthogonal incidence (dotted line). The mean-timer finds this track. But it also finds a ghost track (dashed line). The mechanism of ghost generation in this case is the following: The mean-timer assumes that cell 2 is missing due to inefficiency and it picks up the mirror hit in cell 4. The result is a ghost track that is found a time Δ before the real track. Ghosts of this kind can be suppressed, provided that the real track is found with all 4 cells. The ghost suppression will cancel all track segments of type L (3 cells) that occur within a certain time window before and after a track segment of type H (4 cells).

There is a tradeoff between efficiency and purity. If one wants to increase the purity, one can do that for example by suppressing track segments of the lowest quality (L-). However, a side effect will be a decrease in efficiency.

3.1.2 Endcap

In the endcap the chamber trigger logic is still in the early conceptual design stage. Therefore, the output quantities are not yet well defined. No simulation is available as of now to assess the performance of trigger primitive generation. The trigger primitives in the endcap have traditionally been called track stubs, here the terms track segment and track stub will be used interchangeably.

As described in section 2.2.4, a cathode strip chamber consists of 6 layers of multiwire proportional chambers, with wires running tangentially and strips on the cathode panels running radially. The chamber trigger logic performs local pattern recognition for strips and wires separately. Both the strip cards and the wire cards require a line-up of hits in at least four out of the six layers in order to form a track stub. The central values of the set of wires (strips) hit determine the position coordinates R (ϕ) respectively; the relative combinations of wires (strips) determine the crossing angles. The bunch crossing is assigned using the arrival time of the earliest hits.

This stage is followed by selection stages, where up to two track stubs in

Probability of 2nd TS in chamber

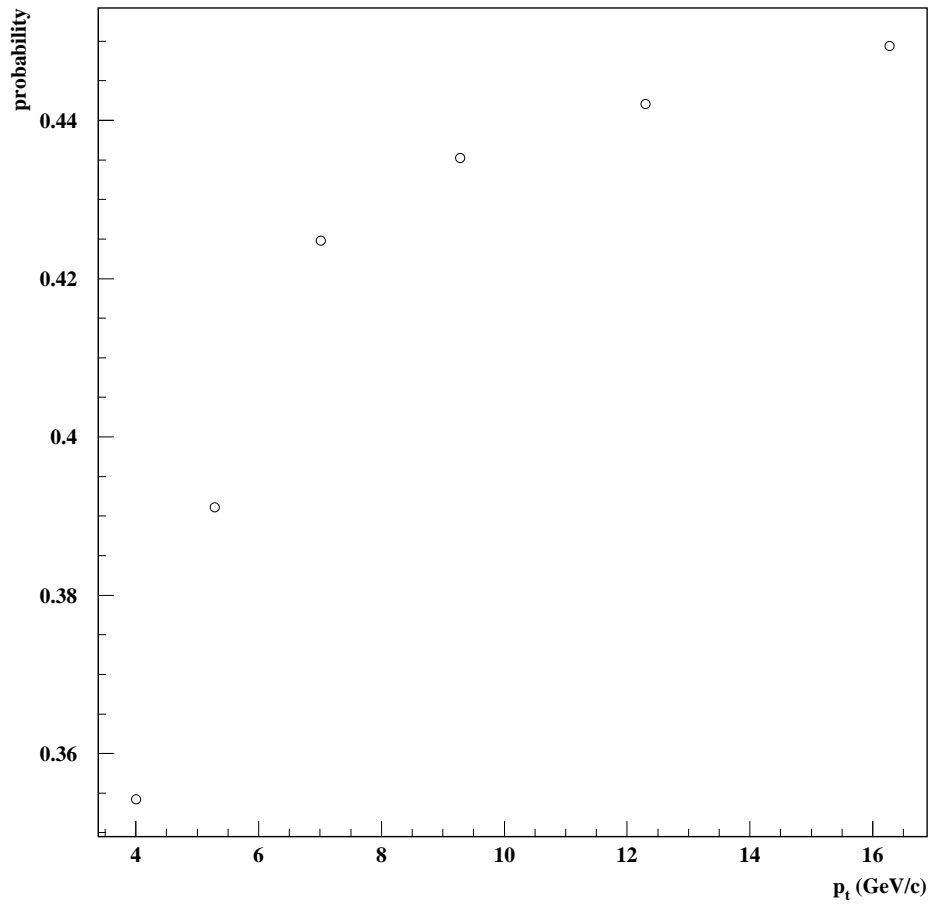


Figure 3.9: Ghost creation probability as a function of muon's transverse momentum p_t

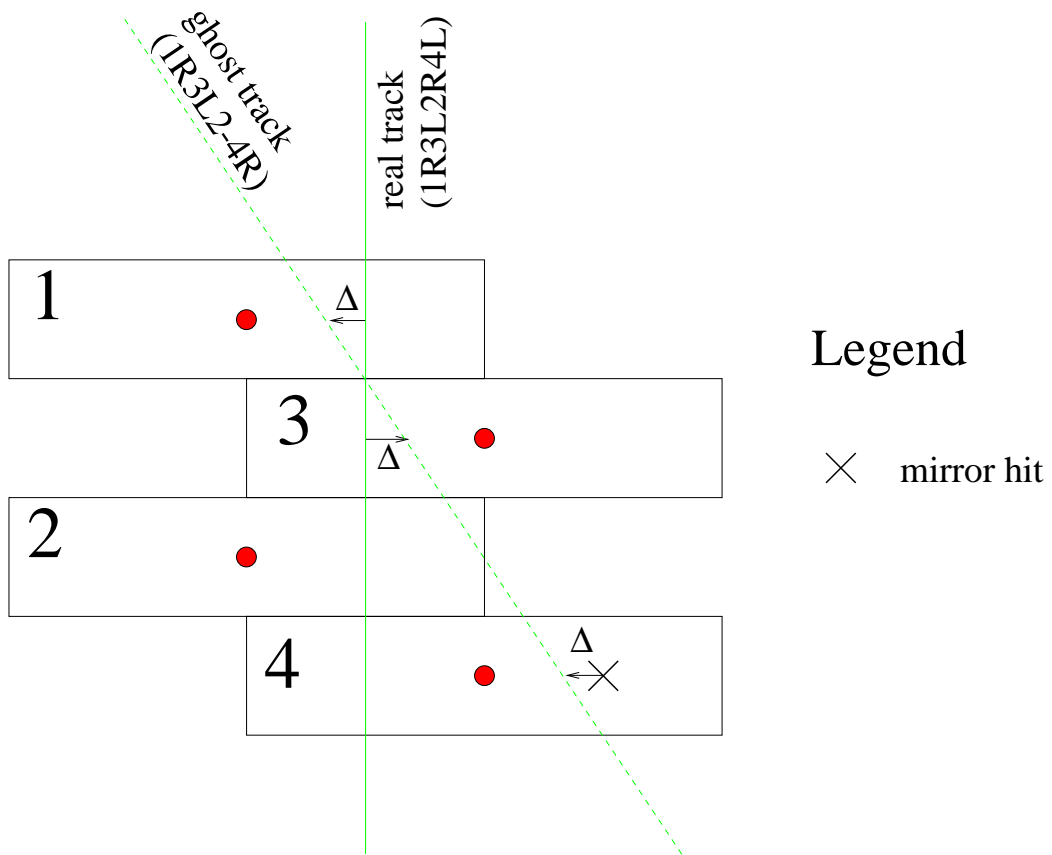


Figure 3.10: Mechanism of ghost generation due to left-right ambiguity in the drift cells; a ghost track is found at a time Δ before the real track

either projection are selected based on the number of layers (4–6) contributing. That is followed by an attempt to match strip and wire information. If only one track passed the chamber and there are no ghosts, there is only one wire track stub and one strip track stub, and matching is straightforward. How to proceed in case of ambiguities is unclear.

In the so-called overlap zone for $0.9 < |\eta| < 1.2$ tracks pass chambers in both the barrel and the endcap chambers. The regional muon trigger should be able to find tracks in that region by combining information from both systems. This task is facilitated, if both systems use similar output data and have a similar segmentation. The physical segmentation of the endcap muon chambers is fixed and is different from the setup in the barrel. While chambers in the barrel cover roughly 30° in azimuth ϕ , those in the endcap cover either 10° or 20° . One way out is to introduce a logical segmentation in the endcap that matches the barrel segmentation by assigning track stubs from a given position in the endcap chamber to the corresponding logical ϕ -sector.

The number of track stubs to be output from each logical sector is again a trade-off between physics performance and hardware expense. The baseline assumption is that three track segments should be output per logical sector if logical sectors are not radially segmented. If each logical ϕ -sector is radially divided into two rings, two track stubs per resulting (ϕ, R) -segment would be sufficient.

The output data from the chamber trigger logic can then be summarized as follows: For the strip track stubs, there will be azimuthal position with respect to the logical segment, a crossing angle and a quality, indicating how many layers (4–6) contributed.

The crossing angle measured by the strips is :

$$\alpha_s := \frac{d\Phi}{dz}$$

Using the following expression for the tangent to the track

$$\vec{t}_p = \begin{pmatrix} \sin \theta_p \cos \phi_p \\ \sin \theta_p \sin \phi_p \\ \cos \theta_p \end{pmatrix}$$

yields

$$\alpha_s = \frac{d\Phi}{dz} = \frac{1}{R} \tan \theta_p \sin \phi_b$$

where R denotes the distance from the beam axis, $R = \sqrt{x^2 + y^2}$, and ϕ_b denotes the bend angle, $\phi_b := \phi_p - \phi$. As will be shown in section 7.2, this quantity can be used directly for p_t -assignment.

For the wire track stubs, there will be no crossing angle information, because tracks are required to point back to the vertex in the (z, R) -projection, hence the crossing angle follows from the position R . The quality information has the same format as for the wire track stub. Moreover, if strip and wire stubs can be matched, that will be indicated. For the simulations presented in this report, only data from the strips has been used. I made some assumptions about the resolution based on a preliminary version of a simulation software [51] and conversations with the people involved in the design of the trigger primitive generator. The resolution for azimuthal position is estimated at 1.4 mrad, the resolution for the slope measured by strips at 30 mrad and the trigger primitive generation efficiency at 97 %.

3.2 Task of the Processor

This section covers the task of the regional muon trigger processor. The regional trigger receives input data from the trigger primitive generator located on the detector, performs some operations on those data and sends the output on to the global muon trigger. The trigger processor's task is the mapping it performs from input data to output data.

The processing of the regional trigger can be logically divided into three stages. The first stage consists of track finding, the second stage of measuring properties of tracks found in the first stage, and the third stage sorts and selects to pass on only the most 'interesting' tracks.

The individual track segments provided by the chamber trigger logic are local in that they comprise data from a very limited region in space. Track finding is the process of joining those local track segments to complete tracks. Before defining an algorithm for track finding, one has to define track finding criteria. Under which conditions does a set of track segments form a valid track? Are different tracks allowed to share track segments? In other words, under which circumstances are different tracks compatible with each other? Those are the questions answered by the specification of track finding criteria. Section 7.1 will state the rationale behind choosing the track finding criteria for the regional muon trigger. For the moment, I shall just list them: A track should be recognized, if it gave a track segment in at least two of the four muon stations. A track should point back to the interaction region. One track segment should not belong to more than one track.

The next stage after finding tracks, is measuring the properties of those tracks. The most important of those properties is the track's transverse momentum, including the charge sign. The next property is the track's direction: The track's pseudo-rapidity η and azimuth ϕ . Finally, each track

is assigned a track quality. Those quantities will be defined in more detail in the following section on output quantities.

At the first level trigger, all data sizes are static, only a fixed amount of data can be transferred for each clock cycle from one stage to the next. That means that selection steps are required to restrict the amount of data to the next stage. Selection steps serve to get rid of ghosts, background and artifacts.

Selection criteria can be based on quality and transverse momentum, tracks of high quality should be preferred to low quality tracks and high momenta are preferable over low momenta. After selection, up to four tracks per wheel can be output to the global muon trigger.

It should be stressed that the regional trigger does NOT make a decision on whether to accept or reject a bunch crossing, it only performs operations on the data provided and passes the result on to the next stage. The trigger decision is reached by the global first level trigger[48], based on the information it receives from the regional muon trigger and other trigger components.

3.3 Output Quantities

This section discusses the interface between the regional muon trigger and the global muon trigger. The regional muon trigger accepts input from the chamber trigger logic and forms tracks, then it assigns track properties to the found tracks. These track properties are the data presented to the global muon trigger[49].

The track parameters measured by the regional muon trigger are the transverse momentum p_t , track direction and quality. For the momentum and the track direction the question arises what should be the reference surface for those quantities. The track loses energy and thus momentum on its way through the detector material, hence the momentum at the vertex is higher than the one in the muon system. Track direction is affected by energy loss, multiple Coulomb scattering and bending in the detector's magnetic field. Which reference surface should be chosen depends on what the consumers of that information — global muon trigger and global trigger, possibly higher level triggers — intend to do with it. When I started designing the regional muon trigger, no blueprint for those devices was in existence, so I chose the reference surfaces that I believed to be most useful.

The reference 'surface' for the track's transverse momentum is the vertex. As the size of momentum is mainly used for applying a transverse momentum cut, the reference surface is not really very important.

Direction information consists of the azimuth ϕ and pseudo-rapidity η . Those quantities are used by the global muon trigger to compare tracks found by the two independent regional muon triggers and by the global trigger to compare muon track information with calorimeter information. For that reason I chose the innermost muon station as reference surface, because it is closest to the calorimeter. The hardware expense can be reduced by using not muon station 1, but the innermost station with a track segment belonging to the track as reference surface. If, for example, a track consists of track segments in stations 2 and 3, station 2 could be used as the reference surface. That way one does not have to extrapolate back from that station to station 1. Moreover, a track that does not have a track segment in station 1, must be of high p_t , hence its direction will not change very strongly between station 1 and the reference station. An alternative would be to use the vertex as reference surface — that is relevant if a higher level trigger wants to use the first level trigger information to measure the invariant mass of a muon pair.

Along with track momentum and direction, the regional trigger generates a quality tag for each found track. This quality tag indicates how many and which stations contributed to the track and what were the qualities of the contributing track segments. It tells the receiving trigger stages how confident they can be that the found track is really a muon track and not a ghost created by the trigger primitive generation and/or track finding. Moreover, it indicates the resolution that can be expected from the p_t -measurement: A track that has track segments in stations 1 and 2 will have a much finer momentum resolution than a track with track segments in stations 3 and 4 only.

The following table gives an overview of the output quantities and the number of bits required/desired by the global trigger.

Quantity	Symbol	# of bits
Transverse momentum	p_t	5
Charge sign	q	1
Pseudo-rapidity	η	2
Azimuth	ϕ	8
Quality		to be defined

The regional muon trigger can transfer up to four tracks per z -wheel to the global muon trigger. For each track the wheel is known, so the number of 2 bits for η in the above table refers to a relative pseudo-rapidity with respect to the wheel which the track belongs to.

3.4 Design Issues and Considerations

3.4.1 Requirements

The following paragraphs list requirements on the regional muon trigger that can be derived from the general requirements on the first level trigger (section 2.3.2).

As far as performance is concerned, the trigger ought to have high acceptance down to the lowest possible transverse momenta, and low contamination by ghost tracks.

The maximum latency of the regional muon trigger is 14 bunch crossings ($0.35 \mu\text{s}$). That is all that remains from the total level 1 latency of $3.2 \mu\text{s}$ after deducting cable propagation delays, trigger primitive generation, global muon trigger and global trigger.

The first level trigger is required by CMS to be deadtime-free. The regional muon trigger, as a component of the first level trigger, has to abide by that rule.

An important design issue is flexibility: The trigger must be able to adapt to unexpected effects, such as higher than expected rates. It should have the capability to deal with noisy and dead channels.

The parameters controlling the algorithm are initially based on simulation studies of the detector, however simulation cannot be fully trusted to accurately describe the real detector. During the experiment's startup phase, the parameters have to be updated based on real measured data.

The muon trigger is a critical component of the detector. Any malfunctioning must be detected as quickly as possible, diagnosis and action to remedy problems must be swift. For that reason, testing, monitoring and diagnosing should be planned into the system from the start.

It must be possible to implement the algorithm in hardware employing today's technology.

3.4.2 Particular Challenges

This section describes the challenges posed by the design of the regional muon triggers.

The most striking of the challenges is the severe timing constraint imposed by the latency bound of 14 bunch crossing intervals of only 25 ns each.

The non-projective geometry in the (z, R) -projection results in muons changing wheels during their journey through the muon system. Moreover, the high magnetic field leads to a strong bending of the tracks. Tracks, particularly at low momenta, are likely to change ϕ -sectors in the muon

system. This means that individual sector processors have to communicate with each other and exchange data, posing a serious interconnection problem. Muons should be identified down to lowest possible transverse momenta. At low momenta, however, muons are more strongly affected by multiple scattering and energy loss fluctuations, which make their trajectories less predictable and increase the number of possible combinations of hits to tracks that have to be considered for track finding.

The system is heterogenous, comprising two different detector types (drift tubes and cathode strip chambers) with different behaviour and geometry.

Chapter 4

Muon Signal and Background Rates

4.1 Muon Rates

Muons in the CMS detector's muon system can originate from several sources.

Prompt muons originate from heavy particles that decay close to their creation vertex in the detector's interaction region. At transverse momenta below about 20 GeV/c this contribution is dominated by decays of b - and c -quark hadrons, above 20 GeV/c the primary source are W -decays. Decays of Z -bosons and t -quarks are additional contributions to the prompt muon rate. Figure 4.1 shows rates for single prompt muons.

On average, one per several hundred bunch crossings will produce a prompt muon that can enter the barrel muon system. Due to the high magnetic field of the CMS detector and energy loss in the calorimeters, muons of low transverse momentum p_t cannot reach the muon system. At $p_t = 3.3 \text{ GeV}/c$, muons have a probability of 50 % to reach muon station 2. Further information about prompt muon rates is available in references [24, 16].

In addition, there are *decay muons*, *accelerator muons* and *cosmic muons*. These will be treated in the section on backgrounds.

4.2 Background

We are primarily interested in prompt muons. Any particle that gives a signal in the muon system and is not a prompt muon is considered background. This section gives an overview of the sources of backgrounds and addresses the effects of background on muon detection.

The sources of background are:

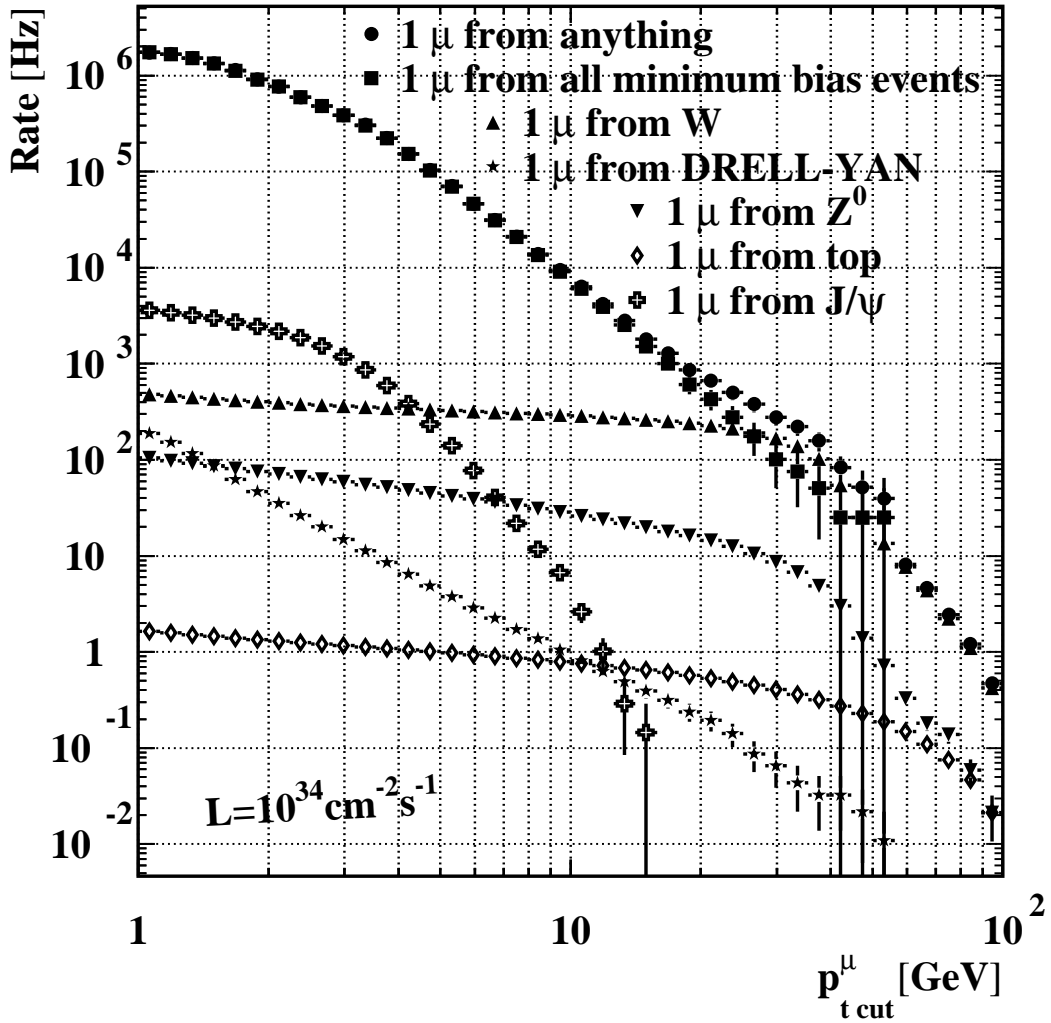


Figure 4.1: Single muon rates[24], where the rate is the rate of events having at least one muon with p_t above the threshold $p_{t \text{ cut}}^\mu$ given by the abscissa.

- Charged hadronic background originating from hadronic showers in the calorimeters and shielding.
 - Punchthrough. Highly energetic hadronic showers are not fully contained in the calorimeter and the shower tails leak into the muon system[15, 57]. If these particles are not energetic enough to pass muon station 1 and reach at least muon station 2, they will not result in tracks.
 - Backsplash from forward calorimeters and beam collimators. Energetic hadronic showers in those components can emit particles at large angles to the direction of the original hadron initiating the shower. These shower particles can reach the endcap muon stations.
- Muon-induced backgrounds.
 - δ -rays are energetic knock-on electrons liberated in a collision between the muon and an atom of the material passed by the muon. Their range is small and the thin walls between individual drift cells or the cathode panels of the CSCs are sufficient to confine them to a single layer. In the case of the drift chambers (DTBX) they can give rise to ghost track segments (section 3.1.1).
 - Muon-induced electromagnetic showers. Muons can interact with matter via the mechanisms of muon bremsstrahlung and pair production. This can touch off an electromagnetic cascade that completely fills the muon chamber with hits and renders its measurement unusable.
- Neutral backgrounds (neutron-induced backgrounds). Neutrons originate from hadronic cascades in detector or accelerator components.

These neutrons can be captured by nuclei, after neutron capture the nuclei deexcite by emitting photons. The neutron capture cross-section is highest for thermal neutrons, but the capture of thermal neutrons can produce photons with energies in the MeV range. Such photons produce electrons via the photo-electric and Compton effect and by pair creation. Because the neutrons have spent a relatively long time being elastically scattered, this background is no longer correlated in time with the bunch crossing.

In a detector medium with high hydrogen content neutrons can give a signal via recoil protons from elastic neutron-proton collisions [35, 25, 26].

This neutral background results in random hits in a single detector layer. The chambers used in the CMS muon system have several layers separated by walls, which these particles rarely penetrate, so this background is suppressed.

- Accelerator muons (tunnel muons) originate from beam losses. Accelerator-related backgrounds are expected to be highest during the first years of LHC operation, but will drop as the performance of the machine improves. Beam losses are caused by interactions between the beam and the residual gas in the beam tube and between off-momentum beam particles and the beam tube. Hadronic and electromagnetic components of these interactions will be suppressed by shielding, but the muon component, produced by π , K and heavy flavor decays, will penetrate the shielding. These muons pass the detector under a small angle to the beam axis, so they will not be seen by the barrel chambers, but they constitute a serious background in the endcap muon chambers. These chambers can reject the accelerator background by applying a cut that requires tracks to point back to the interaction region in the (z, R) -projection. [19]
- Decay muons occur in the decays of hadrons which contain light quarks (u, d, s). These hadrons are mainly π and K -mesons.
- Cosmic muons. The flux of cosmic muons through a horizontal surface at detector level is less than $10^{-1} \text{ m}^{-2}\text{s}^{-1}$ and can be neglected compared to the other background sources.

Effects of background are as follows.

- Fake tracks can be formed either by a line-up of random hits or by punchthrough particles that cross more than one chamber.
- Overestimation of p_t can result by wrongly including background hits in a muon track. This will occur for muon-induced background, which gives hits close to the muon track, and for the case of a muon in a hadronic jet where punchthrough passes the muon chambers close to the muon.
- Loss of a muon trigger primitive due to overcrowding of the chamber. If there are too many hits in a chamber, the trigger primitive generation will possibly not be able to disentangle muon and background hits or will output only trigger primitives corresponding to background.

Chapter 5

Muon Trajectory

On its way through the detector the muon interacts with the magnetic field generated by the detector's superconducting coil and with the material it passes. Those interactions result in a deflection of the particle's movement and a loss of energy. The next section discusses the effect of the magnetic field on the muon's equation of motion and shows how the deflection of the track can be used to measure the muon's momentum. The following section covers the interactions between the muon and the matter it traverses and the stochastic and deterministic effects that these interactions have on the particle trajectory.

5.1 Interaction with the Magnetic Field

This section first describes the magnetic field configuration of the CMS detector. Then the equation of motion of a charged particle moving in a magnetic field will be solved and the effects of the magnetic field will be discussed in detail.

Figure 5.1 shows the magnetic field map for one octant of the CMS detector. The magnetic field is created by a superconducting solenoid, whose axis coincides with the beam axis. Inside the coil the field is practically uniform and parallel to the z -axis. The field flux density has a value of 4 Tesla. Outside the coil the magnetic field is returned by the iron yoke, the muon system is integrated into the yoke. In the barrel muon system the field is almost uniform and anti-parallel to the z -axis, and has a magnetic flux density of 1.8 Tesla. In the corner where endcap and barrel meet, the field lines change direction. In the endcap the field is radial in the transverse plane.

The equation of motion of a relativistic charged particle in an electromag-

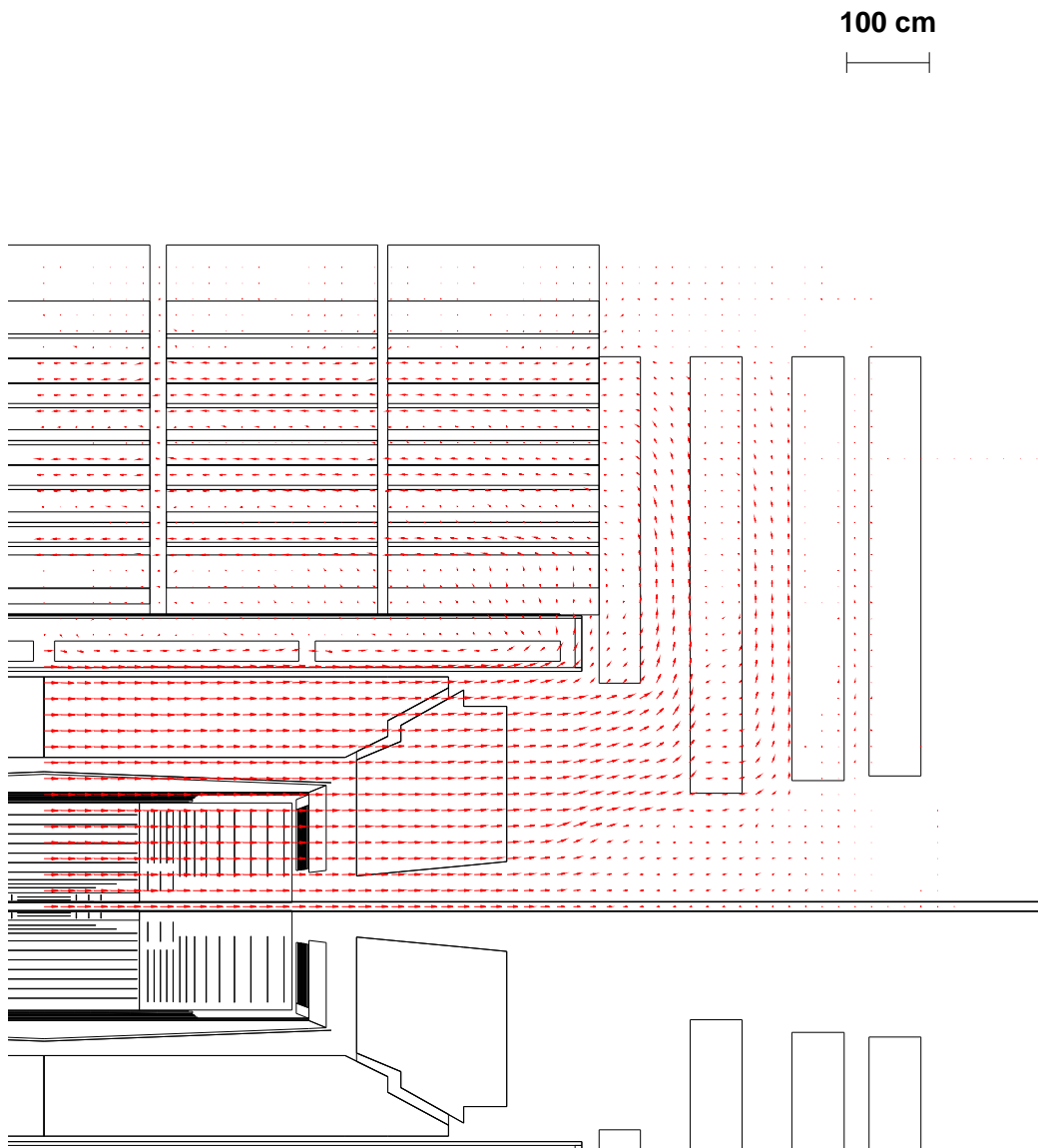


Figure 5.1: Field map of the magnetic field in the CMS detector

netic field is given by

$$\frac{dp^\mu}{d\tau} = qF^{\mu\nu}u_\nu, \quad \mu, \nu = 0, 1, 2, 3 \quad (5.1)$$

where

- p four-momentum of the particle
- u four-velocity of the particle
- τ proper time in the particle's rest frame
- q the particle's charge
- F the electromagnetic field tensor

Solving the equations of motion for the case of a uniform magnetic field and vanishing electric field yields a helix as the particle's trajectory[56]. The helix axis is parallel to the magnetic field. The helix radius is given by (using the SI system)

$$R_{hel} = \frac{p_t}{qB} \quad (5.2)$$

where p_t is the particle's transverse momentum, that is the component of its momentum in the plane perpendicular to the axis of the magnetic field, B is the magnetic field and q is the particle's charge as defined above. Expressed in the units commonly used in high-energy physics, this equation becomes

$$R_{hel}[cm] = \frac{10^2}{0.299\,792\,458} \frac{p_t [\text{GeV}/c]}{q [e_0] B [\text{T}]} \quad (5.3)$$

The helix thread is given by

$$h_{hel} = \frac{p_z}{p_t} R_{hel} = \frac{p_z}{qB} \quad (5.4)$$

where p_z is the particle's longitudinal momentum, the component of its momentum along the axis of the magnetic field.

The parametric representation of the helix is given by

$$\vec{x}(t) = \begin{pmatrix} R_0 \cos \phi_0 \\ R_0 \sin \phi_0 \\ z_0 \end{pmatrix} + \begin{pmatrix} R_{hel} \cos t \\ R_{hel} \sin t \\ \frac{h_{hel}}{2\pi} t \end{pmatrix} \quad (5.5)$$

where

- t denotes the curve parameter
- R_0 distance of the helix axis from the origin
- ϕ_0 azimuth of the helix axis
- R_{hel} helix radius as defined above
- h_{hel} helix thread as defined above

The following subsections cover the behaviour of the track in the bending plane and in the so-called non-bending plane.

5.1.1 Trajectory in the Bending Plane

In the previous paragraphs the equation of motion of a charged particle in a magnetic field has been stated. This section will address the projection of the trajectory into the bending plane, that is the plane perpendicular to the axis of the magnetic field. It is in this projection that bending takes place; the component of the track's momentum in this plane (p_t) can be computed from the curvature according to equation 5.2.

An important quantity that has already been encountered in the discussion of the input quantities (3.1.1) is the bend angle. It is the angle between the direction of a track at a given point and the radius vector through the origin and the point (see figure 3.7). The bend angle ϕ_{bend} can be defined as follows

$$\phi_{bend} := \phi_p - \phi \quad (5.6)$$

where ϕ_p is the azimuth of the track direction and ϕ is the azimuth of the point at which the bend angle is evaluated.

The bend angle has an important relationship with the helix radius and hence the transverse momentum of the track.

The trajectory of the track is a helix with axis perpendicular to the bending plane. The projection of that helix into the bending plane is a circle with equation

$$r \begin{pmatrix} \cos \phi \\ \sin \phi \end{pmatrix} = R_0 \begin{pmatrix} \cos \phi_0 \\ \sin \phi_0 \end{pmatrix} + R_{hel} \begin{pmatrix} \sin \phi_p \\ -\cos \phi_p \end{pmatrix}$$

where

- R_{hel} circle radius (=helix radius)
- R_0 distance of the circle center from the origin
- ϕ_0 azimuth of the circle center
- ϕ_p azimuth of the tangent to the trajectory,
it plays the rôle of curve parameter in this definition of the curve.

Rearranging the last expression gives

$$R_0 \begin{pmatrix} \cos \phi_0 \\ \sin \phi_0 \end{pmatrix} = r \begin{pmatrix} \cos \phi \\ \sin \phi \end{pmatrix} - R_{hel} \begin{pmatrix} \sin \phi_p \\ -\cos \phi_p \end{pmatrix}$$

and squaring both sides yields

$$R_0^2 = R_{hel}^2 + r^2 - 2r R_{hel} \sin(\phi_p - \phi)$$

Hence we obtain for the sine of the bend angle ϕ_{bend}

$$\underbrace{\sin(\phi_p - \phi)}_{\phi_{bend}} = \frac{R_{hel}^2 + r^2 - R_0^2}{2r R_{hel}} \quad (5.7)$$

For a track passing through the origin of the coordinate system we get

$$|R_{hel}| = R_0$$

$$\sin \phi_{bend} = \frac{r}{2R_{hel}}$$

The above formula holds inside the coil. At the coil the direction of the magnetic field reverses and the track's curvature changes sign.

Let a be the radius of the coil. At the intersection of the track with the coil

$$\sin \phi_{bend}|_{r=a} = \frac{a}{2R_{hel}} \quad (5.8)$$

Outside the coil the direction of the magnetic field reverses. The projection of the track into the bending plane is again a circle arc, but with a different circle center and radius. The new circle center is given by

$$\overline{R_0} \begin{pmatrix} \cos \overline{\phi_0} \\ \sin \overline{\phi_0} \end{pmatrix} = a \begin{pmatrix} \cos \phi^a \\ \sin \phi^a \end{pmatrix} - \overline{R_{hel}} \begin{pmatrix} \sin \phi_p^a \\ -\cos \phi_p^a \end{pmatrix}$$

where $\overline{R_{hel}}$ is the helix radius outside the coil and ϕ^a and ϕ_p^a are the corresponding quantities at the coil. $\overline{R_{hel}}$ can be easily computed from the value of the magnetic field outside the coil.

To compute $\overline{R_0}$, the distance of the center of the trajectory circle outside the coil from the origin, we square both sides and get

$$\begin{aligned} \overline{R_0}^2 &= a^2 + \overline{R_{hel}}^2 - 2a\overline{R_{hel}} \sin(\phi_p^a - \phi^a) \\ &= \overline{R_{hel}}^2 + a^2 \left(1 - \frac{\overline{R_{hel}}}{R_{hel}} \right) \end{aligned} \quad (5.9)$$

$$r \begin{pmatrix} \cos \phi \\ \sin \phi \end{pmatrix} = \overline{R_0} \begin{pmatrix} \cos \overline{\phi_0} \\ \sin \overline{\phi_0} \end{pmatrix} + \overline{R_{hel}} \begin{pmatrix} \sin \phi_p \\ -\cos \phi_p \end{pmatrix}$$

In analogy to equation 5.7 the bend angle outside the coil is given by

$$\sin(\phi_p - \phi) = \frac{\overline{R_{hel}}^2 + r^2 - \overline{R_0}^2}{2r\overline{R_{hel}}}$$

Substituting for $\overline{R_0}$, the distance of the center of the trajectory circle outside the coil, yields

$$\sin(\phi_p - \phi) = \frac{1}{2\overline{R_{hel}}} \left(r - \frac{a^2}{r} \left(1 - \frac{\overline{R_{hel}}}{R_{hel}} \right) \right)$$

There will be a zero-crossing of the bend angle $\phi_p - \phi = 0$ at a radius

$$r = a \sqrt{1 - \frac{R_{hel}}{R_{hel}}}$$

In CMS the magnetic field inside the coil is 4 T, outside the coil it is -1.8 T, so

$$\sqrt{1 - \frac{R_{hel}}{R_{hel}}} \approx 1.8$$

Note that according to this equation the position of the zero-crossing does not depend on the track's transverse momentum. The equation takes into account only the effect of the magnetic field, the energy loss of the tracks in the material of the detector is not included. The energy loss results in a momentum-dependence of the radius at which zero-crossing takes place.

Fig 5.2 shows the line of the bend angle's zero crossing superimposed on a transverse view of the detector. It shows that the line of zero crossing is close to muon station 3. This statement holds even when energy loss is taken into account.

Fig 5.3 shows the bend angle as a function of radius for various values of transverse momentum. The plot shows that the bend angle reaches a maximum right at the coil. Therefore this is the best place to compute the transverse momentum from the bend angle. The innermost muon stations, which are closest to the coil, play the most important role in p_t -assignment. The fact that the bend angle has a zero crossing at the radius of muon station 3 means that the bend angle measured in station 3 cannot be used for p_t -assignment. It also implies that extrapolation from station 3 to any other station is ambiguous (section 7.1.3).

One of the effects of the magnetic field is a lower cutoff in transverse momentum p_t . Particles with low p_t curl up inside the coil and can never reach the muon system. This occurs if the helix diameter of the track is less than the coil radius.

Substituting $B = 4$ T, gives a p_t -cutoff of

$$p_t \geq 2\text{GeV}/c$$

It should be pointed out, however, that this calculation does not take into account the energy loss suffered by the particle due to interactions with the matter it passes. Those effects will be covered in section 5.2.2.

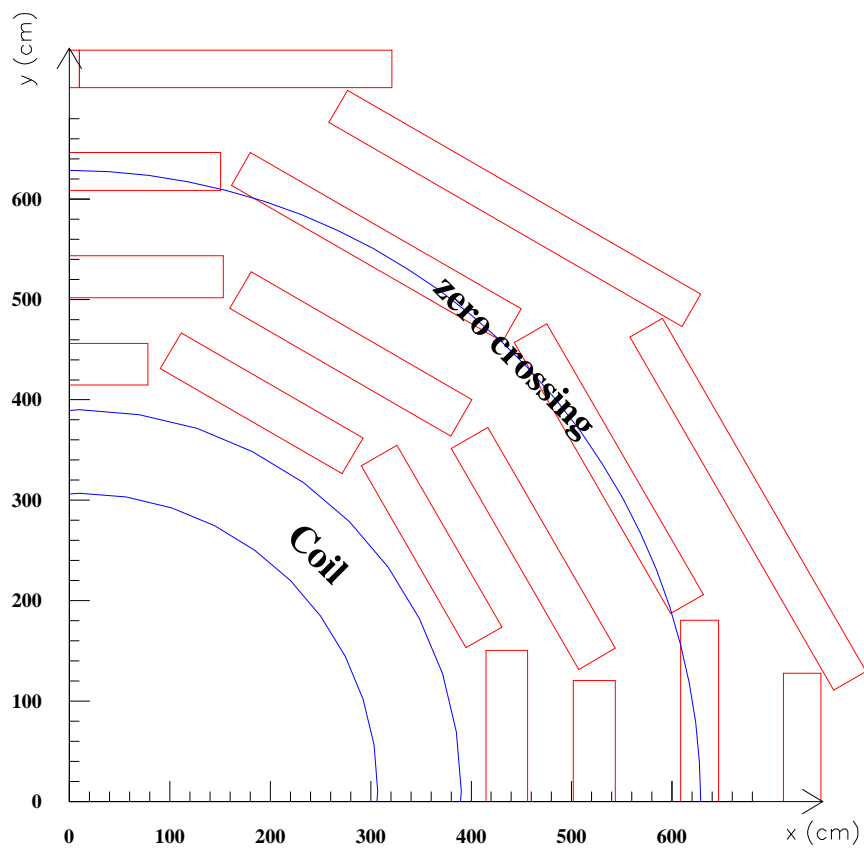


Figure 5.2: The radius where the bend angle passes zero overlaid on a cross-section of one quadrant of the CMS barrel muon system

Bend angle versus radius

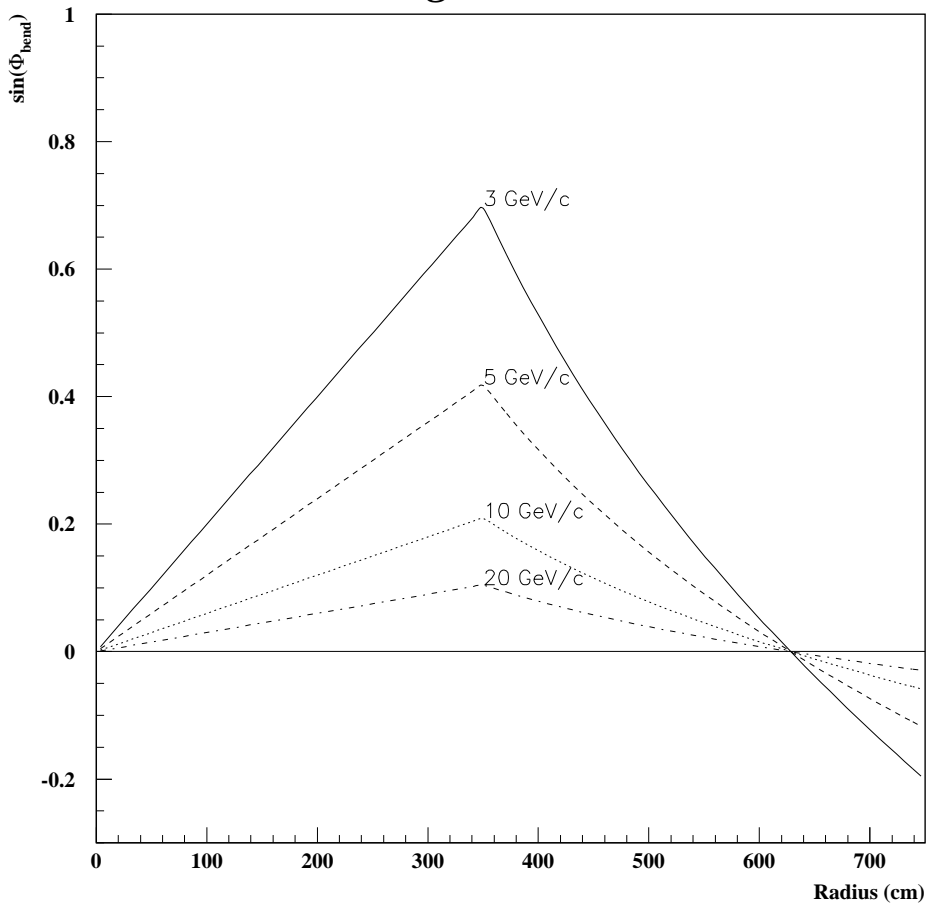


Figure 5.3: The bend angle ϕ_{bend} as a function of radius

5.1.2 Trajectory in the (z, R) -Plane

The previous subsection has discussed the projection of the track into the plane perpendicular to the helix axis. In that plane the bending is strongest, therefore it is called the bending plane. Let us now have a look at the projection of the track into the so-called non-bending plane.

Projecting the trajectory into the plane spanned by the radius $R = \sqrt{x^2 + y^2}$ and z yields a sinoid curve. The parametric representation of the trajectory is given by equation 5.5. Without loss of generality we can set $\phi_0 = 0$. For the radius R we obtain

$$R(t) = (x^2 + y^2)(t) = R_0^2 + R_{hel}^2 + 2R_0R_{hel} \cos t$$

Inside the coil for a track passing through the origin $R_0 = R_{hel}$. So the parametric equation of the projection of the helix into the (z, R) -plane is given by

$$z = \frac{h_{hel}}{2\pi}t \quad (5.10)$$

$$R = 2|R_{hel}|\left|\sin \frac{t}{2}\right| \quad (5.11)$$

$$(5.12)$$

The sinoid function has vanishing curvature at its origin, that is why the (z, R) -projection is sloppily called the non-bending projection, although the track is not a straight line in that projection. However, the curvature is much lower than in the (x, y) -plane and for transverse momenta above 5 GeV/c the tracks look practically straight in the (z, R) -plane. This fact simplifies the design of trigger algorithms. It means that tracks in the (z, R) -plane point back to the vertex.

5.2 Interaction with Matter

The previous section discussed the interaction of the muon track with the magnetic field of the detector. This magnetic field results in a deflection of the track, an effect that is purely deterministic. During its passage through the material of the detector, the muon interacts with the nuclei and electrons of the matter. These interactions result in a deflection and in energy loss of the track. The energy lost by the muon may be released in the form of secondary particles. The effects of the material on the muon track can be classified into deterministic and stochastic effects.

5.2.1 Multiple Coulomb Scattering

A charged particle passing through matter suffers many small-angle Coulomb scatters. The amount of scattering depends on the material, the path length of the track in the material and the charge and kinematics of the particle. The characteristic material constant for multiple scattering is the radiation length X_0 . Multiple Coulomb scattering is a stochastic effect, the average deflection of the particle vanishes, the distribution of deflections can be approximated as Gaussian.

An approximation for the standard deviation of the deflection that is valid in the range $10^{-3} < \frac{s}{X_0} < 10^2$ is [32]

$$\sqrt{\text{var } \theta} = 1.36 \cdot 10^{-2} |z| \frac{1}{\beta p [\text{GeV}/c]} \sqrt{\frac{s}{X_0}} \left(1 + 0.038 \ln \frac{s}{X_0} \right) \quad (5.13)$$

where

- z charge number of the particle
- p its momentum
- β its velocity
- s the path length traversed
- X_0 radiation length of the scatterer's material
- $\frac{s}{X_0}$ is called radiation thickness of the scatterer.

5.2.2 Energy Loss

Muons (and other charged particles) passing through matter lose energy in interactions with that matter. The main energy loss mechanism is excitation of the electrons and ionization of the target atoms. This process is approximated by the Bethe-Bloch formula [11] and usually treated as a continuous process. The latter formula describes the deterministic contribution and gives the average energy loss of the particle. Due the statistical nature of the interactions between incident particle and target atoms, the energy loss fluctuates around the average value and thus displays a stochastic component.

Figure 5.4 shows the average energy loss per unit length for a muon in iron as a function of the muon's energy. It can be seen that the energy loss rises from the minimum to reach the so-called Fermi plateau at high energies. The data used in that figure were extracted from the GEANT detector simulation program [30].

Some of the electrons liberated by collisions have sufficient energy to create secondary ionization. These are referred to as energetic knock-on

Energy loss for μ^+ in Iron

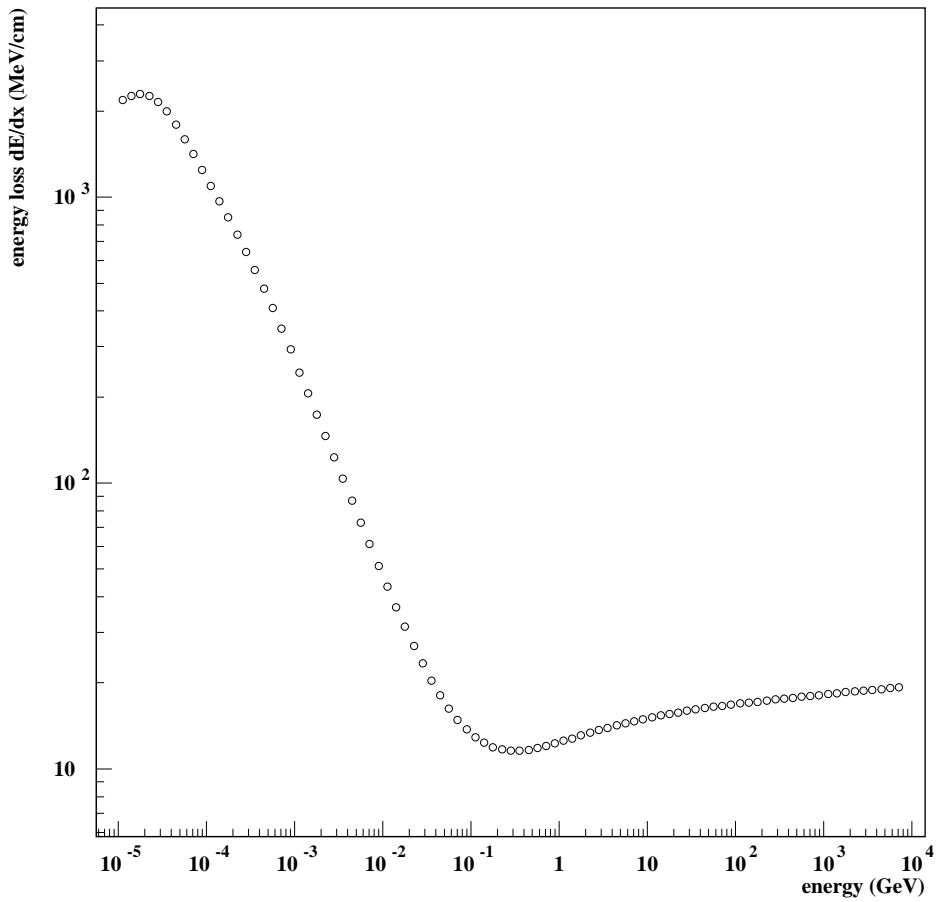


Figure 5.4: The stopping power (energy loss per unit length) for muons in iron as a function of the muon's energy

electrons (δ -electrons). δ -electrons can spoil the drift time measurement in the drift tubes of the barrel muon system (section 2.2.3).

At high muon energies radiative processes play an important role in addition to the energy loss by ionization described in the previous paragraphs. These mechanisms are bremsstrahlung and pair creation.

Figure 5.5 shows the cross section for bremsstrahlung of muons in iron.

Figure 5.6 shows the cross section for pair creation of muons in iron. Note the strong rise with the muon's energy.

The cross section plots demonstrate that radiative processes are of major importance at high muon energies. The secondary particles created by the muons can initiate electromagnetic showers in the iron between the muon stations. This leads to a decrease in efficiency of the trigger primitive generation at high muon energies, because the local pattern recognition logic will often not be able to distinguish the real muon track from the electromagnetic secondaries induced by the muon. It is important that the muon stations are separated by at least 30 cm of iron to contain the showers and decouple the stations.

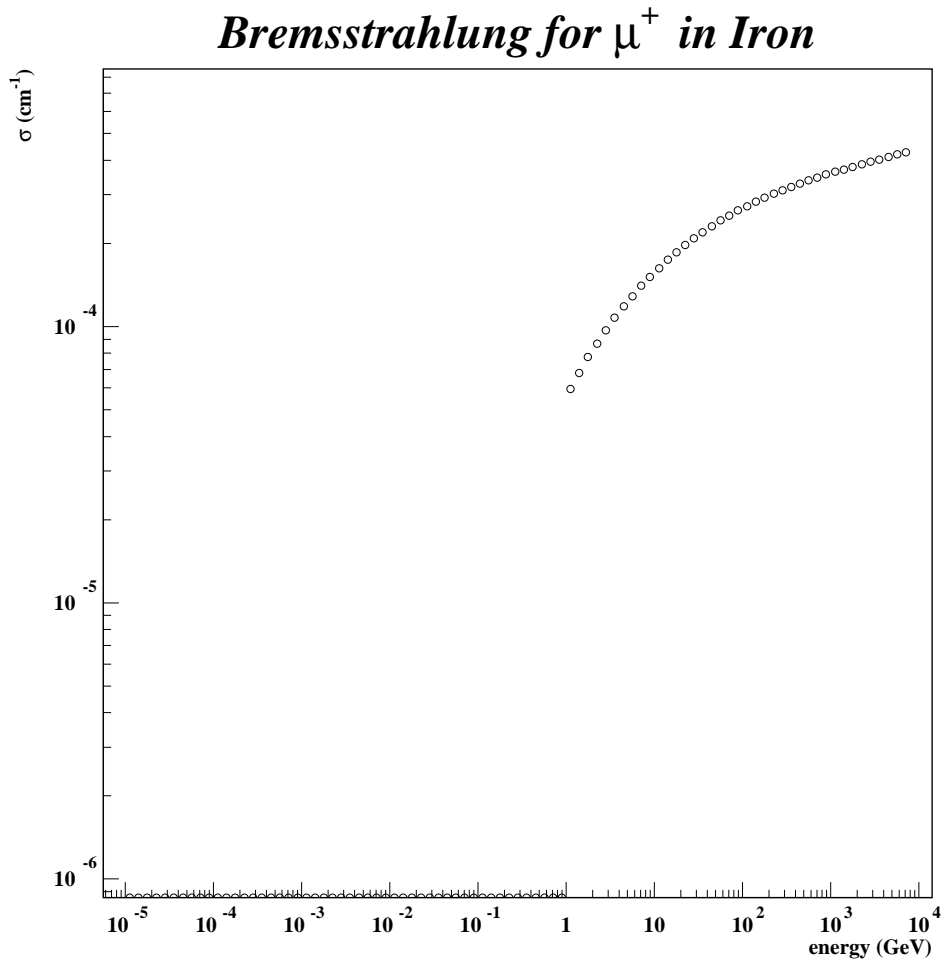


Figure 5.5: The cross section for bremsstrahlung for muons in iron as a function of the muon's energy

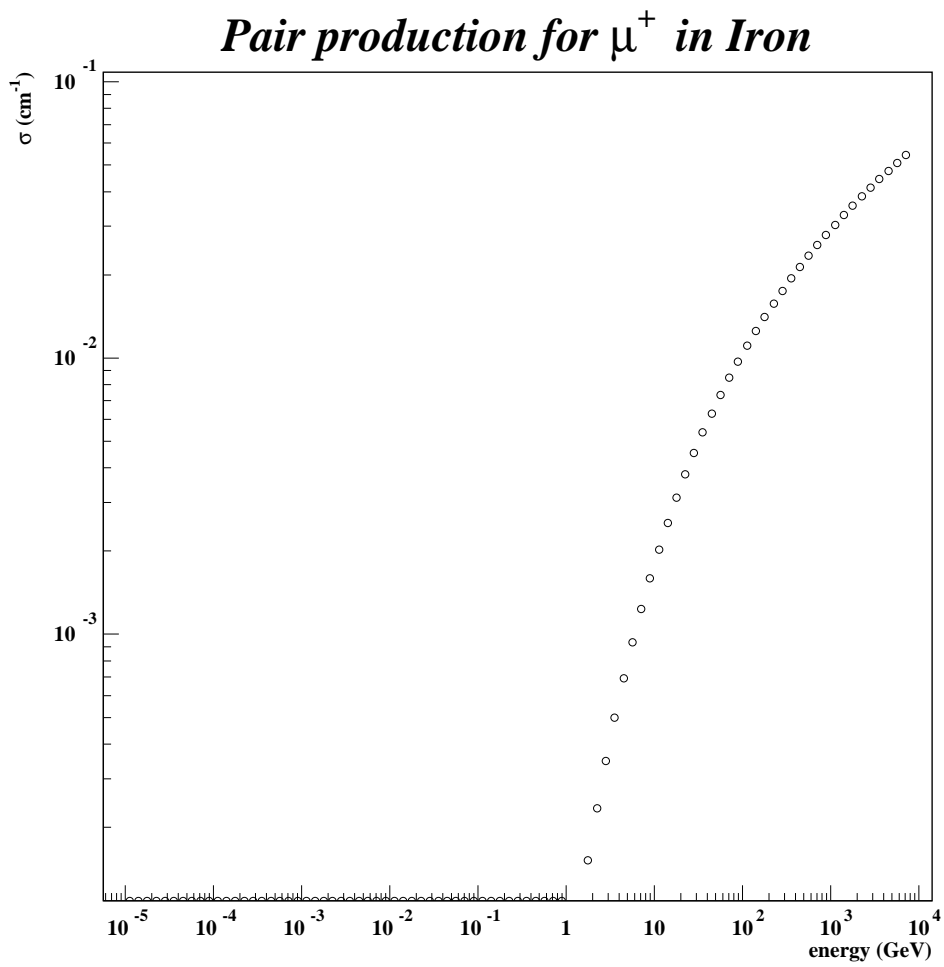


Figure 5.6: The cross section for pair creation for muons in iron

Chapter 6

Implementation Options

This chapter covers some of the methods that are relevant to the task specified in section 3.2. It sets out with a brief introduction to the problem of track finding and gives an overview of technologies and methods that have been used in existing first level muon or track triggers or that are being considered at planned experiments. It gives a brief description of each of these methods and assesses their feasibility in the light of the specifications of the first level regional muon trigger laid down in section 3.

6.1 Track Finding

This section defines track finding and presents several commonly used track finding methods. General introductions to the topic of the reconstruction of charged tracks can be found in references [50] and [29].

Track detectors provide information such as the position or the position and the angle where a track crossed the chamber. These data may be contaminated by noise. Moreover, points can be missing because of chamber inefficiencies. The task of track finding is to take measurements from the input set and join them to tracks.

Many common detectors give a projected position — they do not define a space point where a track passed, but only a point in a projection, for example the bending plane. The track finder can handle this by either working in the projections and finding tracks in each projection independently and trying to match the tracks from the two projections with each other after finding them separately. Or it can work in three dimensions right from the beginning. The drawback of the latter approach is that there are usually ambiguities and the combinatorics increases dramatically. Figure 6.1 shows a trivial example of how such ambiguities can arise due to two-dimensional projective readout.

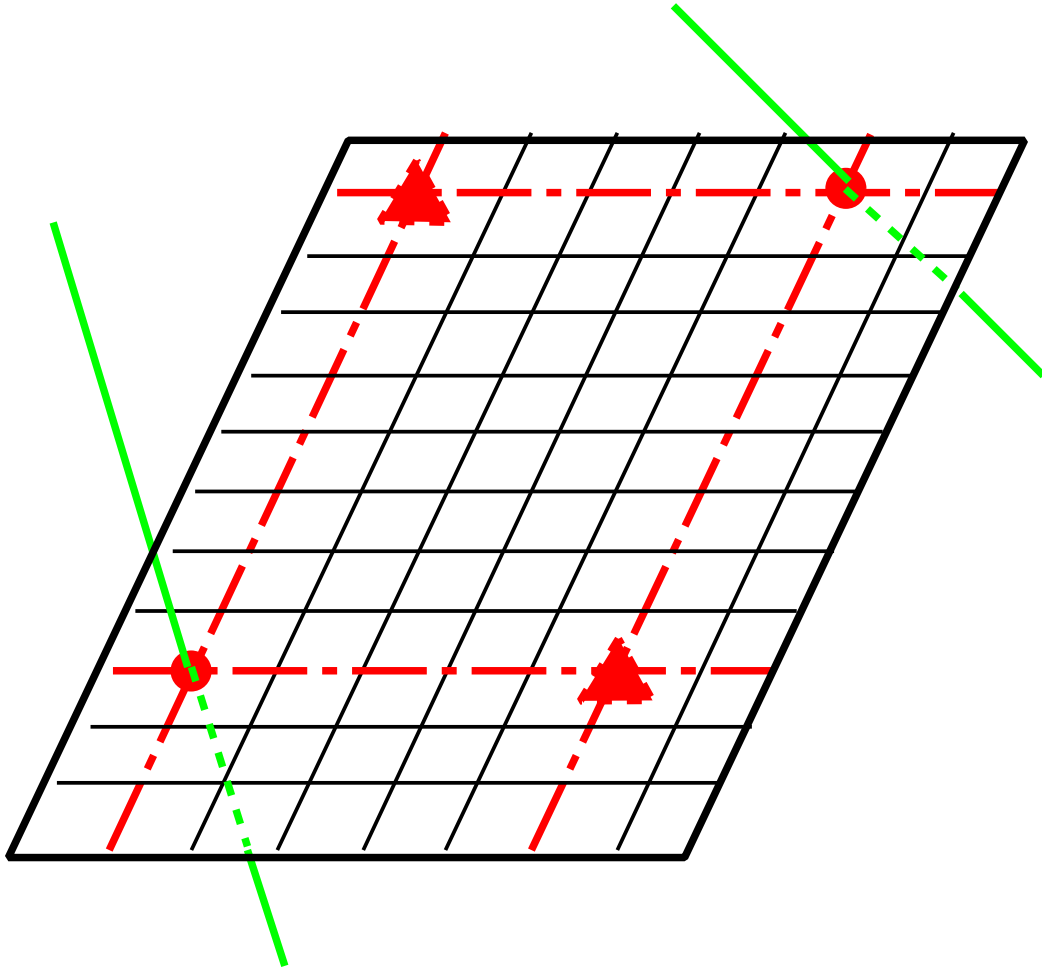


Figure 6.1: Ambiguities due to two-dimensional projective readout. Two tracks pass through the chamber, four tracks are found: Two real tracks (round markers) and two ghost tracks (triangle markers).

Reference [29] classifies track finding methods as either global or local.

Global methods find all candidates in parallel. Local methods determine track candidates one after the other. They usually proceed by using a few measurements to get an initial estimate of the track parameters (track candidate initialisation), then they find additional matching measurements by extrapolating or interpolating, and use those additional data to update the track parameters. If no matches are found, the initial track candidate is rejected.

Global Methods are

- Histogramming, treated in section 6.4.
- Template matching, treated in section 6.2.

The problem from which all global methods suffer is the problem of back-mapping. Global methods indicate that a track has been found and give values for the track parameters, but the information which local measurements contributed to a particular track is usually lost. This is a great concern in our application, because track finding can be performed with a coarse position resolution, whereas fine position resolution is required for precise p_t -assignment. It would therefore be attractive to perform track finding with coarse resolution, keeping the hardware expense for the track finder in check, and then use the full resolution for assignment of transverse momentum. Methods that do not allow back-mapping make such an approach impossible.

Local Methods are

- Track following. This method proceeds by finding a starting track element (point+direction), usually in the region where the track density is lowest, that is far from the interaction region. It then extrapolates the initial track segment towards the interaction region using a track model. This track model can be a full description of the track dynamics including the magnetic field or just a straight line. It intersects the extrapolated track segment with all chambers encountered and adds matching hits to get a track string. Hits match, if they fall into a window about the expected position, the window's size depends on how accurate the initial track parameter estimate is believed to be and on the amount of multiple scattering between the two stations. The knowledge about the track is updated using the new hits. The matching criterion can be refined based on the new knowledge. So the method gets more selective when approaching the crowded region closer to the interaction point.

- Road method. This method produces an initial track candidate by picking hits from the outermost and innermost parts of the detector, defining a road with a certain width about the line joining those points and looking for additional hits within that road.

6.2 Template Matching/Pattern Comparison

The template matching approach to track finding is to predefine all the valid tracks that should be found by the track finder. For each predefined track, called template, the hit coordinates in all chambers are stored in a template memory. Each candidate track is then compared to that set of predefined patterns. If it matches one of the predefined tracks, it is accepted, otherwise rejected.

The output of such a track finder is the identifier of the template track that matched the input pattern. This identifier can be mapped directly to the output quantities, such as transverse momentum.

The number of templates required depends on the hit resolution used, the bending of the tracks and the amount of multiple scattering and energy loss fluctuations. The high magnetic field and large amount of material in the CMS muon chambers let that number skyrocket, if full resolution is used. That means that the templates have to use a coarser resolution to keep the pattern count feasible. Now that poses the following problem: If a coarse input resolution is used, the p_t -resolution will be coarse. Such a device would not fulfill the requirements posed in section 3. A solution is to use the template matching only for track finding, storing the full resolution data in a buffer during the track finder's processing and extracting the data from the buffer once a track has been found. The p_t -assignment unit can then use the full position resolution to assign a precise p_t .

A second way of reducing pattern count is to use a coarse resolution for templates corresponding to low- p_t tracks and a fine resolution for templates corresponding to high- p_t tracks. At low p_t , momentum resolution is limited by multiple scattering rather than trigger primitive resolution, so fine trigger primitive resolution is not required. Due to the larger effect of multiple scattering at low p_t , trajectories of low- p_t tracks have a much larger spread and would therefore require many more patterns if the same resolution as for high p_t were used.

How are the patterns to be stored created? One method is to simulate a large number of tracks and count for each pattern how often it occurs. That number of most probable patterns is accepted whose added probability reaches the desired track finding acceptance.

An alternative is to perform a track fit for each pattern under consideration. If the fit succeeds and the fit's χ^2 is below a defined threshold, the pattern is added to the pattern set. Otherwise the pattern is rejected. The advantage of the first method is that the track finding acceptance is known directly, the second method on the other hand is faster.

A difficulty in a template matching algorithm arises, if one has to deal with incomplete tracks due to detector inefficiencies and geometric acceptance holes. The template corresponds to a complete track; if the real track misses one layer, it would not be found by the standard template. One can either store a separate pattern for all possible cases of inefficiencies. That increases the number of patterns. Or one can make the individual templates more flexible by demanding not a complete match between the candidate track and the template track but only a partial match. In that case, however, several templates can match a given candidate track, and a priority logic is required to choose one of them.

6.3 Neural Networks

A general introduction to artificial neural networks (NN) can be found in [33]. In particle physics neural networks have mainly been used in NN simulation on conventional computers for pattern recognition in off-line analysis. Reference [42] gives an overview over the application of artificial neural networks in particle physics.

For implementing fast pattern recognition in an online environment, neural networks offer a couple of advantages. Their design is characterized by an inherently parallel algorithm, which makes them fast. Feed-forward neural networks reach their decision within a fixed delay. By design, neural networks offer fault tolerance, being able to cope with incomplete and noisy input data. This is an important feature because it makes dealing with hits missing due to chamber inefficiencies easy. Neural networks are trainable, so they provide the flexibility required for the first level trigger as detailed in section 3.4.1.

Feed-forward nets can be easily implemented in hardware; VLSI implementations of digital, analog, and hybrid artificial neural networks are on the market. A review of existing VLSI implementations can be found in [8].

There are two options for outputting a measured quantity in the network's output layer:

- There is one neuron for each measured quantity; the activation of the neuron gives the value of the quantity to be measured. This method can find only one object.

- The measurement range of the quantity is divided into bins, to each bin corresponds a neuron. A measurement can excite one neuron or several neurons. In the latter case the distribution gives the measurement, higher resolution than given by the binning can be achieved. This method can find more than one object.

The following paragraphs give a brief review of existing high-energy physics triggers based on artificial neural networks.

The CPLEAR experiment at CERN [7, 43] has designed a first level track trigger, whose purpose is to determine the number and location of tracks in the detector. The detector consists of 11 layers and is segmented into 64 azimuthal sectors. There is one digital neural network per sector, which processes data from its sector and 4 neighboring adjacent sectors. The input information is in the format of an unencoded hit map, so each ANN-card receives 5×11 input bits. There is one output neuron per sector; if it is activated, it means that a track has been found in that sector. The architecture chosen is a two-layer neural network (input, hidden, output layer) and has been implemented with discrete components. The maximum decision time is less than 75 ns. Note that the input granularity is very coarse and that the trigger does not measure the track's transverse momentum.

The D0 experiment at FNAL [44, 45] uses an analog neural network for local pattern recognition in a 4-layer drift chamber system to determine track segments from data of the individual layers. The output quantities to be determined are the slope and the intercept of track segments. The inputs presented to the neural network's input layer are voltages proportional to the drift times in the four layers. There are two sets of 32 output neurons each for each of the two output quantities. The value of the output quantity is expressed as a bump in the distribution of the activation of output neurons. The implementation uses a commercially available analog NN VLSI chip. In total, processing takes $8 \mu s$.

The WA92 experiment at CERN [9] performs event classification using both a digital and an analog neural network. The input quantities are 16 variables chosen with respect to their significance for pattern classification. The response time is about $8 \mu s$.

After this survey of existing devices, I shall discuss the issues relevant for possible application to the regional muon trigger. The first observation is that analog designs usually have precisions of about a few percent. Given that the position input to the regional trigger has a resolution of 12 bit, corresponding to a fraction of a permille, analog designs are out of question. A further drawback would be that both input and output data are in digital format, so a digital-analog conversion at the input and an analog-digital conversion

at the output would be required. A second observation is that two of the existing designs have latencies far too long for the stringent requirements of the regional muon trigger. Technological progress would have to be significant to overcome that problem.

The trigger processor of the CPLEAR experiment is fast, but the resolution is very coarse and the algorithm is basically a simple coincidence logic that could have easily been implemented without neural networks.

In conclusion, I should like say that neural networks are not a viable option for implementing the first level muon trigger, unless the technological progress is very fast. However, one of the requirements posed to the regional trigger is to be implementable with today's technology. Therefore neural networks do not appear to meet the requirements.

6.4 Histograming Method

Histograming is one global method of pattern recognition. An overview of histograming techniques and their applications in particle physics can be found in [21]. Histograming approaches pattern recognition by transforming the problem of finding tracks to the problem of finding clusters in pattern space, and the latter problem in turn to that of peak-finding in a histogram.

The hardware expense for implementing the histogram table rises strongly with the granularity and the number of dimensions of the histogram. In practical designs, one or two histogram dimensions have been used. That means, that one has to map the input quantities on one or two quantities to be histogramed. For example, we have seen in section 5.1 that the trajectory of a track in the (z, R) -projection is a straight line through the origin for high momentum tracks. If the track gives hits in all four chambers it passes, one can map each of the hits to the quantity η . In the absence of multiple scattering, bending and measurement errors, all four chambers should find the same value of η . Entering the η values into a histogram would give a peak of height 4 at the η of the track. This is the track finding algorithm considered for the (z, R) -projection. The H1 experiment at DESY uses a similar method [20].

Hardware implementation of the histograming method is straightforward: The input quantity is decoded and the corresponding bin is incremented.

A special variant of histograming is the Hough transform [34]. An introduction to the Hough transform is given in [23] and an application for an experiment at GSI is described in [10]. This method can be used for finding arbitrary two-dimensional curves that depend on two parameters, if one knows some points of that curve. It uses a two-dimensional histogram.

In principle, the Hough transform could be applied for track finding in the muon system. However, histogramming methods have a principal drawback for applications that require fine resolution. The number of histogram bins becomes infeasible, if the resolution of the input quantities is too fine. For instance, in our application the tracks in the (x, y) -projection can be described by two parameters, for example p_t and the azimuth at which the track passes the first muon station. This means that the histogram has to be two-dimensional. The position is measured with a resolution of 12 bits, corresponding to 4096 bins in one dimension. So the total number of histogram bins would be prohibitively high. Of course, one does not need the full resolution of the input quantities for track finding, full resolution is only required for the assignment of p_t to found tracks. So one could use a coarser resolution for track finding. However, the problem then is that in a histogramming method one does not know, which of the input track segments belong to the found track. One would know an approximate transverse momentum and position for the found track, but there would be no way of finding the track segments belonging to that track and use their full resolution data for assigning a more precise p_t and position.

My conclusion is that histogramming is a suitable method for track-finding in the non-bending projection, because there one only wants to know at which η a track exists, and the η -resolution does not need to be fine. But it is not a viable method for track-finding in the bending plane, because it does not meet the requirements on p_t -resolution.

6.5 Content-Addressable Memories

Content-addressable Memories (CAM), also called associative memories, are memories that are addressed not by address but by content. Conventional memory is presented an address and outputs the contents of the memory cell with that address. Content-addressable memory is presented with the content, and outputs the address(es) of the cell(s), if any, that hold that content. A comprehensive treatise on CAMs is given in [41]. Several high-energy physics experiments have used CAM-based triggers [17, 5, 4, 18].

Of interest for first level trigger applications are only CAM implementations that perform a parallel search, that means that each memory cell compares its contents with the data presented and raises a flag, if it finds a match. The implementation is that each memory cell is equipped with a comparator, which compares the cell's contents with the input data placed in a comparand register. If the memory cell finds a match, it asserts a match flag to indicate that it has found the data. Of course, there could

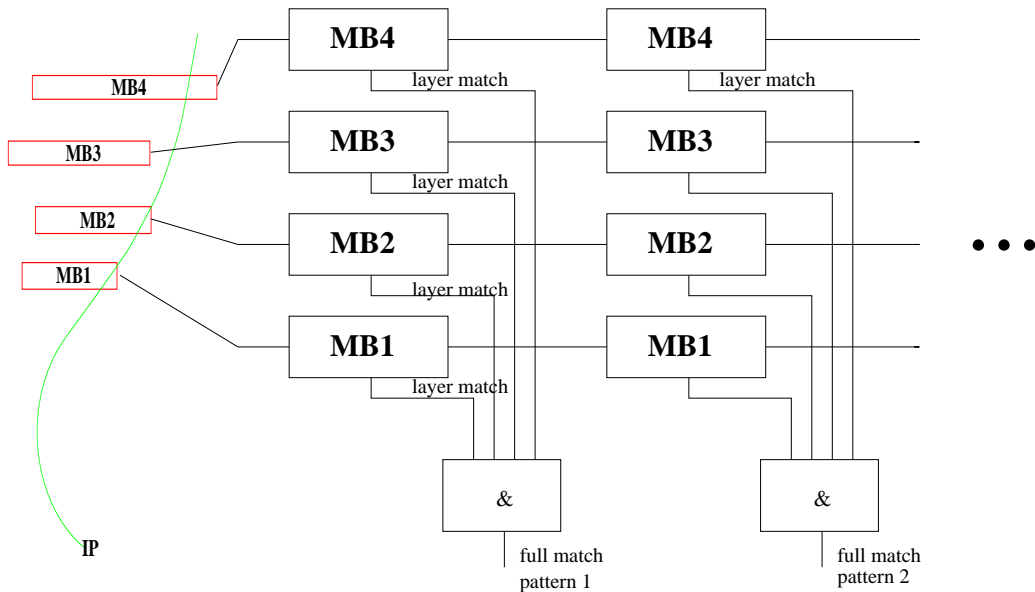


Figure 6.2: Principle of using CAMs for track finding. $MB_i, i = 1, 2, 3, 4$ marks the CAM cell corresponding to muon station i

be several memory cells that match the data in the comparand register. A priority encoder then sorts out which matching location has the top priority. The address of the highest-priority matching location, if any was found, is output.

Implementations of such parallel CAMs are commercially available. For example, there are ICs on the market that can hold up to 1024 128-bit wide patterns or 8192 64-bit wide patterns with priority encoders [52].

Figure 6.2 shows the basic design idea for using CAMs in the regional muon trigger.

Each column of cells in that figure corresponds to one track template pattern. Each cell compares the hit data for the template track it represents with the data measured in the station to which it is assigned and raises the layer match flag if it finds agreement. The AND circuit at the bottom of the figure indicates that the pattern found in the four muon stations agrees with the track template to which that AND belongs.

Our application requires special features not commonly found in commercial CAMs.

- There must be a subdivision according to stations.
- A track should be found even if it did not give hits in all four muon stations, due to chamber inefficiencies.

- There can be more than one track segment per chamber.

There are two possible solutions for the second feature. Either the AND-coincidence shown in the figure can be replaced by a majority logic that allows for partial matches. The majority logic gives a ‘TRUE’ output, if, for example, at least three out of the four layer cells report a match. The drawback is that several patterns can then respond to the same input pattern, necessitating a complex priority logic to select which of them to use.

The second possible solution is to use AND-coincidences, but to store a separate pattern for each combination of missing chambers. Then there would be ANDs that have only layer match inputs from, for example, muon stations 1, 2 and 3, allowing station 4 to be missing, and require station 4 to have no hit. In that case only one stored pattern can fire for a given input pattern. The drawback however is that this method results in a large increase of the number of patterns to be stored. If one chamber is allowed to be missing, the pattern count increases by a factor of 5, if two chambers are allowed to be missing, by a factor of 11.

The chamber trigger logic can output up to two track segments per chamber. The CAM can cope with that by using multiplexing: The two track segments can be transferred to the comparand register one after the other, the layer match flag has to be latched with the information which of the two track segments, if any, matched. Those latched bits can then be output as a track segment address. To summarize, each template track circuit would have the following output:

- 1 bit to indicate match/no match
- 4×2 address bits, because there are four layers and each layer has to indicate whether the first or the second or no track segment matched
- Ideally, it should also output the track segment qualities, because the priority encoder that decides which track to accept in case of clashes should base its decision on the number of track segments in the track and their qualities.

It should be stressed that at the output of such a CAM the addresses of the track segments that were combined to tracks are available. This means that track finding can be done with a coarser resolution, requiring fewer patterns. At the end of the track finding stage, the addresses of the track segments joined to tracks can be used to extract the full-resolution track segment data from a buffer memory where they have been stored during the track finding stage. These full-resolution data can then be used for precise p_t -assignment.

So far, CAM-based track finding appears promising, it is inherently fast due to its parallelism. If the CMS detector consisted of only a single sector, a single CAM could be used for that sector. However, the detector consists of many sectors and muons change sector boundaries. This requires communication between the CAMs, and the amount of interconnection required does not appear feasible.

Chapter 7

Algorithm

This chapter describes the algorithm employed by the regional muon trigger processor. It will explain how the trigger performs the tasks defined in section 3.2. It then demonstrates the feasibility of the described algorithm. Finally it addresses the requirements on the trigger that have been listed in section 3.4.1 and shows that they are met by the presented design.

The discussion is mainly concerned with the regional muon trigger in the barrel, where the trigger's input is already well defined. The endcap region is still in a very preliminary design stage and will be treated at the end.

7.1 Track Finding

7.1.1 Introduction

In this section first the issue of track finding criteria will be addressed. After a few more introductory remarks and considerations, the possible options will be outlined.

In the context of the regional muon trigger, the task of track finding is to map the set of trigger primitives provided by the chamber trigger logic to a (possibly empty) set of tracks. It thus joins track segments to tracks.

The question arises: When should a set of trigger primitives form a valid track? In other words, what are the track finding criteria?

The chambers and the chamber trigger logic are not fully efficient, moreover there are gaps between the chambers and the chamber edges are less sensitive than the interior of the chamber. That means that very often a track will not produce trigger primitives in all stations. So the first question I set out to answer is: How many track segments should be required to form a track? The initial idea was to require at least three stations out of the four

or the innermost two stations. That second condition was to accommodate low p_t tracks. These tracks, due to track bending and energy loss, do not reach the outer chambers.

However, figure 7.1 shows that this requirement yields an unacceptably low track acceptance. The figure was obtained by simulating tracks for each p_t -point and calculating the probability that they have at least three hits or hits in the innermost two stations. No specific assumptions were made about the track finding method employed, and thus the figure gives the upper bound in performance that can be achieved by an ideal track finder.

Based on that simulation result, I decided that the track finding criterion had to be relaxed: Even tracks that yield trigger primitives in only two out of the four muon stations should be accepted. Relaxing the criterion, while improving the efficiency of track finding, decreases its purity. It becomes more likely that a track found by the track finder is not a real track, but originates for example from a random match between hits created by background.

A track, of course, should only be accepted, if it is compatible with the hypothesis that it is a muon originating from the interaction region, that is it should point back to the vertex.

The final track finding criterion deals with the compatibility between different tracks. Are tracks allowed to share trigger primitives? The granularity of the trigger primitives is very fine, so the probability that two real muons overlap is very small. Therefore it appears reasonable to demand that one track segment should not belong to more than one track.

Having defined the track finding criteria, the next question is whether one can order tracks by quality. The algorithm has to include selection stages, where it chooses between tracks and passes only the better tracks on to the next stage. That decision would ideally be based on the qualities of the individual track segments which make up the track and on the information of how many and which stations contributed to the track. Due to limitations on the amount of information transfer between processing units, it may be necessary to make a selection based on the second criterion only. What should the preferences be, if such a decision has to be made?

Each possible combination of stations that can form a valid track is called a track class. For the track-finding criterion specified above (two out of four) there are 11 track classes

1234, 123, 124, 134, 234, 12, 13, 14, 23, 24, 34.

The digits in the identifier of the track class indicate which stations belong to that track class. A priority-ordering is defined on the set of track classes. For example, the best track class (1234) has track segments in all 4 stations and is therefore ‘better’ than all the others. This priority-ordering will play

Acceptance Study

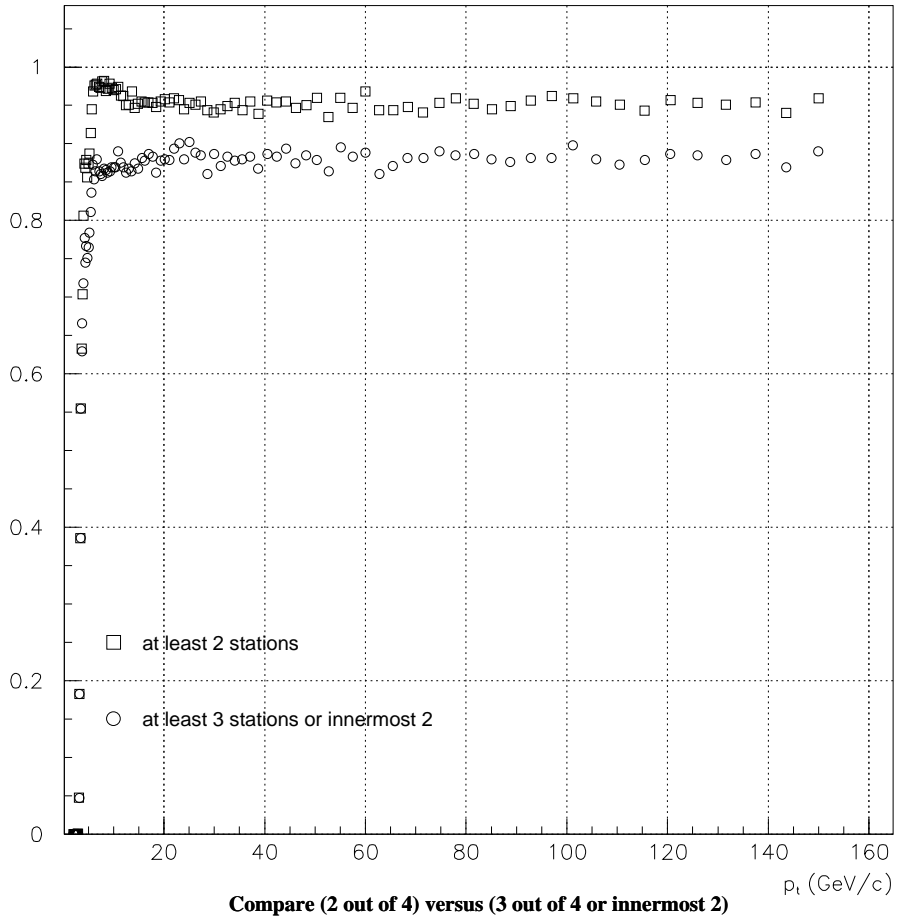


Figure 7.1: This figure compares two requirements for track finding. Square markers show the acceptance if one requires at least two track segments for one track. Circular markers show the requirement of at least three track segments or two track segments in the two innermost stations to accommodate low momentum tracks.

an important role when the algorithm has to make selections to pass only the ‘best’ tracks on to the next stage.

But the ordering is not obvious. While it is evident that 1234 should have higher priority than any other class, it is not obvious whether track class 12 is better than class 34. On the one hand, 34 is more likely to be a real track and not faked by punchthrough, on the other hand p_t can be measured much more precisely for a track of class 12 than for a track of class 34. For the moment, an ordering has been defined. The hardware implementation provides sufficient flexibility to change that ordering, so the optimal ordering can be chosen as soon as backgrounds are known after startup of the detector, based on real measured data.

A track is a three-dimensional object. The trigger primitives, however, are two-dimensional objects, because the chambers that create them use projective readout. The track finding can proceed either independently in the two projections, the bending plane (x, y) and the non-bending projection (z, R) . Those two projections almost decouple in the barrel zone as I shall show in section 7.6.1. In the endcap and overlap zone, however, the picture is more complicated.

Alternatively, the track finder can try to find tracks in all three dimensions right from the beginning. The drawback is the much higher hardware expense. The measurements from the two projections cannot be combined locally in the chamber due to ambiguities (see figure 6.1).

The track finding processor has to be segmented due to the large amount of data and the complexity of the problem. A serious technological challenge is the interconnection between the various components of the trigger processor. The hardware segmentation of the track finder processor should mirror the detector segmentation to alleviate that challenge.

After these general remarks on track finding in the regional trigger, the next question is which algorithm should be chosen. Chapter 6 has already listed a few methods that have been successfully used in previous experiments.

One candidate is the pattern comparison/template matching method (section 6.2). One of its drawbacks is that one has to use a coarser resolution for track finding to keep the pattern count within reasonable limits. The difficulty is then to recover the full resolution data for use in the p_t -assignment. Moreover, that method does not include the bend angle measurement provided by the trigger primitive generation and thus does not make full use of the available information. Finally, this method is used by the muon trigger based on resistive plate chambers [13]. The two systems are supposed to have a high degree of complementarity, so it is preferable that they employ different algorithms.

7.1.2 The Pairwise Matching Method

For the reasons mentioned above, a different algorithm was developed. Track segments are joined to tracks by pairwise matching. If two track segments from different stations are found to be compatible with originating from a single track, they form a track segment pair. If one of those two track segments is in turn compatible with a third track segment from a station different than the two, a track segment triple is formed. A compatible fourth track segment yields a track segment quadruple. In short, a string of matching track segments forms a track.

This algorithm has a high degree of intrinsic parallelism: All the comparisons required can be carried out in parallel.

The station pairings required depend on the track selection criteria. Two track segments from two different stations already form a valid track, so a total of $\binom{4}{2}$ station pairings have to be examined: 1-2, 1-3, 1-4, 2-3, 2-4, 3-4.

Tracks do not necessarily stay in the same ϕ -segment and z -wheel as they traverse the muon system. They cross sector boundaries in ϕ due to their bending in the magnetic field and multiple scattering. Due to the non-projective geometry in the (z, R) -projection they cross z -wheel boundaries. A bit of terminology: From now on the slice of the muon system spanned by a ϕ -sector and a z -wheel will be called a detector segment.

There are two ways of combining information from adjacent detector segments:

- Overlapping logical sectors: One logical sector comprises two physical sectors and logical sectors overlap by half their width. This approach doubles the number of sectors and hence the hardware expense.
- Exchange of data between neighbouring segment processors. This is the path chosen.

Figure 7.2 shows all the pairings of detector segments that have to communicate with one another.

Combining all the above figures yields the total number of comparisons required: $2 \times 2 \times 6 \times 12 \times 3 \times (3 + 2 \times 2 + 2 \times 1) \approx 7800$. The first two factors are the number of track segments in each chamber, 6 is the number of station pairings, 12 the number of ϕ -sectors, 3 the number of ϕ -sectors into which each ϕ -sector has to look (itself and the neighbours on either side), the term in parentheses stems from the inter-wheel combinations.

The question clearly arises: How does one check that two track segments from different stations are compatible with each other?

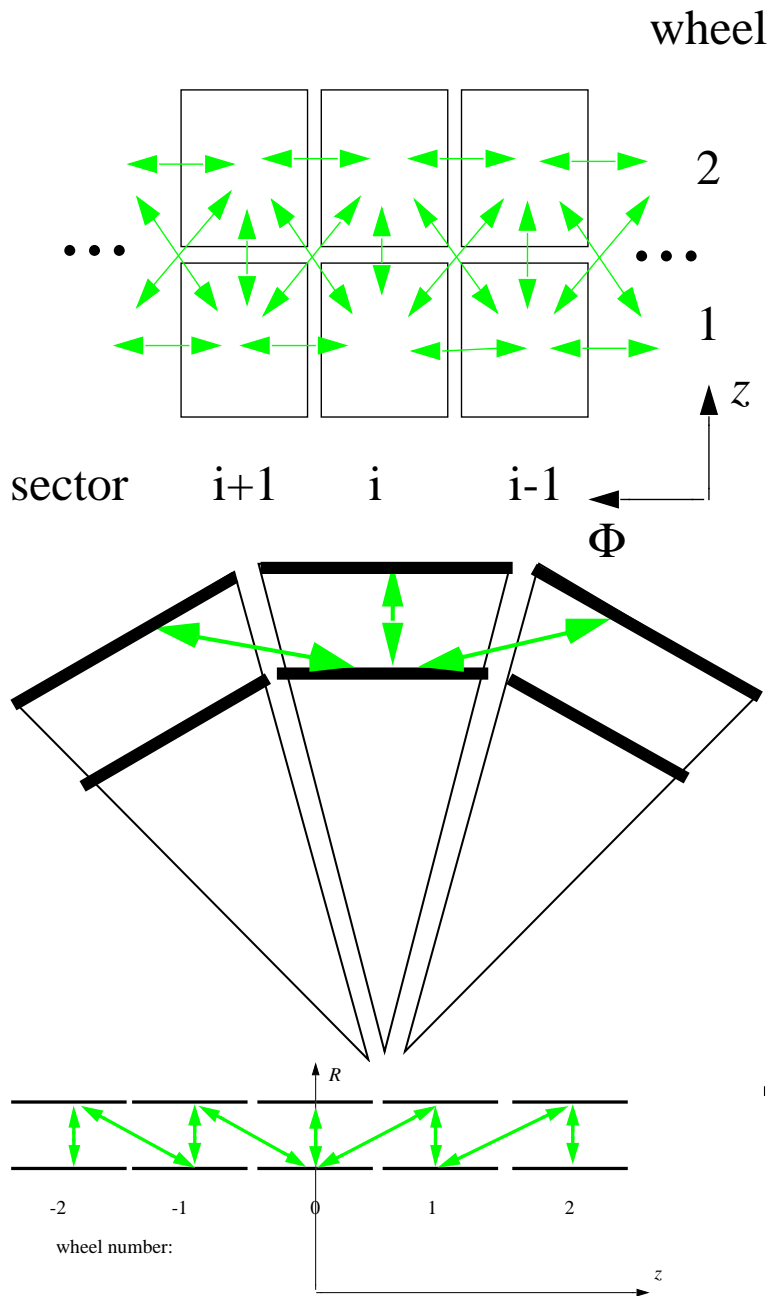


Figure 7.2: Matching of track segments between neighboring detector segments.

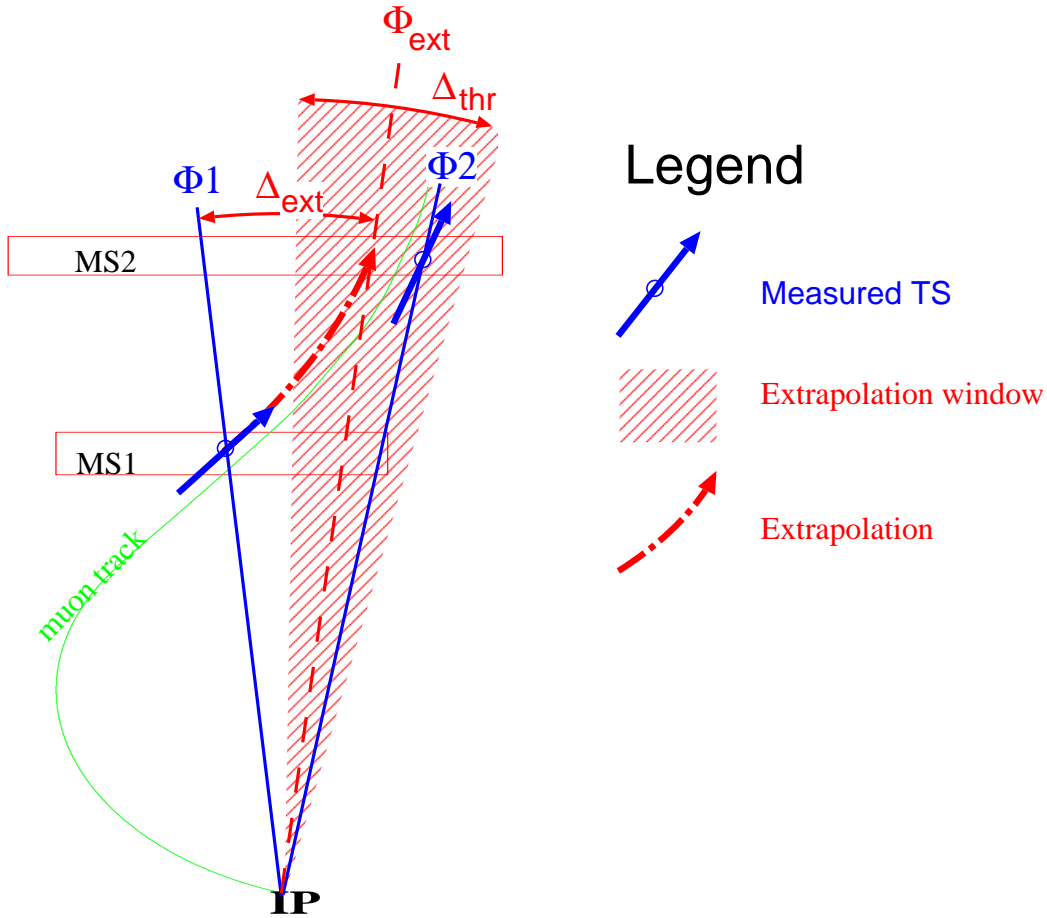


Figure 7.3: Principle of the extrapolation method: The track segment's measured bend angle in muon station 1 (MS1) is used to extrapolate to the target station (MS2). The difference between extrapolated (ϕ_{ext}) and measured (ϕ_2) position in MS2 must be below the threshold Δ_{thr} for a match.

7.1.3 Pairwise Matching by Extrapolation

The previous section has explained how tracks are built by pairwise matching of track segments. This matching between track segments can be carried out by extrapolation.

The principle of the extrapolation method is shown in figure 7.3. In the following discussion, the track segment which is extrapolated will be called source track segment, the track segment to whose chamber the source track segment is extrapolated will be called target track segment. Track segments come with position and bend angle. The procedure is to extrapolate the source track segment to the station of the target track segment, using the

former's measured bend angle. The bend angle is a function of transverse momentum, so the extrapolation takes the track's curvature into account. In principle, one could use a simpler extrapolation, such as a zeroth order extrapolation, where the extrapolated azimuthal position is simply the same as the source track segment's measured position. That approach, however, while simplifying the design would have a lower acceptance for strongly bent low p_t tracks and hence violate one of the basic requirements put down for the trigger processor in section 3.4.1.

The second step is to check that the difference between extrapolated position and measured position of the target track segment is below a specific threshold. That threshold should depend on transverse momentum p_t , because the stochastic effects that smear the particle's trajectory on its way from one station to the next depend on transverse momentum. Those effects are multiple scattering and energy loss fluctuations. Again, the bend angle is related to p_t , so that p_t -dependence can be taken into account by making the threshold depend on the bend angle of the source track segment. The matching criterion can be written as

$$\|\phi_{pos}^i + \Delta_{ext}(\phi_{bend}^i) - \phi_{pos}^{ii}\| \leq \Delta_{thr}(\phi_{bend}^i) \quad (7.1)$$

where

ϕ_{pos}^i : measured azimuthal position of the source track segment

ϕ_{bend}^i : measured bend angle of the source track segment

$\Delta_{ext}(\phi_{bend}^i)$: expected change of azimuthal position between source and target station as a function of the bend angle

$\phi_{pos}^i + \Delta_{ext}(\phi_{bend}^i)$: expected azimuthal position in the target station

ϕ_{pos}^{ii} : measured azimuthal position of the target track segment

$\phi_{pos}^i + \Delta_{ext}(\phi_{bend}^i) - \phi_{pos}^{ii}$: extrapolation deviation, that is the difference between expected and measured position

$\Delta_{thr}(\phi_{bend}^i)$: extrapolation threshold, that is the maximum allowed extrapolation deviation for a match

A refinement of the matching could be achieved by extrapolating not only the track segment's position but also its bend angle. That means, that one predicts not only the position but also the bend angle in the station of the target track segment and compares predicted and measured bend angle along

with position. The potential gain in performance, however, was not deemed to justify the increase in hardware expense.

Figure 7.4 shows station pairings for which unambiguous extrapolation is possible. The abscissa in these plots displays the bend angle of the source track segment. The ordinate shows the difference between the azimuthal positions of the target and the source track segment. The data were obtained by simulation using the CMSIM simulation software package[1]. Due to the zero crossing of the bend angle near station 3 (see 5.1.1), extrapolation from station 3 to any other station is ambiguous. This is shown in figure 7.5. That is not a problem because one can extrapolate from any other station to station 3.

It has been mentioned above that the size of the threshold for matching extrapolated and measured position should depend on transverse momentum p_t . The dependence can be parametrized as follows:

$$\frac{1}{\Delta_{thr}} = \alpha p_T - \beta$$

This proportionality can be understood from the momentum dependence of multiple scattering (equation 5.13). Figure 7.6 shows the functional dependence of the spread of the extrapolation deviation on p_t for each of the station pairings that allow unambiguous extrapolation. It can be seen that the spread is small compared to the chamber size (a chamber spans about $2\pi/12 \approx 0.5$ in azimuth ϕ). It is thus possible to choose the extrapolation thresholds such that high acceptance is combined with good background rejection.

The previous paragraphs have outlined the idea behind pairwise matching by extrapolation. How can that be implemented in hardware?

Figure 7.7 shows my original idea for the implementation of the matching step, and figure 7.8 for the implementation of joining matching pairs to strings.

Extrapolation itself can be carried out by RAM-based look-up tables. In principle, of course, one can compute the expected value for the position, knowing the functional dependence, but that would take too long. Look-up tables offer a fast and simple implementation of a complicated function that is computationally expensive to generate. Moreover, since they are RAM-based, their values can be updated easily if experimental conditions such as magnetic field or amount of material change.

The same holds for the implementation of extrapolation thresholds. The threshold values can be stored in look-up tables.

Extrapolations

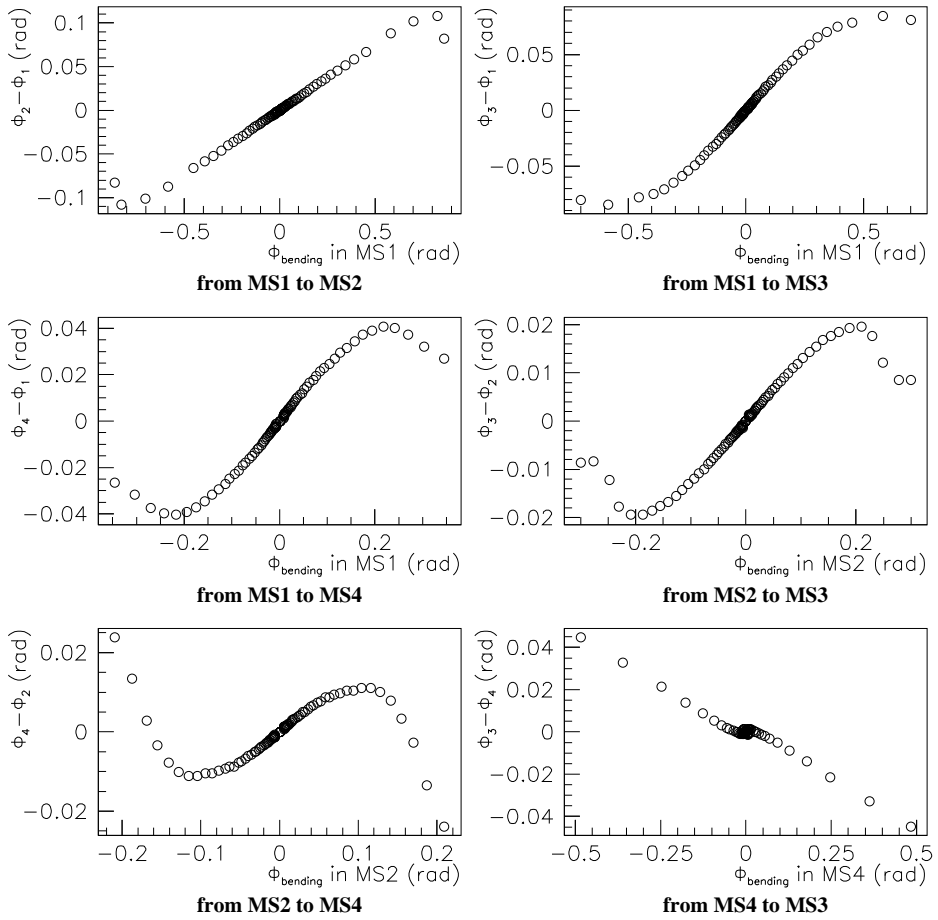


Figure 7.4: Unambiguous extrapolation. Knowing the track's bend angle and position in the source station, one can unambiguously infer the track's position in the target station for the station pairings shown here.

No unambiguous extrapolation possible

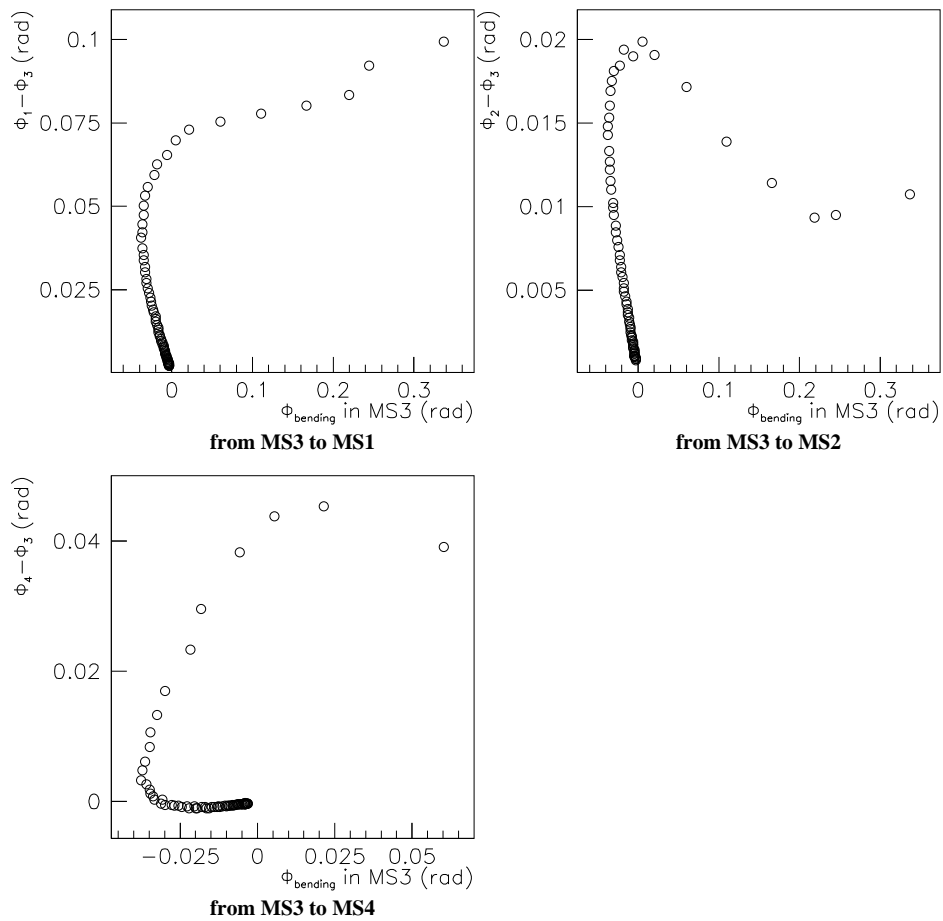


Figure 7.5: Ambiguous extrapolation. Due to the zero-crossing of the bend angle near station 3 no unambiguous extrapolation from station 3 to any other station is possible.

Extrapolation deviations

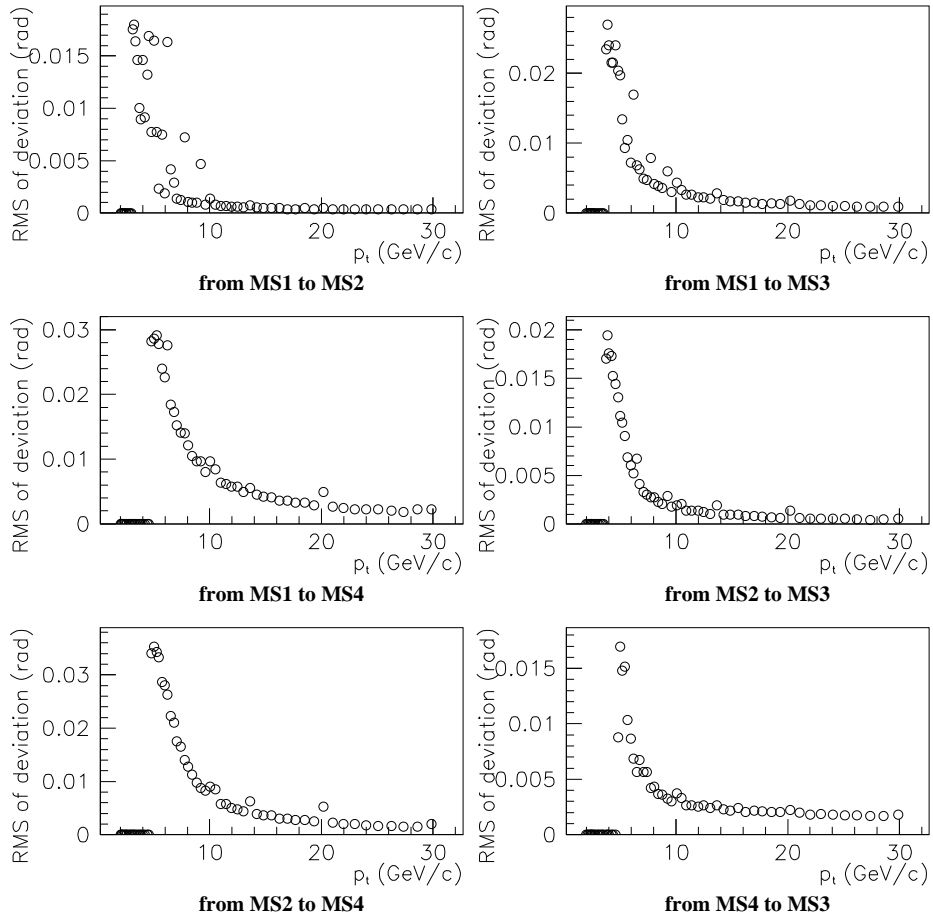


Figure 7.6: RMS of the extrapolation deviation as a function of track's transverse momentum p_t

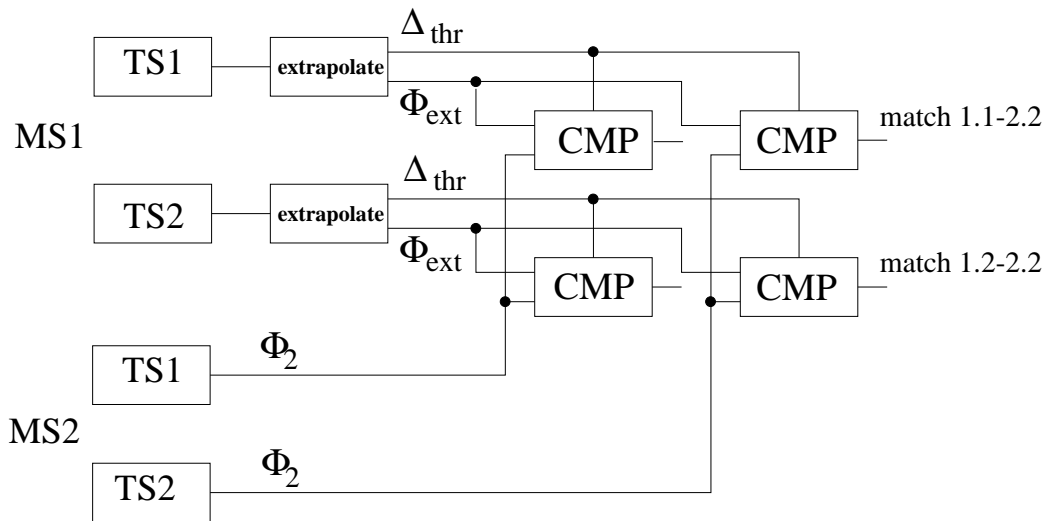


Figure 7.7: First idea of implementation of pairwise matching by extrapolation in hardware; TS=track segment; MS=muon station

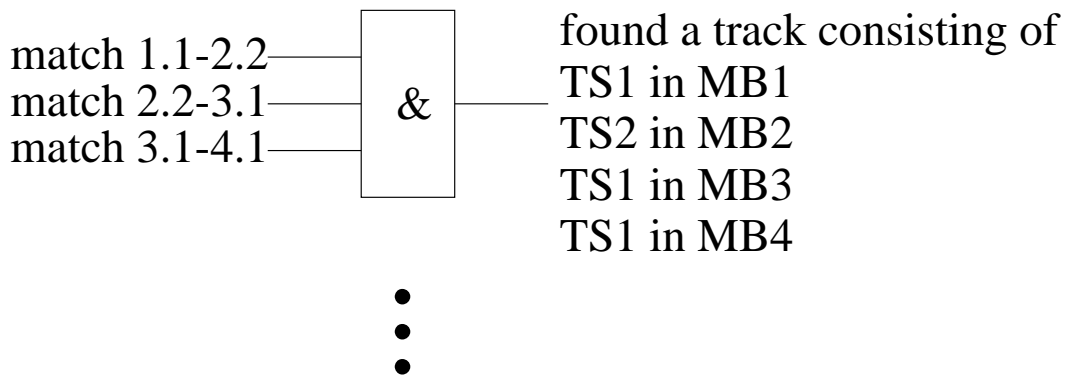


Figure 7.8: First idea of implementation of pairwise matching by extrapolation in hardware - this step shows the joining of track segment pairs to full tracks

7.2 p_T Assignment

Once a track candidate has been identified by the track finding stage, the p_t -assignment unit determines the track's transverse momentum p_t . This value is used by later trigger stages for applying a p_t -cut, thus accepting only muons that pass a given threshold.

Measurement of transverse momentum is based on the momentum-dependence of the track's deflection in the magnetic field of the detector. Section 5.1 demonstrated that in the barrel region bending takes place mainly in the projection perpendicular to the beam axis, and for that reason this (x, y) -plane is called bending plane.

At low momenta, resolution is limited by multiple scattering and energy loss fluctuations in the absorber material. At high momenta, the resolution is limited by the position resolution of the trigger primitive generation.

Using data from the muon system alone, there are two basic ways of measuring the transverse momentum. First, one can use the track's bend angle, that is the angle between the tangent to the track and the radius vector in the bending plane, as defined in figure 3.7. This method implicitly uses a vertex constraint. Secondly, the track's sagitta can be used as a measure of p_t .

The following two subsections will investigate those two methods.

7.2.1 Bend Angle Method

This method makes use of the vertex constraint: It assumes that the position of the vertex of the track is known and is the interaction point. Thus the vertex enters the algorithm as a virtual measurement with resolution equal to the size of the interaction region. The size of the interaction region in the bending plane is very small ($15 \mu\text{m} \times 15 \mu\text{m}$), the vertex constraint thus corresponds to a measurement of excellent resolution.

In section 5.1 it was shown that the absolute value of the sine of the bend angle rises linearly with radius inside the coil, reaches a maximum at the coil and decreases until it crosses zero. The best bend-angle based p_t -resolution can therefore be achieved by measuring the bend angle right after the coil.

At the coil we have for the bend angle ϕ_{bend}

$$\sin \phi_{bend} = \frac{a}{2R_{hel}} \quad (7.2)$$

where a is the radius of the coil and $R_{hel} = \frac{pt}{qB_z}$ is the helix radius of the track trajectory. For high p_t , $a \ll |R_{hel}|$ holds, hence the bend angle is small

and we get an inversely proportional relationship between p_t and ϕ_{bend}

$$p_t = \frac{a q B_z}{2 \phi_{bend}} \quad (7.3)$$

Figure 7.9 shows that this proportionality holds well over a wide range of p_t .

Abbreviating the constants in (7.3) to α ,

$$p_t = \alpha \frac{1}{\phi_{bend}}$$

we get for the p_t resolution, discounting all stochastic effects on the trajectory,

$$\begin{aligned} \sigma(p_t) &= |\alpha| \frac{1}{\phi_{bend}^2} \sigma(\phi_{bend}) \\ &= \frac{1}{|\alpha|} p_t^2 \sigma(\phi_{bend}) \end{aligned} \quad (7.4)$$

where I have used the error propagation law. This equation does not take into account multiple scattering and energy loss fluctuations, so it is valid only for high transverse momenta. It shows that resolution gets worse as p_t increases.

We have seen that transverse momentum can be computed from the bend angle. The next question is how to determine the bend angle from directly measured quantities. As discussed in section 3.1.1, each station measures bend angle and azimuthal position of the track. The bend angle can thus be taken directly as the measured bend angle from a single station, or it can be determined from the difference of measured positions in two stations.

Let us discuss first the option of determining the bend angle from the data measured in a single station. Figure 7.10 shows the bend angle as a function of transverse momentum in all four muon stations. One sees that the bend angle changes sign between station 2 and station 4. The zero-crossing of the bend angle (figures 5.3,5.2) occurs near station 3, so the bend angle measured in station 3 does not allow unambiguous determination of p_t . The best resolution is achieved by using the bend angle from muon station 1, because the magnitude of the bend angle is highest here right after the coil and because the muon has crossed less material. The space between the muon stations is filled with the iron plates of the return yoke, giving rise to multiple scattering and energy loss of the particles.

The conclusion is that the measured bend angle in stations 1, 2 or 4 can be used, with station 1 however giving the best resolution.

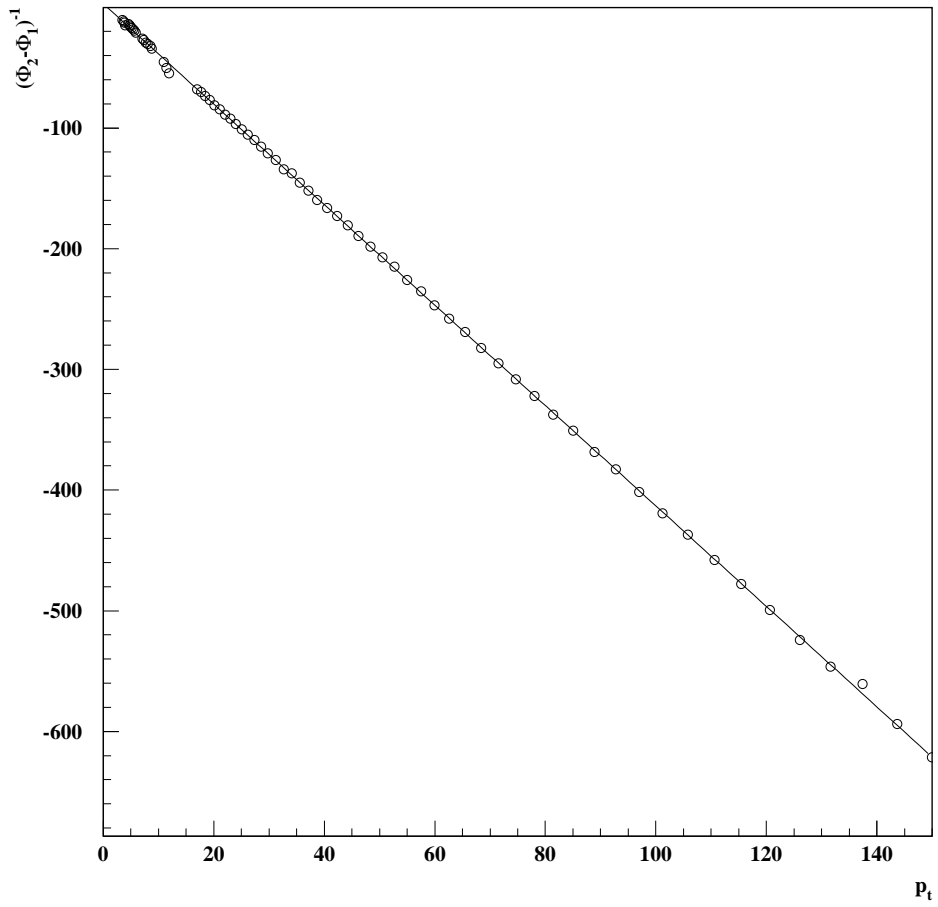


Figure 7.9: Relationship between transverse momentum p_t (in GeV/c) and the inverse of the change of azimuthal position between stations 1 and 2 — the latter quantity is proportional to the bend angle ϕ_{bend} (in rad^{-1}); round markers show simulated data points, the solid line is a straight line fit to those data

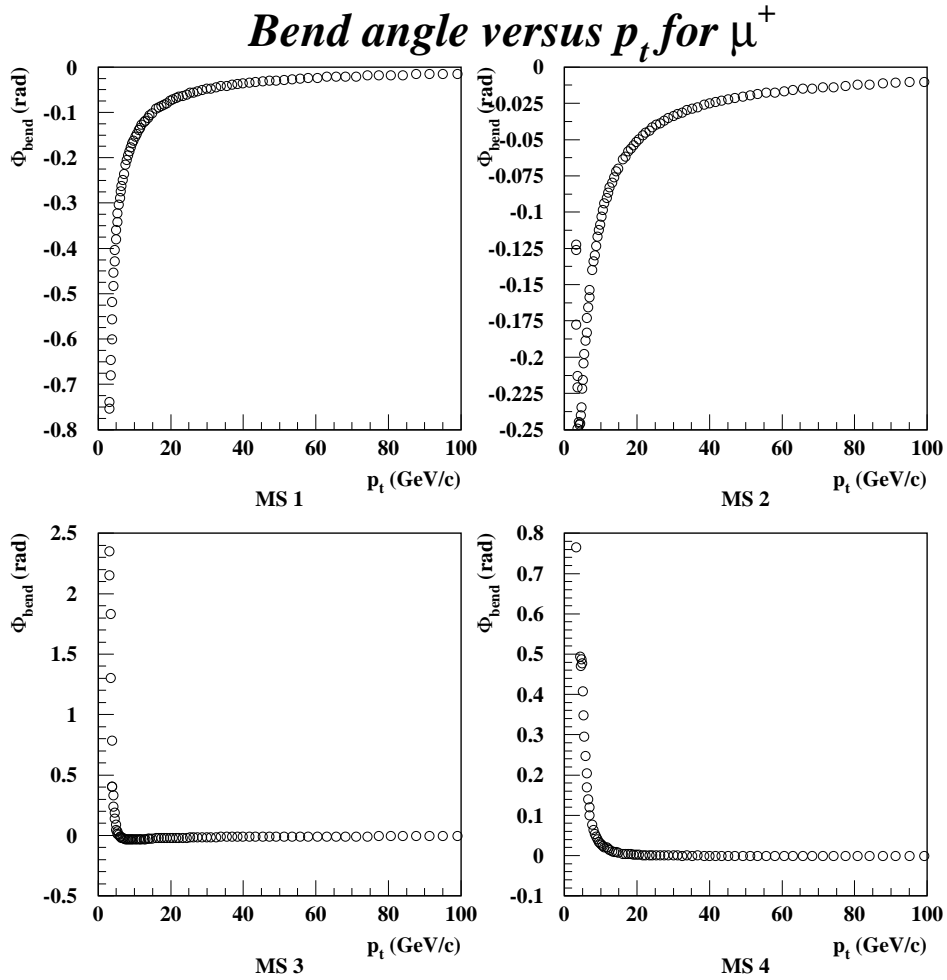


Figure 7.10: Bend angle ϕ_{bend} as a function of transverse momentum p_t in all four muon stations in the barrel

The second possibility of determining the bend angle (or rather a quantity that has a unique relationship with the bend angle) is to take the difference of two azimuthal positions measured in two stations.

Figure 7.11 shows that quantity as a function of transverse momentum p_t for all station pairings.

It can be seen that only for the station pairing MS1-MS2 is that function monotonous. That means that for all other pairings, the determination of p_t from the azimuthal difference is ambiguous. The effect that such an ambiguous mapping would have on the efficiency curves of the muon trigger is shown in figure 7.12. Those efficiency curves were created by using the ambiguous mappings, and always assigning the higher p_t when two values of p_t mapped to one azimuthal difference. As a result, a bump at a p_t of about 5 GeV/c appears in the efficiency curves.

The hardware implementation of this p_t -assignment method is straightforward: The mapping from bend angle to p_t is accomplished by a look-up table. If the bend angle is computed from the difference of two azimuthal positions, the positions are first routed to a subtractor, and the difference is then sent to the look-up table.

7.2.2 Sagitta Method

The second method of determining the track's transverse momentum from muon system data alone is the sagitta method. The sagitta is a measure of the track's curvature and hence of its transverse momentum.

The sagitta can be determined either from two measured bend angles or from three measured azimuthal positions. Using two measured bend angles yields a poor resolution and will not receive further discussion.

If one uses three positions to compute the sagitta, there are $\binom{4}{3} = 4$ possibilities: One can use the station triples 123, 124, 134 or 234.

In this discussion, sagitta is defined by equation 7.6, because this quantity is directly related to the sagitta in the proper sense, but is easier to compute than the latter. Figure 7.13 shows the sagitta as defined above as a function of the track's transverse momentum. Error bars indicate the spread of the sagitta due to multiple scattering and energy loss fluctuations. As the size of the error bars indicates, determining sagitta from the triple of stations (1,2,4) is the least favorable option.

The method can be easily implemented in hardware. The sagitta for station triple (1,2,3) is

$$s_{123} = (\phi_3 - \phi_2) - (\phi_2 - \phi_1) \quad (7.5)$$

$$= \phi_3 - 2\phi_2 + \phi_1 \quad (7.6)$$

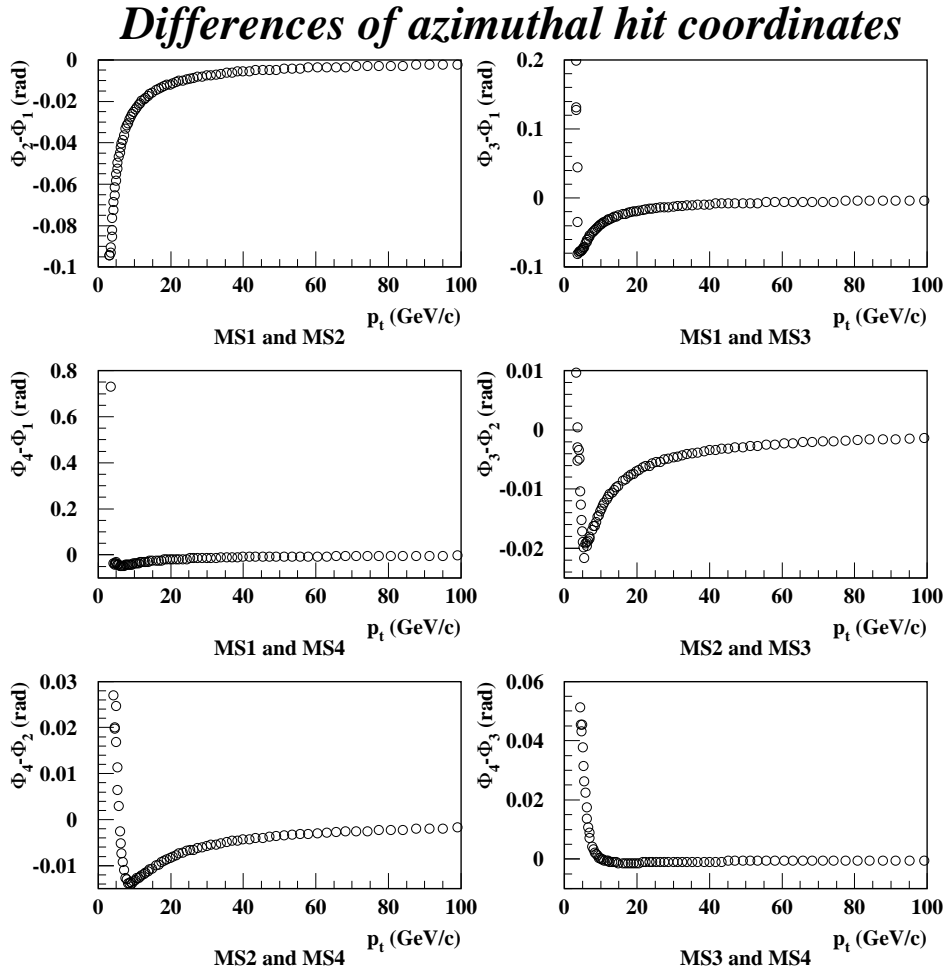


Figure 7.11: Difference of measured azimuthal positions as a function of transverse momentum p_t for all station pairings

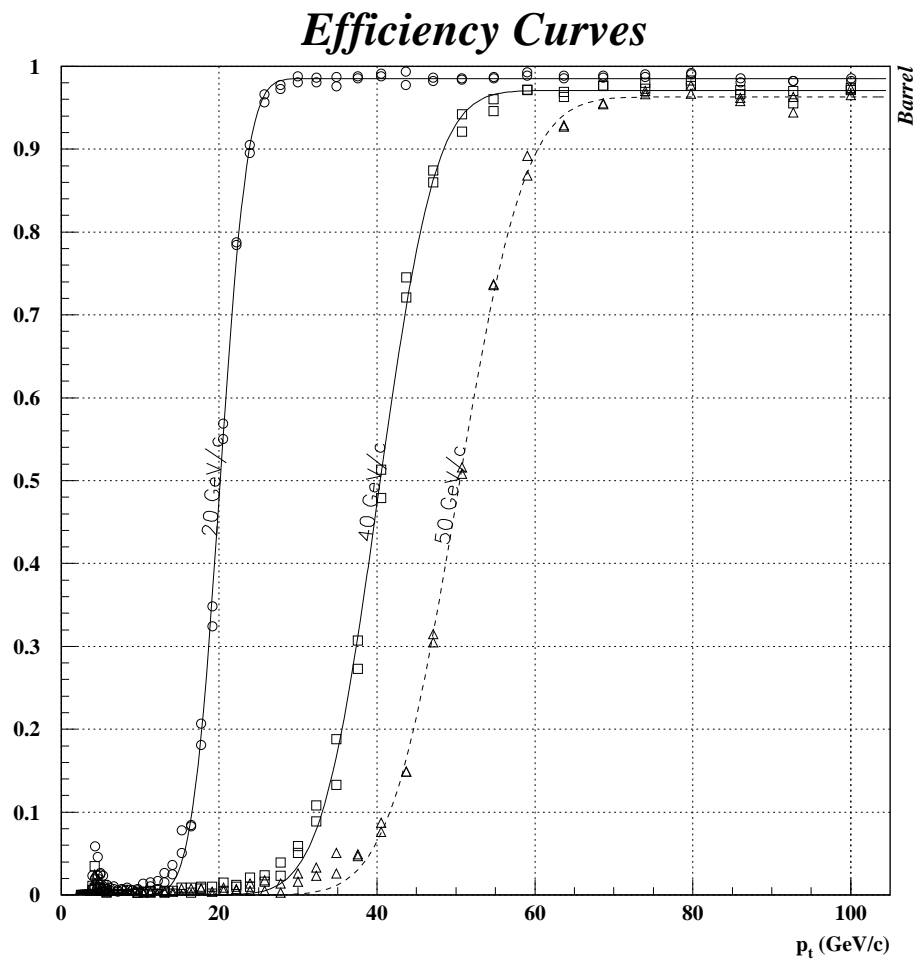


Figure 7.12: These efficiency curves show a bump at a transverse momentum of 5 GeV/c

Sagitta for PAU

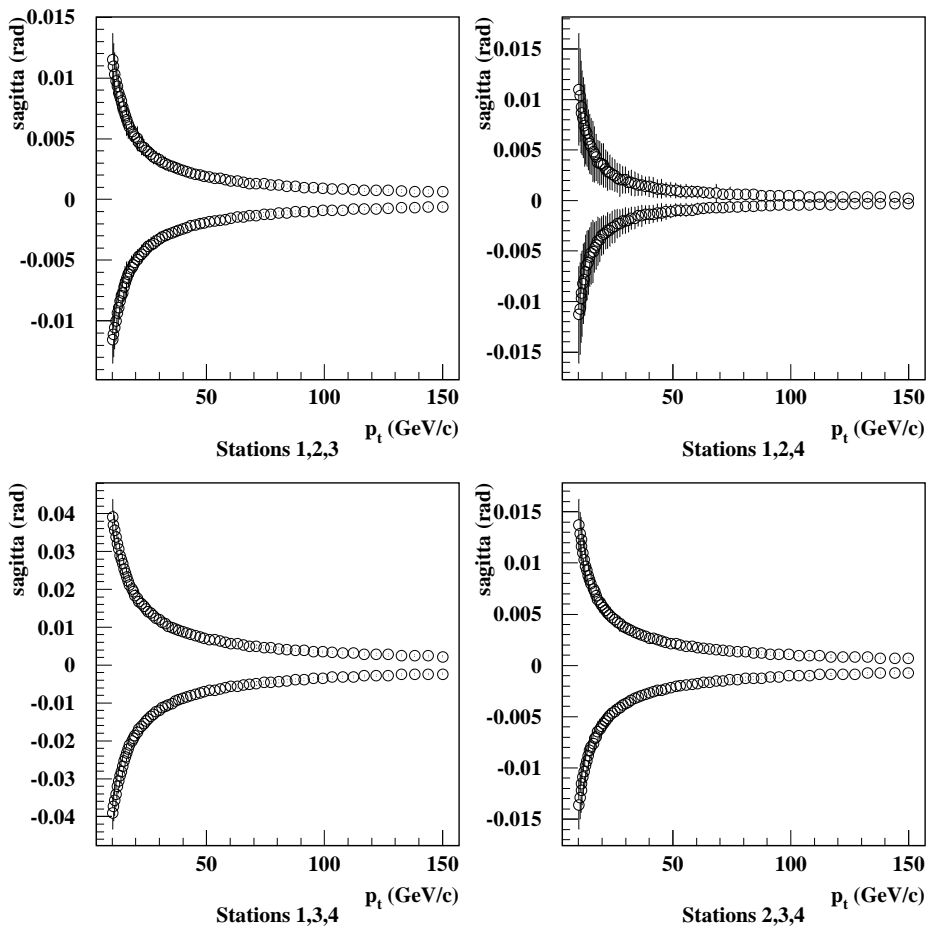


Figure 7.13: Sagitta as a function of transverse momentum p_t for all station triples

The first line in that equation corresponds to a tree of subtractors, requiring a total of three subtractors. The second line represents an implementation that adds three quantities at once with a three-input adder. The multiplication by two is implemented by a bitwise left-shift by one binary digit.

7.2.3 Implementation in Hardware

Hardware implementation of the p_t -assignment algorithm can be divided into two tasks. The primary task is the p_t -assignment itself and has been already described for each of the assignment methods. The second task is to decide which p_t -assignment method is to be used for a given track. For a track with track segments in only stations 1 and 2, for example, there are three possibilities: use the bend angle from station 1 only, the bend angle from station 2 only, or the difference of the azimuthal positions. In that example, using the difference of azimuthal positions yields the best resolution and is the method of choice.

The optimal p_t -assignment method is chosen by converting the quadruple of track segment qualities of the track to a code that determines which method is to be used. That conversion can be implemented with a look-up table. The reason for using the full quality information and not only the 1-bit information (station present/not present in the track) is that it provides the possibility to take into account the resolution with which the track segment quantities have been measured. Recall that the track segment's bend angle is much more precise, if both superlayers of the chamber contribute to the track segment.

That method code is used as select input to a multiplexer which routes the result from the selected p_t -assignment method to the output. In that implementation all p_t -assignment methods run in parallel and offer their outputs, but only one of them is chosen.

7.2.4 Resolution

The p_t -assignment has a measurement error and hence a finite p_t -resolution. Several effects contribute to that measurement error:

- The trajectory of the muon in matter is not deterministic due to
 - multiple scattering in the material of the calorimeter and the iron yoke (section 5.2.1) and
 - energy loss fluctuations and catastrophic energy loss (section 5.2.2).

Those effects come into play primarily at low momenta.

- The intrinsic trigger primitive resolution (section 3.1). It is the dominant effect at high p_t .
- η/ϕ -dependence of the track behaviour. The exact form of the relationship between bend angle/sagitta and p_t depends on the location of the track (sections 7.6.2,7.6.3). The look-up tables used for p_t -assignment take that effect only partly into account. Each chamber can have its own look-up table, but all tracks passing through the chamber, no matter whether they pass in the corner or the center of the chamber, will be processed with that look-up table.
- Chamber misalignment. The actual chamber position will deviate from its nominal position. There is an alignment system in place to determine its actual position, but that too has a finite resolution. However, the resolution of the alignment system should be better than the off-line resolution of the muon chambers of approximately 200 μm , so this effect is negligible compared to the other factors mentioned.
- Spread of the vertex. The vertex position is used implicitly as a virtual measurement. With the vertex size of about 15 μm this contribution is completely negligible.

Another important effect is background-related. Background hits in the vicinity of the real hits of the muon track can be included in the track instead of the real muon hits and distort the p_t -measurement.

Assessing the importance of the different factors, it can be said that at low p_t the measurement is limited by multiple scattering and at high p_t by the trigger primitive resolution.

Figure 10.1 shows the simulated p_t -resolution for the algorithm described.

7.2.5 Charge Sign

p_t -assignment includes the determination of the particle's charge sign. The charge sign is directly related to the sign of the bend angle or sagitta and can be stored in the p_t -assignment look-up table along with p_t . Charge assignment is unproblematic at low momenta. Track curvature is large and it is easy to determine the curvature's sign. At high momenta by contrast curvatures are low, the tracks are almost straight and determining the charge sign gets increasingly difficult. Wrong assignment becomes more and more probable.

7.3 Direction Assignment

7.3.1 Pseudo-rapidity η

There are two ways to determine the pseudo-rapidity η . The first way is to derive it from the combination of z -wheels contributing to the track. A track of $\eta = 0$, for example, will stay in the central wheel (wheel 0). As η increases, the track will pass station 4 in wheel 1, increasing η further, the track will pass stations 1 and 2 in wheel 0 and stations 3 and 4 in wheel 1 and so on. Figure 7.14 shows η -assignment based on this method. It can be seen that the η -resolution varies widely with η .

A complementary approach is to do track finding in the (z, R) -projection in parallel with track finding in the bending plane. Tracks found in the (z, R) -projection come directly with their η . Their ϕ is known roughly from the ϕ -sector in which they were found. Those two values (η, ϕ) can be used to match tracks found in either projection and use the more precise η of the track found in (z, R) .

7.3.2 Azimuth ϕ

The azimuthal location of the track ϕ can be determined from the measured azimuthal position values of the track segments forming that track. The track segment's azimuthal position is given with a resolution of 12 bits and refers to the axis of the sector in which the track is found. The azimuthal position to be output to the global muon trigger should have a resolution of 8 bits and refer to the global detector coordinate system. The easiest implementation is to use the 7 or so most significant bits of the track segment's ϕ as input to a look-up table that performs the mapping to the global coordinate system.

An open question is the reference surface for the ϕ value (section 3.3). The reference surface requiring least hardware expense is the innermost muon station that has a track segment belonging to the track. That means, however, that different tracks can have different reference surfaces. Using existing extrapolation look-up tables, one could extrapolate back from that innermost station to muon station 1 and use the latter as reference surface. The hardware expense for that solution is moderate. If ϕ at the vertex is desired, additional look-up tables have to be introduced for that extrapolation. Due to the long lever arm of such an extrapolation, the ϕ -resolution at the vertex would be rather poor.

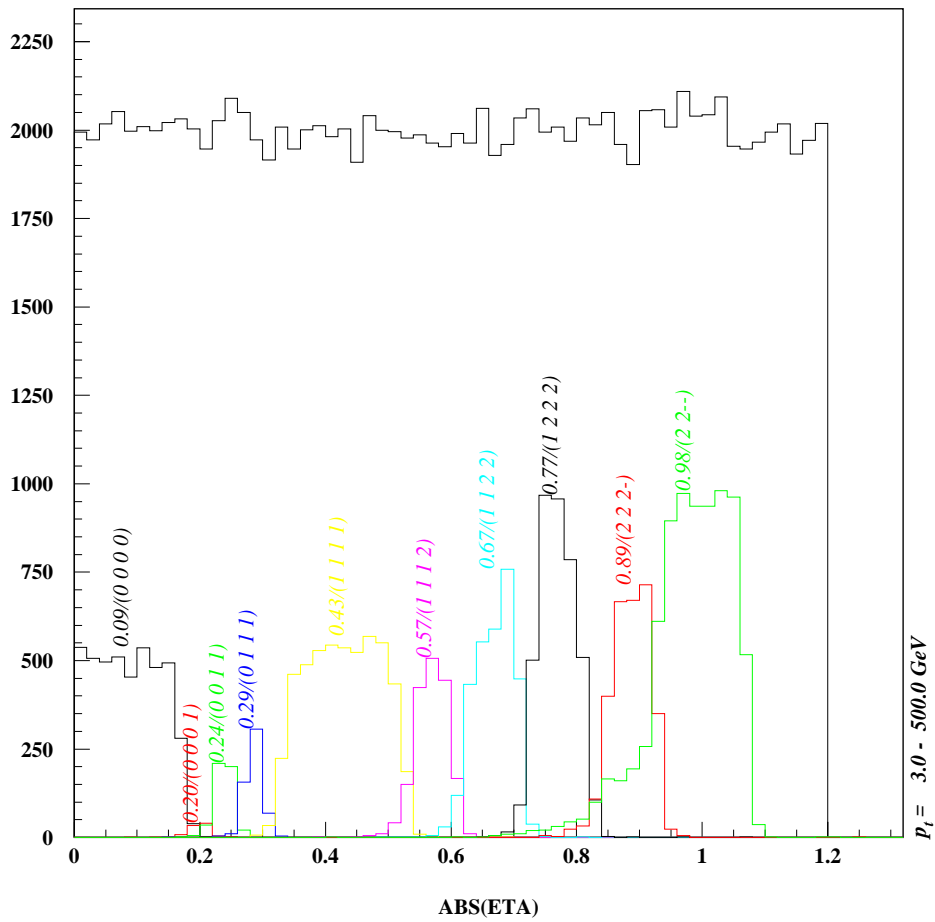


Figure 7.14: The pseudo-rapidity η is assigned from the combination of z -wheels that contribute to this track. Each of the peaks in the histogram has a label that indicates the η of the mean of the peak and the corresponding z -wheel combination

7.4 Quality Assignment

The quality of a track is determined from the qualities of the contributing track segments. A missing track segment is assigned a quality of 0. Hardware implementation is a simple look-up table.

7.5 Selection Steps

At several stages, the trigger algorithm has to perform selections. Selection serves to reduce combinatorics and to suppress background. For example, track segment pair matching has to compare one source track segment in a given station to up to 12 target track segments in a different station. It is very unlikely that all those 12 target track segments exist, and even less likely that they all match. Each potential match, however, has to be provided for in hardware and the expense for the hardware would increase dramatically due to the combinatorics of all the possible matches. For these reasons, it is both safe from the point of view of performance and economical from the point of view of hardware implementation to make a selection among the 12 possible matches of the example and pass on only two to the next stage.

Selection is also important from the point of view of background suppression. The chamber trigger logic generates a high number of ghosts (section 3.1.1). A single muon track of 10 GeV/c creating a track segment in a chamber has a probability of about 45 % to give a second track segment in the same chamber. The second (ghost) track segment is usually close to the muon track in position and bend angle. It is therefore likely that it, too, will match a track segment matched by the first track segment. This gives rise to ghost tracks in the track finder, for instance the bifurcating tracks shown in figure 7.15. The ghost track segment usually has a lower quality than the ‘right’ track segment. This can be used to perform a selection based on the quality of the track segments forming a track. Such a selection can reduce the fraction of ghost tracks in the track finding output to less than 4 %. Moreover, the design of the trigger primitive generation is being modified to reduce the rate of ghost track segments generated.

The price to pay for all kinds of selection is a drop in efficiency, particularly in the case where two muon tracks are close to each other in angle. The consequence is a worsening of the two-track resolution.

Selection criteria that can be applied at the various selection stages are

- Track class. A priority-ordering is defined on the set of track classes, see section 7.1.

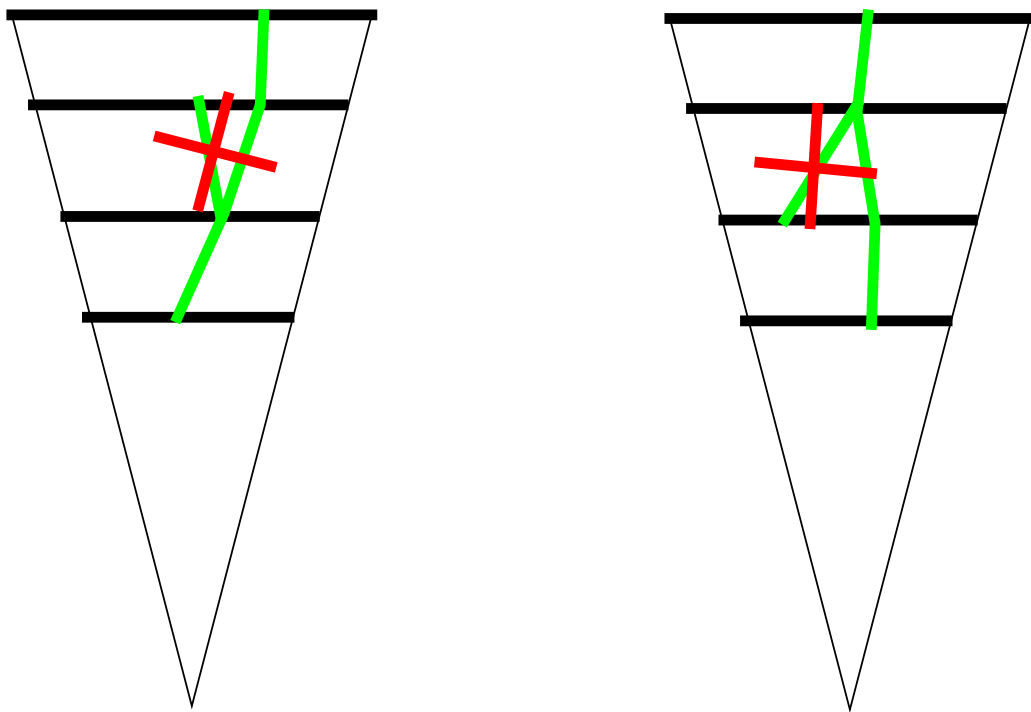


Figure 7.15: Ghost tracks and their cancelation in one sector of the muon system. These ghost tracks here are due to ghost track segments, which are close to the real track segment.

- Track segment qualities. These are the best indicators to decide whether a track segment is real or a ghost.

7.6 Feasibility

The previous sections have described a possible algorithm for the regional muon trigger. The present section discusses some of the aspects related to the feasibility of that algorithm. First of all, the algorithm should be feasible from the point of view of physics: that means that all assumptions made about track behaviour are borne out and that the algorithm can maintain good efficiency of finding muons while effectively suppressing background. Secondly, the algorithm should be implementable in hardware. Along with the discussion of the individual components of the algorithm, hints on their possible hardware implementation have been given. A detailed study of a hardware implementation can be found in [40].

The track finding algorithm described proceeds independently in two two-dimensional projections. This requires that those projections ‘decouple’. That is the topic of subsection 7.6.1.

Closely related is the topic of η - and ϕ -dependence of track behaviour. The presented algorithm takes η and ϕ of the tracks only partially into account for both track finding and p_t -assignment. It has to be shown that this approach is valid (subsections 7.6.2,7.6.3).

A third issue is the tradeoff between efficiency and purity whenever a cut is made in pattern recognition. The cut under discussion in track finding is the size of the upper bound on the deviation to be used in matching track segment pairs by extrapolation. That this threshold is small compared to the chamber size has already been demonstrated in section 7.1.3.

7.6.1 Decoupling

A particle trajectory is a three-dimensional object. It can sometimes be advantageous to work only with two-dimensional projections of the trajectory into two independent planes (section 6.1). This section shows that in the barrel region, the two projections decouple approximately. The two projections used in this context are

- the bending plane projection — the projection of the trajectory into the plane perpendicular to the magnetic field axis; it maps each point (x, y, z) to (x, y) .
- the (z, R) -projection — it maps each point (x, y, z) to $(z, R = \sqrt{x^2 + y^2})$.

By decoupling I mean that one can perform track finding in the bending plane without knowing the track's pseudo-rapidity η and track finding in the (z, R) -projection without knowing the track's ϕ more precisely than what is defined by the muon system's segmentation into sectors and wheels.

The first statement — one can approximately perform track finding in the bending plane without knowing the track's η — follows from the fact that the track behaviour depends only very weakly on η . This weak dependence is shown in section 7.6.2.

The second statement — one can approximately perform track finding in the (z, R) -plane without knowing the track's ϕ — follows from the observation that the trajectory in that projection is very close to a straight line (section 5.1.2).

7.6.2 η -Dependence

In the barrel, the projection of a track of given transverse momentum p_t into the bending plane does not depend strongly on the track's pseudo-rapidity η . This section will explain first why that is advantageous for the design of the trigger device, and secondly what the reason behind that weak dependence is.

Section 6.1 pointed out that track finding can be performed either in projections or in three-dimensional space. It was also mentioned that track finding in projections is easier to implement. For that reason, the preferable solution for track finding in the muon trigger is to find tracks in the (z, R) -projection and the (x, y) -(bending)-projection independently. That means that when determining whether a subset of track segments is compatible with having been caused by a muon track, one does not know the exact η to which these track segments correspond. Knowing the chamber and hence the z -wheel of the track segment gives of course a rough estimate of η . If the η -dependence of track behaviour were very strong, then one would have to know the track's η precisely in order to perform track finding.

A similar reasoning applies to p_t -assignment. p_t -assignment is more precise, if one takes the track's pseudo-rapidity into account to full precision. Using only the coarse information on η derived from the z -wheel in which one operates, yields a worse resolution for p_t . How serious that effect is, depends again on how strongly quantities such as bend angle and track curvature for a given p_t depend on η . Because that η -dependence is not very pronounced, one can assign p_t without knowing η very precisely and can implement the algorithm with minimal hardware expense.

Now let me come to the reasons why the η -dependence is weak. The particle's trajectory is defined by its interaction with the magnetic field and

the matter it passes. As for the magnetic field, the track's equation has been derived in section 5.1 and the projection of the track into the bending plane depends on the track's transverse momentum p_t and the value of the magnetic field only. As long as the field is uniform, the effect of the magnetic field is indifferent to η . The next contribution to the track's trajectory is the deterministic part of energy loss ($\frac{dE}{dx}$). It results in a decrease of the particle's energy and hence transverse momentum as it passes through matter. After having traversed a path length s_t (s_t is the path length of the track in the bending plane projection), the particle acquires a reduced transverse momentum given by

$$p_t(s_t) = p_t(0) + \int_0^{s_t} \frac{dp_t}{ds'_t} ds'_t$$

From

$$\begin{aligned} p &= p_t \cosh \eta \\ s &= s_t \cosh \eta \end{aligned}$$

with p being the particle's momentum and s the full three-dimensional path length, follows

$$\frac{dp_t}{ds_t} = \frac{dp}{ds}$$

Furthermore

$$\frac{dp}{ds} \approx \frac{dE}{ds} \approx \text{const at the Fermi plateau}$$

The first approximate equality holds for relativistic particles, the second follows from the shape of the energy loss curve (section 5.2.2) at high momenta. That means that $p_t(s_t)$ does not depend on η in this approximation, which holds for high momenta. We however expect some η -dependence for low momentum tracks.

Figure 7.16 verifies these results.

Figure 7.17 shows two muon tracks with $p_t = 5 \text{ GeV}/c$ superimposed. In spite of the fact that their η differs by 1.0, their projections are still very close to each other.

It should be pointed out that the results presented hold for the barrel region, where the magnetic field is uniform. In the endcap the magnetic field is not uniform and varies rapidly; the consequence is that track trajectories depend strongly on η and the two projections do not decouple.

7.6.3 ϕ -Dependence

The polygonal symmetry of the CMS detector's muon system results in a ϕ -dependence. That is due to the fact that the distance between the chamber

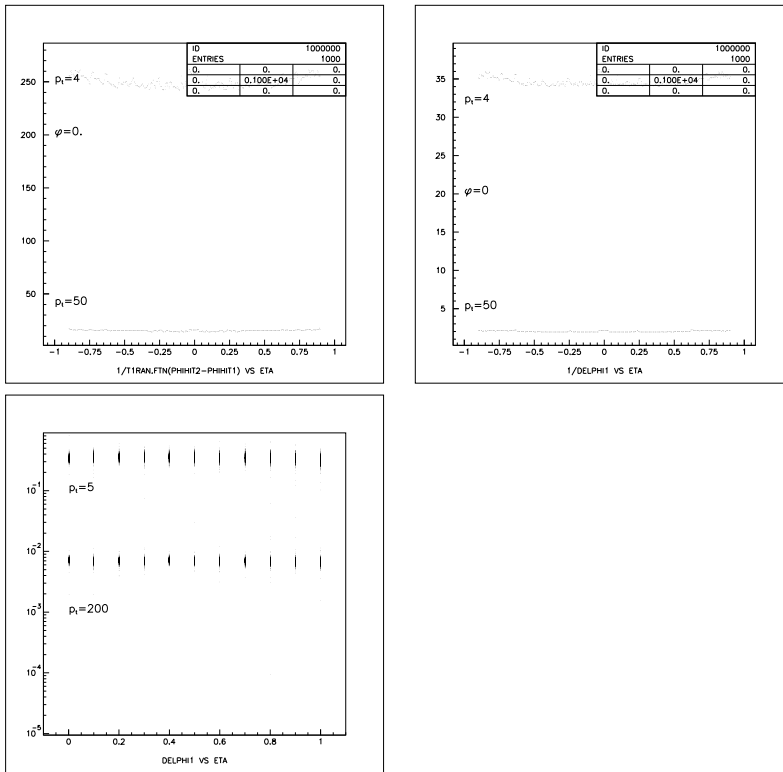


Figure 7.16: η -dependence:

The top left diagram shows the inverse of the bend angle as determined from the difference of azimuthal hit coordinates in stations 1 and 2 as a function of the track's η for two values of p_t .

The top right plot shows the same for the bend angle obtained from station 1 alone.

The bottom diagram shows the spread in bend angle caused by multiple scattering and energy loss fluctuations for a set of discrete η , and allows to compare that effect to the effect of η -dependence. One sees that the latter effect is negligible compared to the former.

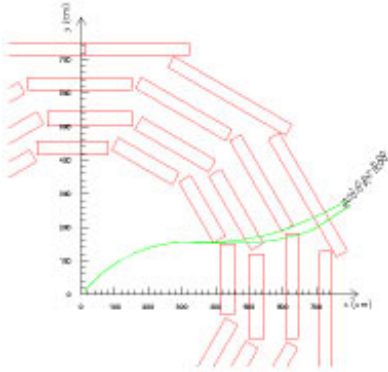


Figure 7.17: η -dependence: Two muons, one with $\eta = 0$, the other with $\eta = 1$; their p_t is 5 GeV/c. Despite the large difference in η , the projections of the two trajectories almost coincide.

and the origin differs between the center and the edge of the chamber, since the chambers are planar and not cylindrical. The radius where the track crosses the chamber hence depends on ϕ and varies by about 20 cm. Figure 7.18 shows that the effect is more pronounced at low transverse momentum and is negligible compared to the spread due to multiple scattering and energy loss fluctuations.

7.7 Assessment

Section 3.4.1 has defined the requirements on the trigger device. The current section will verify whether the presented design meets those requirements, and whether a hardware implementation based on this algorithm has the potential to meet the requirements.

- Physics performance. This is discussed in section 10.
- Latency. Depends on the hardware implementation. A full description of a possible hardware design is given in [40]. The conclusion of that reference is that the algorithm can be completed within 14 bunch crossing intervals.
- Deadtime. The algorithm lends itself to a pipelined design, which is inherently deadtime-free.
- Flexibility. All parameters of the algorithm are stored in RAM-based look-up tables, rendering modifications in situ trouble-free. The initial

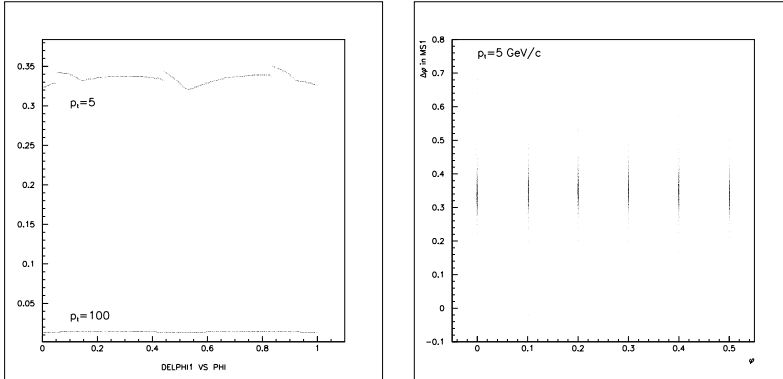


Figure 7.18: ϕ -dependence:

The left plot shows the bend angle in station 1 as a function of the track's azimuth at the vertex, for two values of p_t . The right plot compares the relative effect of multiple scattering and ϕ -dependence over the ϕ -range of one sector.

set of parameters will be based on simulation results and can be updated using real data once the experiment starts taking data.

Several handles are built into the algorithm to cope with higher than expected backgrounds. Input track segments can be rejected if their quality is below a set threshold. By default, all track segments, even those based on only 3 layers out of the 2×4 layers of a chamber, are accepted. The size of the extrapolation window for track segment matching can be scaled by a p_t -dependent scaling factor. That allows to keep the full acceptance for the more interesting high- p_t tracks while reducing the acceptance for low- p_t tracks. The number of track classes accepted can be decreased. By default, even a track producing track segments in stations 3 and 4 only is accepted.

- Errors. Recording the trigger's input and output data as well as the state of the system at intermediate stages allows easy diagnosing by comparing the recorded data with those expected from the algorithm's simulation software. The hardware implementation presented in [40] provides for recording of those data.

7.8 Endcap and Overlap Regions

Up to now the triggering algorithm in the muon system's barrel region has been discussed. In this region the design of trigger primitive generation is

well advanced. By contrast, in the endcap, where cathode strip chambers are used, the design of the chamber trigger logic is still in a very early stage. For that reason, only some very preliminary ideas have been developed for that region.

For reasons of economic use of resources, both in terms of time spent on development and money spent on hardware, it is desirable to use a design in the endcap region that is as close as possible to the one in the barrel region. Ideally, the same hardware ought to be used.

There are, however, fundamental differences between the barrel and the endcap region. The η -dependence of track behaviour is much stronger in the endcap than in the barrel (see the discussion in section 7.6.2 for the barrel). This is mainly due to the fact that the magnetic field in the endcap is not uniform. In the barrel, the slight η -dependence is taken into account only by providing separate look-up tables for each wheel. For example, a track passing station 1 in wheel 0 and station 2 in wheel 1 will have its p_t assigned according to a look-up table for wheel 0. That approach will not be sufficient to achieve satisfactory momentum resolution in the endcap. There are two possible solutions to that problem.

One solution is to work in all three dimensions instead of in the two projections independently. The algorithm in that case uses both the track segment's wire and strip data to fix the track segment's point and direction in three-dimensional space. Look-up tables are then two-dimensional and accept both the track segment's wire and strip data to perform extrapolation and assign p_t . This method, while very appealing from an esthetic point of view, has a major drawback in implementation. The chamber trigger logic cannot resolve the ambiguities between wires and strips. If two particles cross the chamber, two wire and two strip track segments will be output, but which wire belongs to which strip will not be known. The algorithm thus has to work with four three-dimensional track segments, increasing the hardware expense.

The second solution is to take η -dependence into account by using a different look-up table for each combination of R -rings. In the barrel the algorithm uses the same look-up table for all extrapolations from wheel 0, no matter whether the extrapolation is to wheel 0 or wheel 1. The endcap muon system is physically segmented into rings along radius R . By using a different look-up table for extrapolation from ring 0 (innermost ring) to ring 0 and from ring 0 to ring 1, η is taken into account more precisely.

For the purpose of this study, the second approach has been adopted. Apart from the difference in using additional look-up tables, the algorithm studied is identical with the one in the barrel. A few parameters are different, because in the endcap neighboring chambers overlap and geometric accep-

tance is higher than in the barrel. For that reason, one can use a more restrictive track finding criterion, and require at least three trigger primitives to form a track.

Extrapolation and p_t -assignment can proceed as in the barrel. Figure 7.19 shows extrapolation in the endcap, and figure 7.20 shows how the angle measured by the strips can be used for p_t -assignment.

The overlap zone is the region of η where tracks pass chambers both in the barrel and the endcap muon systems. Figure 7.21 shows a longitudinal cut through the muon system with tracks in the overlap zone.

This zone is the most challenging one. The η -dependence of track behaviour is even stronger than in the endcap because the magnetic field changes direction from a uniform field along z in the barrel to a radial field in the endcap. There are two different detector types, with different segmentation and possibly different trigger primitive data formats. Moreover, the algorithm in the barrel is simplified by the fact that the muon chambers can be essentially treated as coaxial cylinder shells at fixed radii R , and in the endcap the muon chambers can be viewed abstractly as disks at fixed values of z . The overlap zone does not profit from such simplifications.

The easiest option would be to simply find tracks in the barrel and the endcap independently. A later stage could then combine those independently found tracks. Such a design, however, could not find a track at $\eta = 1.1$, which passes only station 1 in the barrel and thus produces no track in the barrel track finder, and passes only station 1 and 2 in the endcap and thus gives no track in the endcap track finder, which requires at least three stations for a track. The result of that would be a dip in the acceptance curve at the overlap region of η .

Having dismissed the easiest way out, we have to come up with a scheme to combine barrel and endcap trigger primitives to tracks. Can extrapolation be used to match barrel and endcap trigger primitives?

Extrapolation from the endcap to the barrel is ambiguous even if one uses three-dimensional trigger primitives by joining the strip and wire trigger primitives.

Three-dimensional extrapolation from the barrel to the endcap works very well in principle. However, in that region of η the crossing angle in the (z, R) -projection between track and chamber is outside the angular acceptance range of the mean-timer algorithm, and only the bending-plane track segments will be available. If one performs extrapolation using the bending-plane track segment only, one suffers from the strong η -dependence, which can be taken in account only partially by using a different look-up table for each z -wheel in the barrel/ R -ring in the endcap pairing. That problem can be tackled by using wider extrapolation windows. The drawback of that

Extrapolation FWD; wheels 00

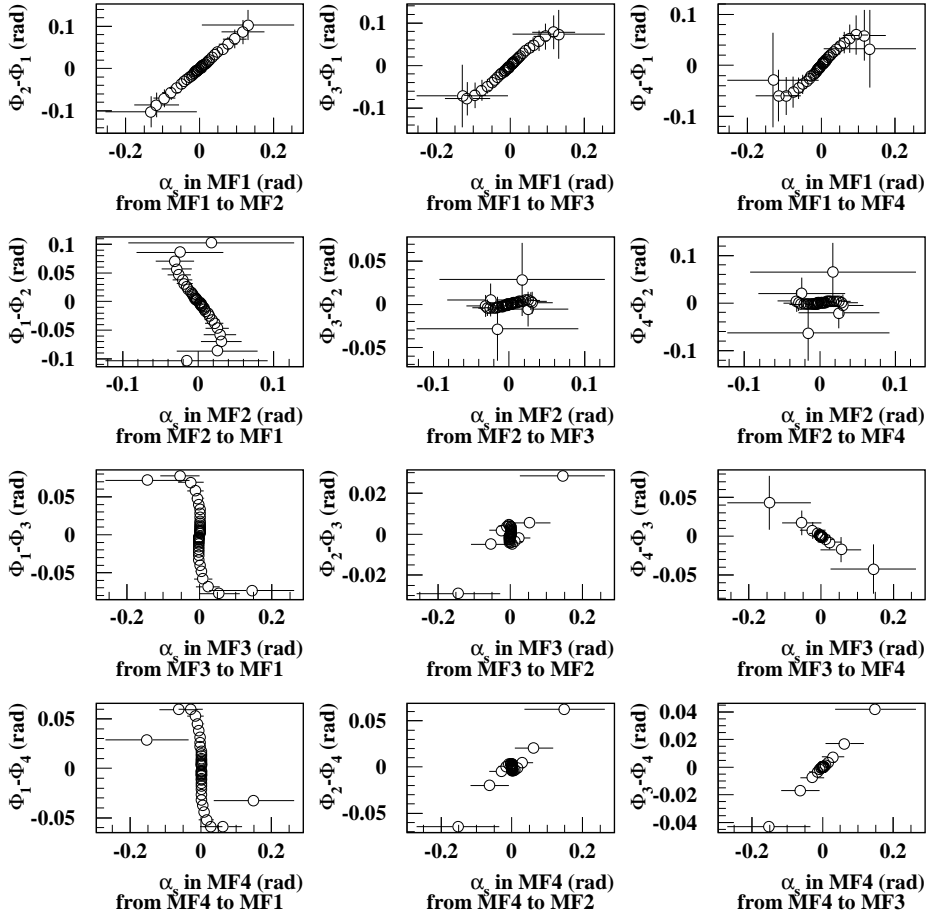


Figure 7.19: Extrapolation in the endcap: The figure shows the relationship between α_s , the angle measured by the strips, of the source track segment and the difference of azimuthal positions of source and target track segment for all station pairings. The error bars show the effects of multiple scattering and energy loss fluctuations. All the plots are for the innermost R -rings (wheels 00) of the endcap muon system. Some of the extrapolations are unambiguous and can be used for track finding, others cannot.

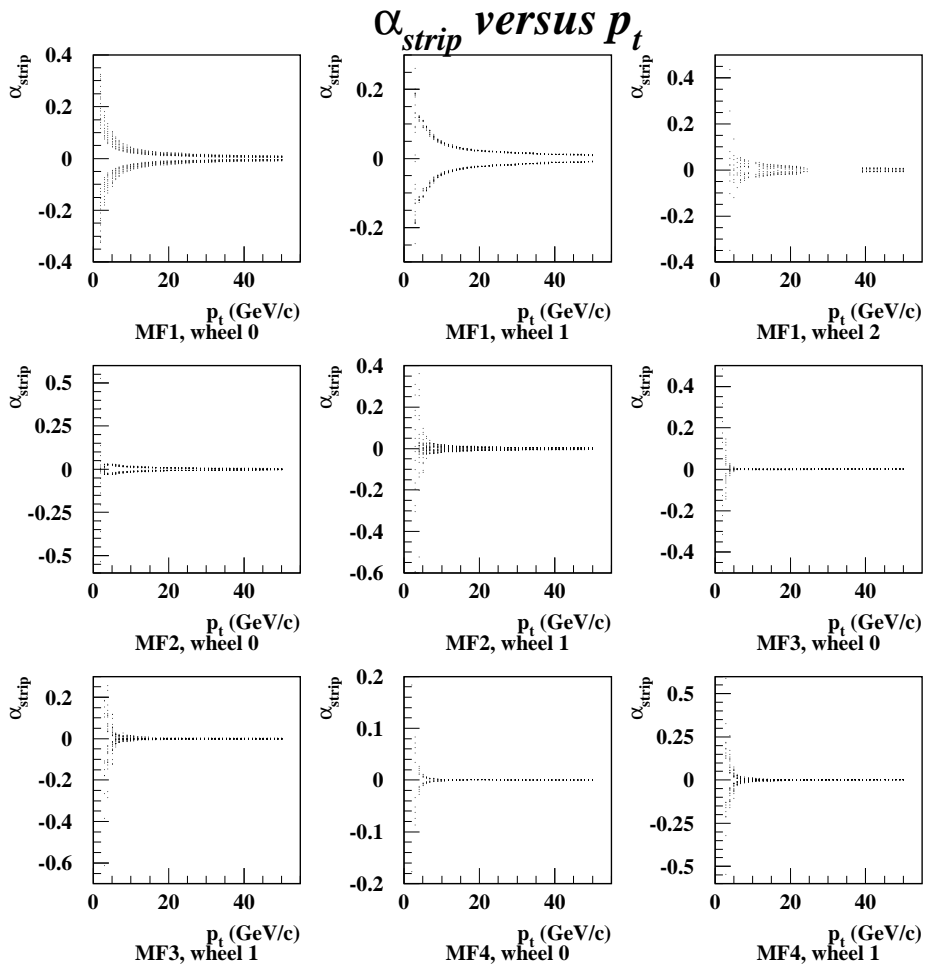


Figure 7.20: p_t -assignment in the endcap: The figure shows the relationship between the strip angle α_s and p_t for all stations and R -rings (=wheels). Muons of both charge signs are included, yielding the two branches shown in each plot. The spread due to multiple scattering, energy loss fluctuations and η -dependence is indicated by the error bars. It can be seen, that this particular quantity can be expected to yield reasonable p_t resolution in rings 0 and 1 of station 1, but not in the other stations.

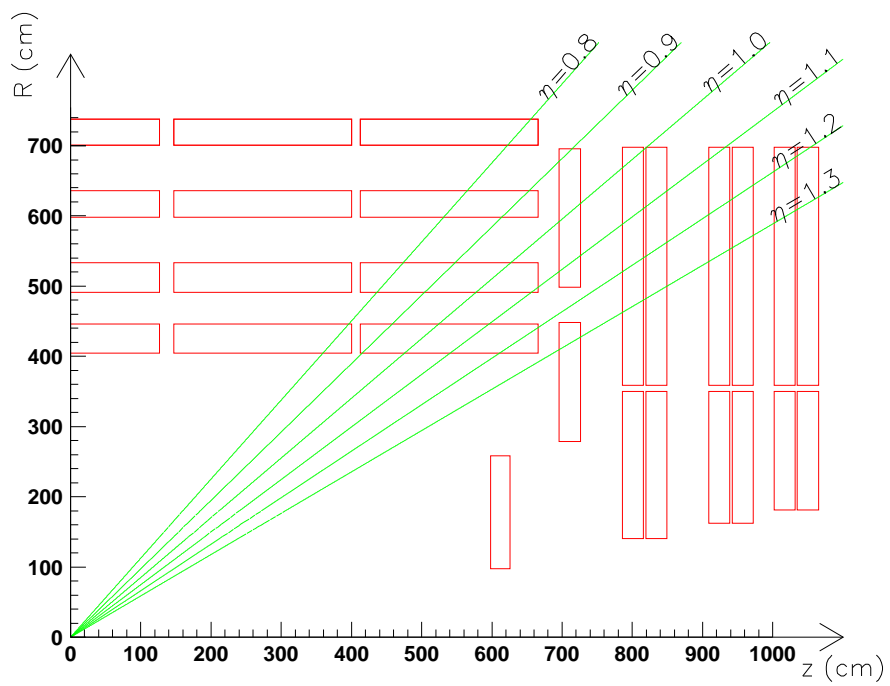


Figure 7.21: Straight tracks in the overlap zone, longitudinal view of one octant of CMS

approach is however that it is sensitive to background and might result in a decrease of purity. That effect cannot be assessed, before a full simulation of the endcap trigger primitive generation is available.

p_t -assignment in the overlap zone can be based on the barrel and endcap algorithms. A mixed mode, where track segment data from the barrel and the endcap are combined into a p_t -measurement, does not seem feasible due to the problems mentioned above.

Chapter 8

Hardware

A detailed description of the trigger algorithm's hardware implementation can be found in [40, 37, 38, 39].

Figure 8.1 shows the top-level block diagram of the hardware. Trigger primitive data from the chamber trigger logic enter the system from the left. The track finder links the track segments to tracks and outputs the *addresses* of track segments that were combined to tracks. Based on these addresses the track segment *data* are extracted from the pipeline, where they have been stored during the track finder's processing, by the track router. The track router passes the track segment data for each found track on to the assignment units, which compute the track parameters from the track segment data.

The hardware shown covers one detector segment, corresponding to a sector of about 30° in azimuth ϕ and a z -wheel of 2.6 m length. Each of these detector segment processors can output up to two tracks. Tracks from the twelve ϕ -segments of one z -wheel are sent to the ring sorter, which selects the four highest-momentum tracks. The ring sorter passes the data of all found tracks on to the global muon trigger [49].

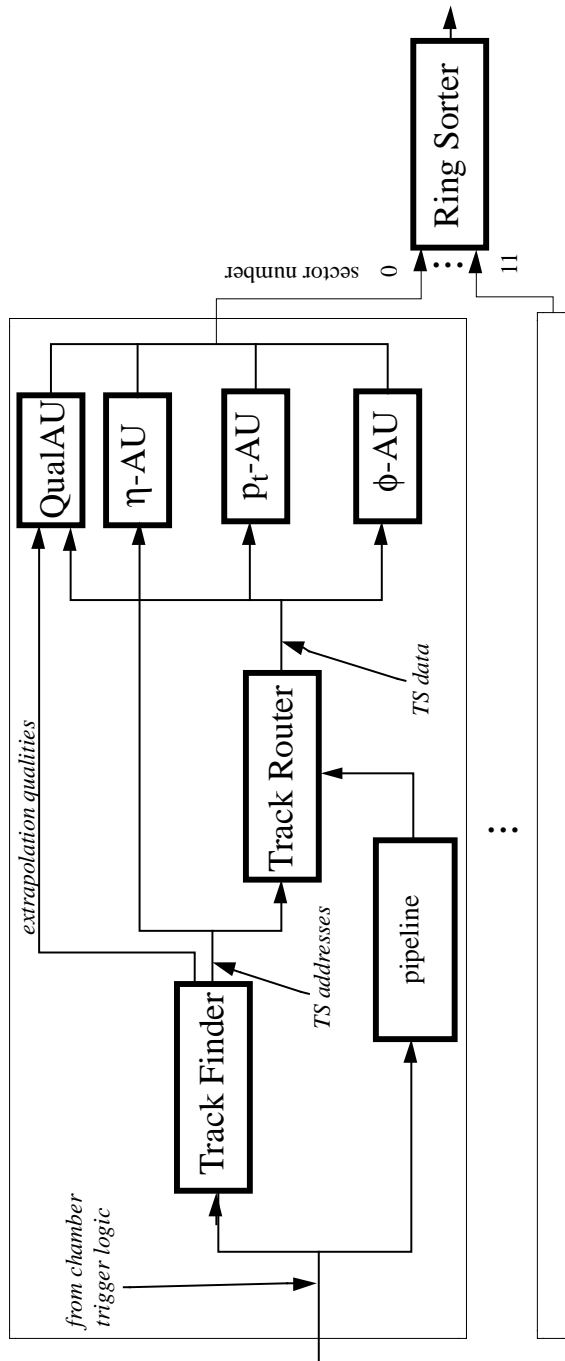


Figure 8.1: Block diagram of the regional muon trigger for one wheel in the barrel.

TS = track segment; AU = assignment unit.

Chapter 9

Simulation Software

A simulation and analysis software package has been written to verify the presented algorithm, assess its performance and optimise its parameters. Detailed documentation of the package can be found in [55].

The primary task of the simulation software is to implement the presented trigger algorithm and to allow assessing its performance. The algorithm had to be implemented with sufficient flexibility to test new ideas and optimise all of its parameters.

The simulation software is integrated into the CMS simulation software package CMSIM [1]. On the input side it provides an interface to the drift tube trigger primitive simulation[28, 58]. Due to the absence of trigger primitive simulation for the endcap chambers, I wrote a very simple simulation for the chamber trigger logic, which takes resolution, geometric acceptance and efficiency into account. On the output side, the regional trigger simulation is interfaced to the global muon trigger simulation code[49].

In parallel to the simulation program described here, a simulation of the hardware design was written in the hardware description language VHDL by A. Kluge[40]. To ensure that both simulation programs deliver identical output for a given input, a set of tools for automatic comparison of their respective output data was created.

Moreover the simulation provides data structures that can be used for visualisation by means of the PAW program [31]. For each simulated event, generated and reconstructed tracks along with data from the intermediate stages can be stored. That serves for assessing the performance of the algorithm by interactively analyzing the output data and for verifying that the simulation correctly implements the algorithm.

Moreover, there is a package of utility programs to

- Test the trigger primitive generation and assess its performance. Results are shown in section 3.1.1.

- Visualise the relationship between quantities such as bend angle and transverse momentum.
- Create the look up-tables required by the algorithm.
- Create test data to be sent to a prototype board of the processor hardware.

Chapter 10

Simulated Performance

This chapter covers the performance of the regional muon trigger algorithm presented in this report. The performance was estimated by simulating physics events as they will take place in the interaction region of the detector and analyzing the response of the detector, chamber trigger logic and regional muon trigger algorithm to these events.

Physics events were generated with the Monte Carlo event generator PYTHIA [53]. The GEANT detector simulation package [30] was used to describe the response of the detector to these events. The setup of the detector with a detailed description of geometry, material and magnetic field was incorporated into GEANT from the CMS simulation software CMSIM [1]. CMSIM contains the simulation of the trigger primitive generation for the barrel muon chambers. The software package described in chapter 9 was used to simulate the regional muon trigger algorithm.

Section 2.3.3 named two important criteria that can serve as figures of merit of a muon trigger.

One of these criteria is the quality of the set of efficiency curves. The efficiency curve for a given p_t -threshold is sigmoid-shaped. The two relevant parameters are the steepness of the curve's slope and the height of the plateau that it reaches for high momenta. Ideally that curve should be a unit step function at the threshold momentum. The finite p_t -resolution of the algorithm leads to a smearing of the sharp edge. At low momenta the resolution is limited primarily by multiple scattering and energy loss fluctuations, at high momenta the intrinsic trigger primitive resolution is to blame for limiting the resolution. The geometric acceptance of the muon system as well as cuts applied by the trigger primitive generation and the regional trigger limit the height of the plateau.

The second important criterion is the purity of the output provided by the trigger. Not all the tracks found by the algorithm are associated with

real muons passing through the muon system. Backgrounds (section 4.2), ghosts created by the trigger primitive generation (section 3.1) and geometric ambiguities conspire to produce ghost tracks.

The following sections present the performance for each of the three zones of the regional trigger processor. The design for the barrel zone is well advanced and the results given are a realistic estimate of its performance. For the endcap and overlap zone, however, the results shown here can be considered only a first estimate of what can be achieved.

10.1 Barrel zone

Figure 10.1 shows the p_t -resolution as a function of the track's p_t . The resolution is due to the effects described in subsection 7.2.4. Moreover, the resolutions that can be achieved vary widely among the different methods described in section 7.2. A track that has track segments in stations 1 and 2 can be assigned a p_t with very fine resolution. A track with track segments in stations 3 and 4 only will have its p_t measured with a much poorer resolution.

Figure 10.2 shows the efficiency curves for the barrel region for p_t -thresholds of 20, 40 and 50 GeV/c.

The contamination of the output tracks by ghost tracks is about 5 % for the trigger primitive ghost rate given in section 3.1.1. Efforts to reduce the ghost rate on the trigger primitive level will improve that number. A residual source of ghosts that is entirely due to the track finding algorithm and not to backgrounds or trigger primitive ghosts is the following: If a track gives track segments in all four stations, and if pairwise matching between e.g. station 1 and 2 on the one hand and station 3 and 4 on the other hand is successful, but there is no match between track segments in station 2 and 3, the track finding algorithm will output two tracks, one consisting of stations 1 and 2 and the other consisting of stations 3 and 4. The rate of this type of ghost is less than 1 % of the total number of tracks.

10.2 Endcap zone

Figure 10.3 gives an idea of the p_t -resolution that could be achieved for an ideal trigger primitive generation. It shows efficiency curves for muon tracks generated with a pseudo-rapidity $\eta = 1.75$.

The following figure 10.4 takes trigger primitive resolution into account. The values assumed for the position and angular resolution of the trigger primitive and for the efficiency of its generation are given in section 3.1.2.

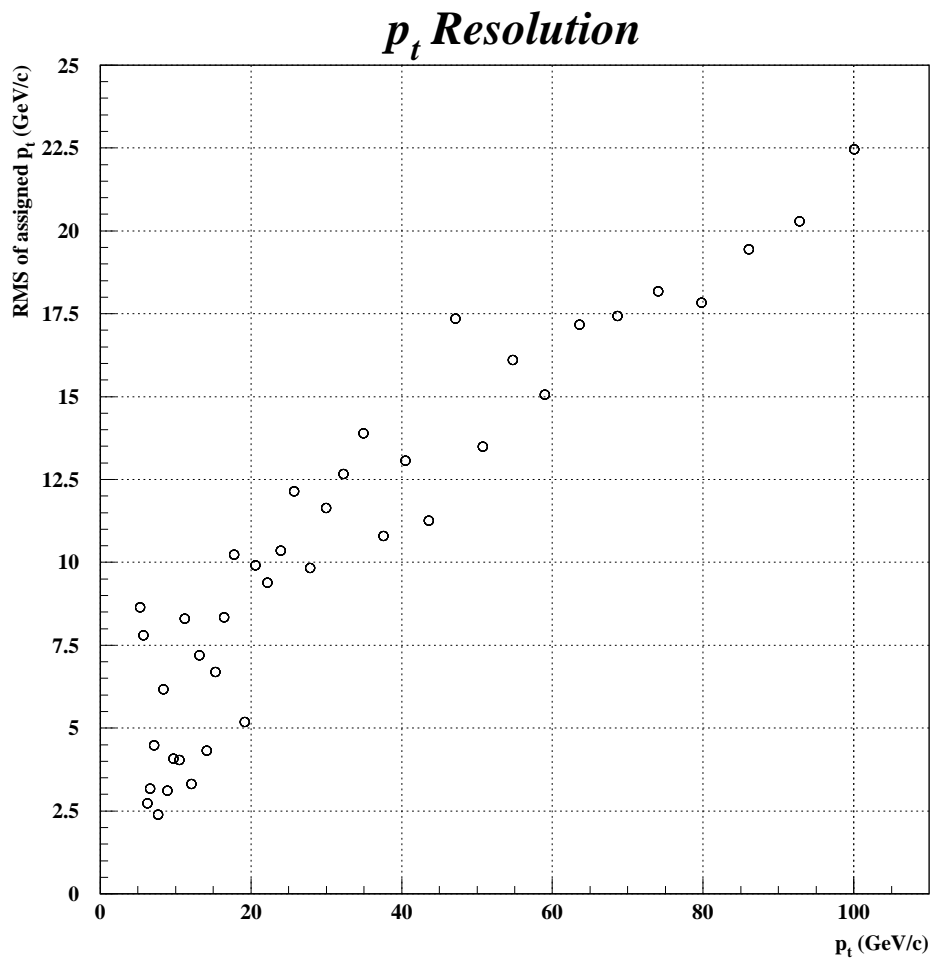


Figure 10.1: p_t -resolution in the barrel zone

Efficiency Curves

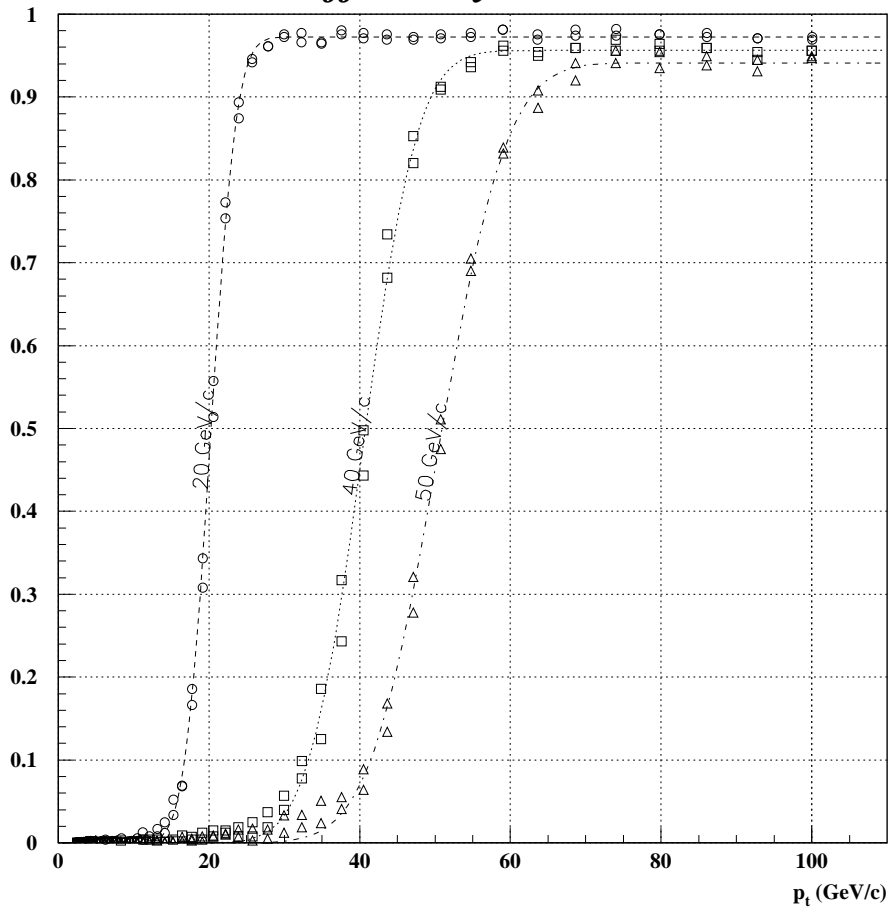


Figure 10.2: Efficiency curves in the central z -wheel of the barrel zone

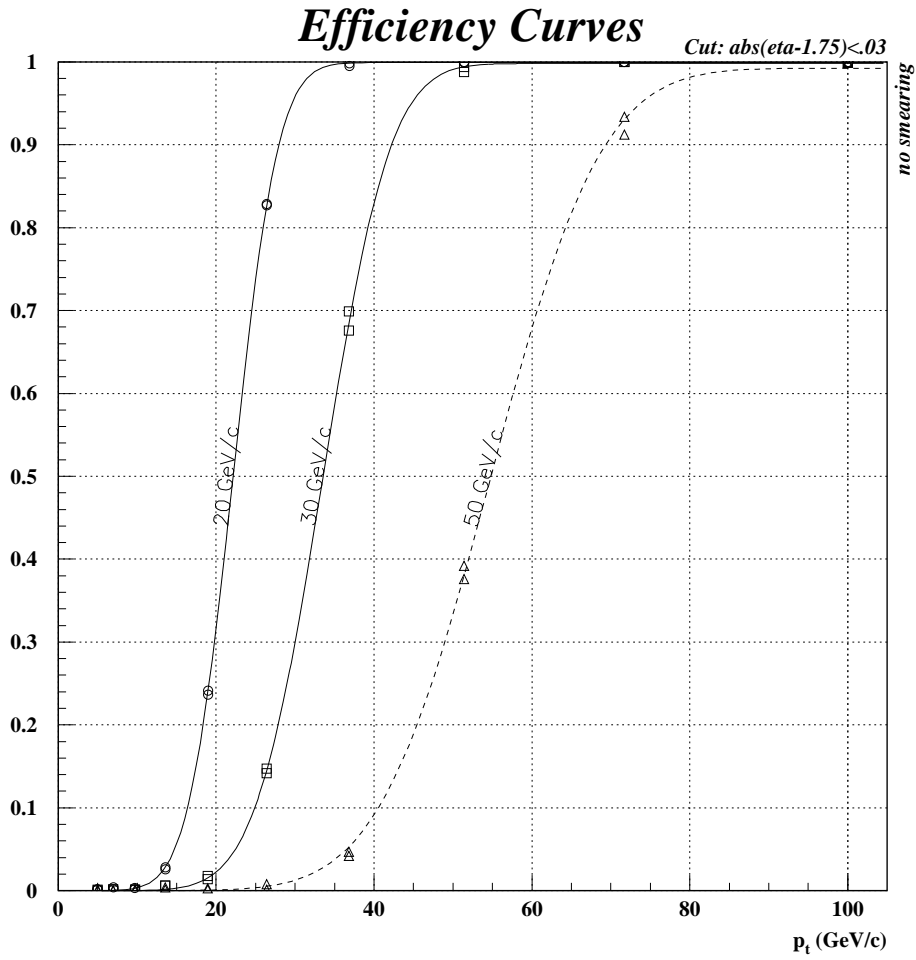


Figure 10.3: Efficiency curves in the endcap zone ($\eta = 1.75$) without trigger primitive resolution effects

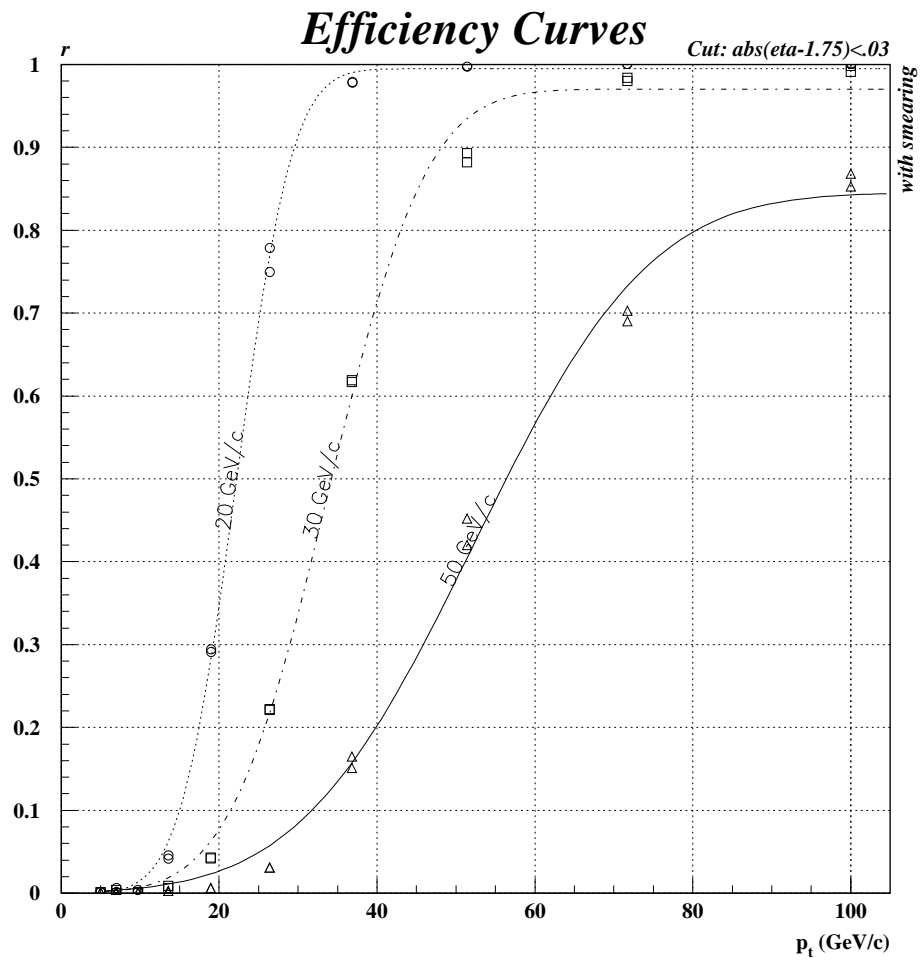


Figure 10.4: Efficiency curves in the endcap zone ($\eta = 1.75$)

10.3 Overlap zone

Figure 10.5 shows efficiency curves for the overlap zone by itself. Note that track finding proceeds in the barrel, endcap and overlap zone independently and in parallel. A track that passes through the overlap zone can be found by all three zone track finders. The figure shows the efficiency for only those tracks found by the overlap zone track finder. The level of the plateau is less than 90 %.

The tracks found by the three zones can be combined to improve the overall track finding efficiency. Figure 10.6 shows the efficiency curves for that case. The plateau reaches almost 100 %.

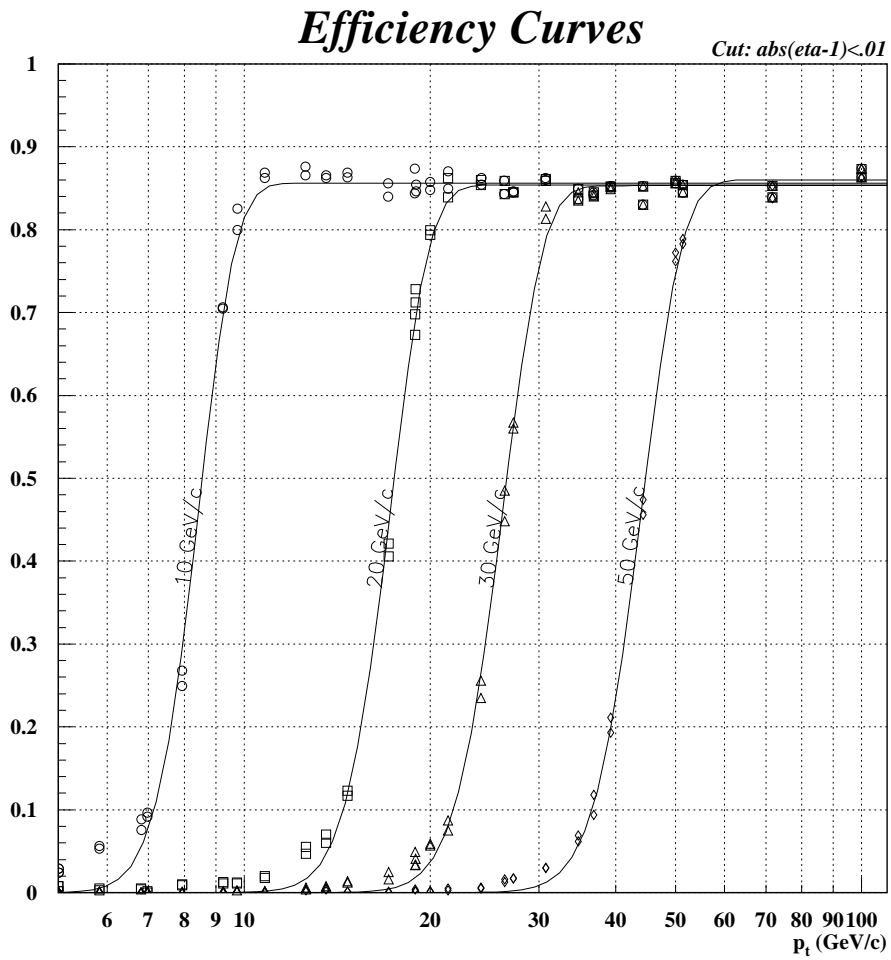


Figure 10.5: Efficiency curves for the overlap zone alone at $\eta = 1$; note that the fit function is misleading at p_t below the threshold

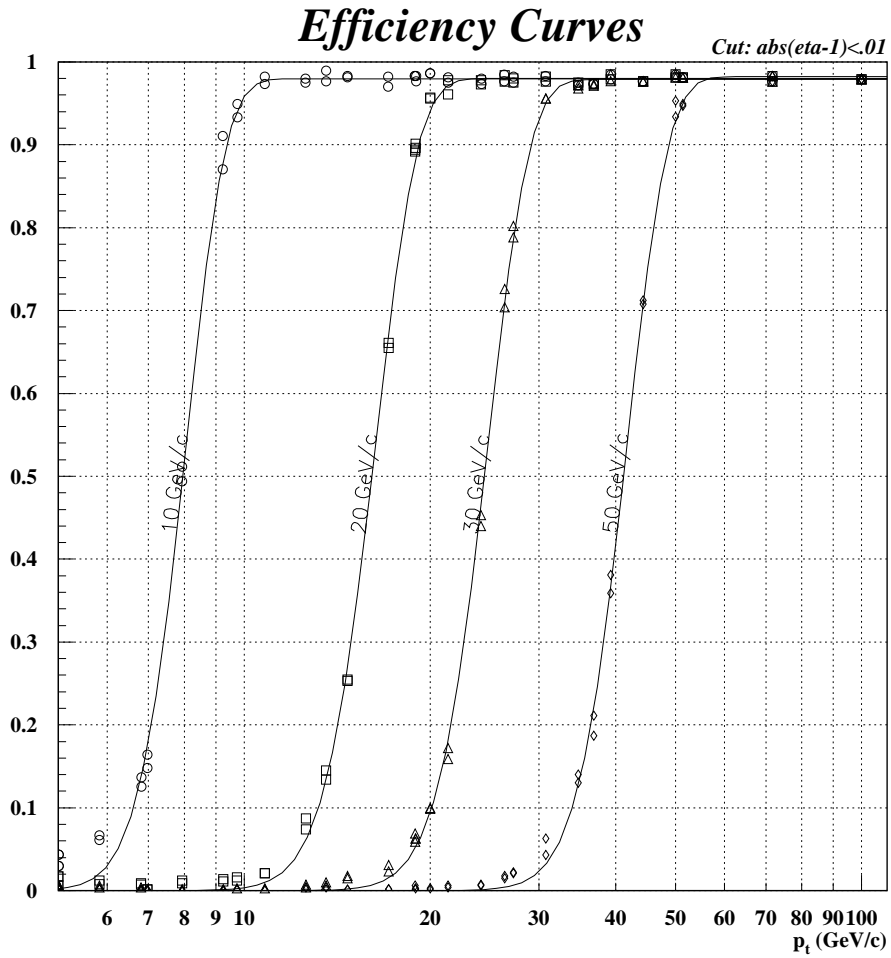


Figure 10.6: Efficiency curves for the track finders of all three zones combined at $\eta = 1$; note that the fit function is misleading at p_t below the threshold

Chapter 11

Operation

This chapter outlines how I imagine the operation of the regional muon trigger, particularly during the startup phase. The first section of this chapter presents ‘operating instructions’ for installing and commissioning the regional trigger.

Error detection is a very important aspect of trigger operation and will be covered in the second section.

11.1 Operating Instructions

The first step before installing the modules is thorough testing. For this purpose a mock-up of the trigger logic of at least one detector segment should be set up. Preferably this mock-up should be integrated with the test facilities of the chamber trigger logic and the global muon trigger, allowing complete testing of the trigger chain including the interconnects. Possibly, the mock-up could even be integrated with a chamber test bench, enabling a combined testing of the analog and digital part of the system with cosmic rays or radio-active sources. After testing all modules individually, they can be installed in their racks in the control room and the whole system can be tested by feeding it simulated data. The next step could again be a test including the chambers, now installed in the detector, using cosmic rays. Cosmic muons do not pass through the detector’s interaction region, so to use cosmic muons for trigger testing, the track finder must not require tracks to point to the vertex. For that end, the extrapolation windows of the track finder have to be wide open and the (z, R) -trigger, which checks that tracks point to the vertex in the (z, R) -plane, has to be disabled.

During the initial low-luminosity phase of the accelerator, where background is not a concern, the trigger’s acceptance can be kept high by using

wide extrapolation windows for track finding.

At first, the look-up tables of the regional muon trigger will be filled with data obtained from simulation. This simulation cannot be completely relied upon to accurately describe the detector, so the look-up tables have to be updated using measured data. The look-up tables used for p_t -assignment can be calibrated by comparing the momenta determined by the trigger with those obtained by the full track reconstruction. The extrapolation look-up tables can be updated most easily, if the extrapolation deviations (see equation 7.1) are histogrammed. The mean of that histogram then represents the correction to be applied to the extrapolation look-up table and the spread is a measure of the extrapolation threshold to be used.

During the initial low-luminosity operation, backgrounds will very likely not pose a problem. If it turns out that backgrounds and rates are higher than expected, several measures can be taken to address that problem. They are listed in section 7.7.

11.2 Monitoring and Diagnostics

The trigger is crucial to the success of the experiment. For that reason errors should be avoided. If they occur, they must be detected, diagnosed and fixed as quickly as possible.

It goes without saying that all trigger modules will be extensively tested before being installed in the control room of the CMS detector by feeding test patterns into the input and verifying the module's test response. For two reasons this is not sufficient to prove that the module is working correctly. First of all, the total number of possible test stimuli is so huge that exhaustive testing is impossible. Secondly, the environment during actual data taking may be very different from the one in the test setup, due to electromagnetic interference from other devices in the neighborhood and temperature effects.

The same test bench that is used for commissioning the modules to be installed in the control room can also serve for testing spares and modules that have been removed from the control room because they are suspected of malfunctioning. It would be desirable to design a common test bench in collaboration with the groups who design the chamber trigger logic and the global muon trigger, so that the whole trigger chain can be tested at once including all the interfaces between its components.

Monitoring the trigger function, while the trigger is in operation, helps to detect errors without disrupting trigger operation. Trigger input and output data are available both on-line and off-line and can be used to compare the actual trigger output with the expected output obtained by running the

trigger simulation code on the trigger's actual input data. An alarm should be raised, if any discrepancy is found.

An additional level of monitoring should be provided by the global muon trigger that combines information from the trigger systems. By logging summaries of the discrepancies between the two systems' output data, it can help to detect rare errors.

Once an error has been reported, diagnosis has to be performed to pinpoint the error. Spy registers on the modules intercept data at the input, intermediate and output stages of the trigger's components and allow tracking down the source of the error. Boundary scan (JTAG) is an IEEE standard, whose objective is to enable a system user to observe a device's input and output pins [36].

A desirable feature is the possibility to inject test patterns into the trigger inputs in situ. This allows testing the modules while they are in their crates, so that there is no need to remove them for testing.

To conclude, I want to stress the importance of planning efficient facilities for testing and diagnosing into the trigger device from the outset.

Chapter 12

Conclusion and Outlook

The present thesis describes my work on the first level muon trigger of the planned CMS experiment. Starting from detailed specifications of the trigger's input, output, task and general requirements, this report lists options for implementing the trigger. Based on a comparison of these options with the requirements, and taking into account the hardware feasibility of these options, it describes the chosen algorithm in detail. Then the feasibility of this algorithm is shown. For each of the steps of the algorithm, hints for possible implementation in hardware are presented. An assessment of the algorithm's compliance with the stated requirements concludes the description of the algorithm.

The performance of the algorithm has been determined using simulation by software. The results are presented and discussed.

A final chapter discusses how I imagine the commissioning and operation of the trigger device, once the CMS detector starts up in the year 2005.

It should be stressed that the presented design is far from final. This report presents a linear process, leading from a specification to a consideration of possible options. Options are assessed with respect to their performance potential and technical feasibility. From this assessment emanates a design that is shown to fulfill the requirements and has satisfactory performance. Real life is more complicated than that and the design process is cyclic. For instance, the input provided by the chamber trigger logic of the barrel drift tubes to the regional muon trigger has not yet been fixed, but had to be adapted to the needs of the regional muon trigger. Similarly, the specification of the output quantities of the regional to the global muon trigger has evolved and is evolving with the global muon trigger's design.

For these reasons, the presented design represents only the current status in the cycle of iterations of the development process. In the years leading up to the actual manufacturing of the device, the specifications will very likely

be redefined as they have been several times during the period that I have been working on the project. In particular for the endcap muon chambers, the input to the regional muon trigger is still not precisely defined because the chamber trigger logic is in an early design stage. Much work remains to be done, and I am certainly curious to see what the final design will be.

Appendix A

The Pseudo-Rapidity η

The pseudo-rapidity η of a track with four-momentum (E, \vec{p}) is defined as

$$\eta := \frac{1}{2} \ln \frac{p + p_l}{p - p_l}. \quad (\text{A.1})$$

where p_l is the longitudinal component of the momentum. It is the limit of the rapidity y

$$y := \frac{1}{2} \ln \frac{E + cp_l}{E - cp_l}$$

in the limit $E \rightarrow cp$. The pseudo-rapidity η depends only on the polar angle θ_p of the momentum:

$$\cos \theta_p = \frac{p_l}{p}.$$

Using $\cos \alpha = \cos^2 \frac{\alpha}{2} - \sin^2 \frac{\alpha}{2}$, we get

$$\begin{aligned} \eta &= \frac{1}{2} \ln \frac{1 + \cos \theta_p}{1 - \cos \theta_p} \\ &= \frac{1}{2} \ln \frac{\cos^2 \frac{\theta_p}{2}}{\sin^2 \frac{\theta_p}{2}} \\ &= \ln \cot \frac{\theta_p}{2} \\ &= -\ln \tan \frac{\theta_p}{2} \end{aligned}$$

If, on the other hand, one wants to compute the polar angle θ_p from the pseudo-rapidity η , the following equations can be used:

$$\theta_p = 2 \arctan e^{-\eta}$$

$$\begin{aligned}\sin \theta_p &= \frac{1}{\cosh \eta} \\ \cos \theta_p &= \tanh \eta \\ \tan \theta_p &= \frac{1}{\sinh \eta}\end{aligned}$$

Bibliography

- [1] CMS Simulation Package CMSIM - User's Guide and Reference Manual.
- [2] Proceedings of the ECFA Large Hadron Collider Workshop, 1990.
- [3] The LHC Conceptual Design Report, 1995.
- [4] S. R. Amendolia et al. The AMchip: a full-custom CMOS VLSI associative memory for pattern recognition. *IEEE Trans. Nucl. Sci.*, Vol. 39, No. 4, 1992:795–797.
- [5] S. R. Amendolia et al. The AMchip: a VLSI associative memory for track finding. *Nucl. Instr. and Meth.*, A315 (1992):446–448.
- [6] M. Andlinger et al. *Nucl. Instr. and Meth.*, A370 (1996):389–395.
- [7] G. Athanasiu et al. Real time track identification with artificial neural networks. *Nucl. Instr. and Meth.*, A324 (1993):320–329.
- [8] C. Baldanza et al. Hardware and software structure of a neural network trigger based on the ETANN and MA16 chips. *Nucl. Instr. and Meth.*, A373 (1996):261–281.
- [9] C. Baldanza et al. Results from an on-line non-leptonic neural trigger implemented in an experiment looking for beauty. *Nucl. Instr. and Meth.*, A361 (1995):506–518.
- [10] D. Best. Tracking mit der Hough-Transformation für die Zentrale Driftkammer des GSI-4 π -Experiments. Diplomarbeit, Universität Mainz, 1992.
- [11] H. A. Bethe. *Annalen der Physik*, 5 (1930) 325.
- [12] S. Cittolin. Trigger and Data Acquisition at Large Hadron Collider. In *Proceedings, 1996 CERN School of Computing*, 1997.

- [13] CMS Collaboration. CMS Technical Proposal.
- [14] RD5 Collaboration. Bunch crossing identification at LHC using a mean-timer technique. *Nucl. Instr. and Meth.*, A336 (1993):91–97.
- [15] RD5 Collaboration. Measurement of hadronic shower punchthrough in magnetic field. *Z. Phys. C*, 69:415–425, 1996.
- [16] M. Ćwiok and G. Wrochna. Muon rates in UA1, D0, CDF and CMS predicted by PYTHIA 5.7. CMS Technical Note CMS TN/95-150, 1996.
- [17] M. Dell’Orso and L. Ristori. VLSI structures for track finding. *Nucl. Instr. and Meth.*, A278 (1989):436–440.
- [18] D. C. Doughty et al. A Massively Parallel Track-Finding System for the Level 2 Trigger in the CLAS Detector at CEBAF. *IEEE Trans. Nucl. Sci.*, Vol. 41, No. 1, February 1994:267–273.
- [19] A. I. Drozhdin et al. Accelerator Related Background in the CMS Detector at LHC. CMS Technical Note CMS TN/96-056.
- [20] Stefan Eichenberger. *A Fast Pipelined Trigger for the H1 Experiment at HERA Based on Multiwire Proportional Chamber Signals*. PhD thesis, Universität Zürich, 1993.
- [21] H. Eichinger. Global Methods of Pattern Recognition. *Nucl. Instr. and Meth.*, 176 (1980):417–424.
- [22] E. Eisenhandler. Level-1 Triggers for LHC Experiments. In *Proceedings, 1993 CERN School of Computing*, 1994.
- [23] Yu. Ermolin and C. Ljuslin. *Nucl. Instr. and Meth.*, A289 (1990):592–596.
- [24] A. Fengler. *Double Muon Trigger Rates in CMS Experiment*. PhD thesis, Warszawa University, 1996.
- [25] Yu. Fisyak. Evaluation of the CMS Muon Endcap Shielding. CMS Technical Note CMS TN/96-076.
- [26] Yu. Fisyak and R. Breedon. Comments on the simulation of background for the CMS muon system. CMS Technical Note CMS TN/96-019.
- [27] F. Gasparini et al. Performance of a DTBX Prototyptpe. *Nucl. Instr. and Meth.*, A344 (1994):137.

- [28] M. De Giorgi et al. Design and Simulation of the Trigger Electronics for the CMS Muon Barrel Chambers. CMS Technical Note CMS TN/95-01.
- [29] H. Grote. *Rep. Prog. Phys.*, 50 (1987):473–500.
- [30] Application Software Group. GEANT - Detector Description and Simulation Tool. CERN Program Library Long Writeup W5013, 1994.
- [31] CERN Application Software Group. PAW Reference Manual. CERN Program Library Long Writeup Q121, 1996. <http://wwwcn.cern.ch/pl/paw/index.html>.
- [32] Particle Data Group. *Physical Review*, D54, 1 (1996).
- [33] S. Haykin. *Neural Networks*. Macmillan College Publishing Company, 1994.
- [34] P. V. Hough. Methods and means to recognize complex patterns. U.S. patent 3.069.654, 1962.
- [35] M. Huhtinen. Radiation Environment Simulation for the CMS Detector. CMS Technical Note CMS TN/95-198.
- [36] IEEE. IEEE Std 1149.1, 1990.
- [37] A. Kluge and T. Wildschek. Track Finding Processor in the DTBX Based CMS Barrel Muon Trigger. In *Proceedings of the First Workshop on Electronics for LHC Experiments*, 1995.
- [38] A. Kluge and T. Wildschek. Track Finding Processor in the DTBX Based CMS Barrel Muon Trigger. In *Proceedings of the Second Workshop on Electronics for LHC Experiments*, 1996.
- [39] A. Kluge and T. Wildschek. The Track Finder of the CMS First Level Muon Trigger. In *Proceedings of the Third Workshop on Electronics for LHC Experiments*, 1997.
- [40] Alexander Kluge. *The Hardware Track Finder Processor in CMS at CERN*. PhD thesis, Technische Universität Wien, 1997.
- [41] T. Kohonen. *Content-Addressable Memories*. Springer, 1987.
- [42] H. Kolanoski. Application of artificial neural networks in particle physics. *Nucl. Instr. and Meth.*, A367 (1995):14–20.

- [43] F. R. Leimgruber et al. Hardware realization of a fast neural network algorithm for real-time tracking in HEP experiments. *Nucl. Instr. and Meth.*, A365 (1995):198–202.
- [44] C. S. Lindsey et al. Drift chamber tracking with neural networks. *IEEE Trans. Nucl. Sci.*, Vol. 40, No. 4, August 1993:607–614.
- [45] C. S. Lindsey et al. Real time track finding in a drift chamber with a VLSI neural network. *Nucl. Instr. and Meth.*, A317 (1992):346–356.
- [46] L. Mapelli. The challenge of triggering and data acquisition at supercollider experiments. *Nucl. Instr. and Meth.*, A315 (1992):460–471.
- [47] L. Mapelli. Collisions at future Supercolliders: the first 10 microseconds. In *Proceedings, 1991 CERN School of Computing*, 1994.
- [48] N. Neumeister et al. CMS Global Trigger. CMS Note 1997/009.
- [49] N. Neumeister et al. Simulation of the global muon trigger. CMS Internal Note CMS IN-1997/023.
- [50] M. Regler and R. Frühwirth. Reconstruction of Charged Tracks. In Thomas Ferbel, editor, *Techniques and Concepts of High-Energy Physics V*, volume Series B: Physics Vol. 204 of *NATO ASI Series*. Plenum Press, 1990.
- [51] J. Rowe. CSC Trigger Simulation in CMSIM 100. CMS Technical Note CMS TN/96-069.
- [52] MUSIC Semiconductors. MU9C1480 Specification, 1993.
- [53] T. Sjöstrand. *Comput. Phys. Commun.*, 82 (1994) 74.
- [54] W. Smith et al. In *Proc. Int. Conf. on Computing in High Energy Physics*, 1992.
- [55] T. Wildschek. CMS Muon Trigger Track Finder — Simulation Software. <http://sungraz.cern.ch/CMS/trigger/muonTrigger/Simulation/AnIndex.html>.
- [56] T. Wildschek. Simulation of the Silicon Tracker/Vertex Detector of the ATLAS Experiment at the Large Hadron Collider at CERN. Diplomarbeit, Technische Universität Wien, 1993.
- [57] G. Wrochna. Punchthrough in the barrel muon stations with and without the Tail Catcher. CMS Internal Note CMS IN-1996/011.

[58] P. Zotto. <http://warco.pd.infn.it/~zotto/CMS.html>.

Acknowledgements

Professor Manfred Markytan has been my thesis adviser, and I would like to thank him for his constant support and encouragement and his very careful proof-reading of my thesis report. I would also like to express my thanks to Professor Christian Fabjan for being my co-supervisor.

Dr. Alexander Kluge has been a great colleague, and I have greatly enjoyed and appreciated our teamwork in designing the regional muon trigger.

Many wonderful colleagues from the CMS collaboration have provided valuable input to my work and I am grateful to them all. Pierluigi Zotto, Anna Meneguzzo, Jeff Rowe and Yuri Fisyak have contributed to the simulation software of the trigger primitive generation, and have made my life exciting by providing many documented and undocumented features in the programs. I would like to thank Grzegorz Wrochna for numerous fruitful discussions on the muon trigger in general.

My stay at CERN was made possible by a generous scholarship program for doctoral students, which is managed by CERN and financed by the Austrian tax-payers. During the last seven months of my stay at CERN, I was employed by the Institute of High-Energy Physics of the Austrian Academy of Sciences. I wish to thank Professor Walter Majerotto and Dr. Claudia Wulz for their support in providing me that position.

Dr. Friedrich Szonzo and Dr. Claudia Wulz have given me complete freedom in my work on the regional muon trigger, and I appreciate that freedom very much.

Lebenslauf

Persönliche Daten

Name: Torsten Wildschek
Geburtsdatum: 18. 01. 1968
Staatsangehörigkeit: Österreicher
Anschrift: ZEUS Wisconsin
DESY
D-22607 Hamburg

Email: Torsten.Wildschek@desy.de
WWW: <http://www.desy.de/~wildsche/>

Ausbildung

- 1994 – 1998: Doktoratsstudent an der Technischen Universität Wien
Ausführung der Forschungsarbeit am CERN, Genf
 - 1988 – 1993: Technische Physik an der Technischen Universität Wien
Abschluß: Diplom-Ingenieur, mit Auszeichnung
Ausführung der Diplomarbeit am CERN, Genf
 - 1986 – 1987: Elektrotechnik an der Technischen Universität Wien
 - 1978 – 1986: Gymnasium in Wien
Matura mit Auszeichnung
-

Beruflicher Werdegang

- 02/1998 – jetzt: University of Wisconsin
Research Associate, Mitarbeit im ZEUS-Experiment am Forschungszentrum
DESY
- 05/1994 – 01/1998: CERN, Genf/Institut für Hochenergiephysik, Wien
Entwurf und Simulation des Myontriggers für das CMS-Experiment

- 07/1992 – 11/1993: CERN, Genf/Institut für Hochenergiephysik, Wien
Simulation des Silizium-Spur/Vertex-Detektors für das ATLAS-Experiment
(Diplomarbeit)
- 09/1986 – 02/1987: Philips BU-PC, Wien
freier Mitarbeiter
Testen von Anwendungssoftware, Kundenunterstützung (Hotline)

Curriculum Vitae

Personal Information

Name: Torsten Wildschek
Birth date: January 18, 1968
Nationality: Austrian
Address: ZEUS Wisconsin
DESY
D-22607 Hamburg
Germany

Email: Torsten.Wildschek@desy.de
WWW: <http://www.desy.de/~wildsche/>

Education

- 1994 – 1998: Graduate Student at Technical University of Vienna, Austria
Research work carried out at CERN
 - 1988 – 1993: Physics Engineering at Technical University of Vienna, Austria
Degree obtained: Diplom-Ingenieur, graduation with First Class Honours
Diploma thesis work carried out at CERN
 - 1986 – 1987: Electrical Engineering at Technical University of Vienna, Austria
 - 1978 – 1986: Secondary school in Vienna, Austria
Final exams (Matura) with First Class Honours
-

Employment History

- 02/1998 – present: University of Wisconsin
Research Associate, working on the ZEUS experiment at DESY
- 05/1994 – 01/1998: CERN/HEPHY Wien
Design and simulation of the CMS first level muon trigger track finder (PhD thesis)

- 07/1992 – 11/1993: CERN/HEPHY Wien
Simulation of the ATLAS Silicon Inner Tracker/Vertex Detector (Diploma thesis)
- 09/1986 – 02/1987: Philips BU-PC, Wien, Austria
Contractor
Software testing, customer support (hotline)